Hyaluronic acid-coated gold nanoparticles as an anticancer drug delivery system – Biological characterization and efficacy

Hanna Parkkola

UNIVERSITAT DE BARCELONA

FACULTAT DE FARMÀCIA

DEPARTAMENT DE FARMÀCIA I TECNOLOGIA FARMACÈUTICA

PROGRAMA DE DOCTORAT:
NANOCIÈNCIES

HYALURONIC ACID-COATED GOLD NANOPARTICLES AS AN ANTICANCER DRUG DELIVERY SYSTEM – BIOLOGICAL CHARACTERIZATION AND EFFICACY

Memòria presentada per Hanna Parkkola per optar al títol de doctor per la Universitat de Barcelona

Directora: Judith Sendra Cuadal

Doctoranda: Hanna Parkkola

Tutora: Ana Calpena Campmany

Hanna Parkkola
Barcelona, 2014

UNIVERSITAT DE BARCELONA

FACULTAT DE FARMÀCIA

DEPARTAMENT DE FARMÀCIA I TECNOLOGIA FARMACÈUTICA

HYALURONIC ACID-COATED GOLD NANOPARTICLES AS AN ANTICANCER DRUG DELIVERY SYSTEM – BIOLOGICAL CHARACTERIZATION AND EFFICACY

Hanna Parkkola 2014

To my parents

To Tuomas

To Joan

ACKNOWLEDGEMENTS

I would like to thank the personnel of Endor Nanotechnologies for the opportunity to realize this doctoral thesis. Especially the CEO and founder of the company, Joaquin Querol, and the director of this thesis, Dr. Judith Sendra, from whom I have learned discipline, to pay plenty of attention on the smallest possible details and to think about EDS even in my sleep. I also want to thank Júlian Peña, for his professional advice and sharing the same interest in music, and Luciano Sobrevals and Rafa Miñana for their friendship, for teaching me so much about the flora and the fauna and for sharing the cell culture hood during the long hours of time consuming experiments. Very special thanks to Laura Vivero, for sitting next to me every day during almost five years, I appreciate your help, patience and friendship deeply, thank you for sharing this part of my life with me.

During this project we have collaborated with various entities, including Leitat Technological Centre, PCB Toxicology Unit and CIBBIM Nanomedicine, which deserve my gratitude. Thank you for your professionalism, advice and sharing your knowledge.

Thank you also all my “new” friends that I have met in Barcelona for sharing amazing experiences with me, for showing me new places and for making me feel like home. You are too numerous to mention one by one, and I don’t want to leave anyone out, but you know who you are!

Suvi, Katrin, Natalia, Michela, Dr. Katrin and Antonija, I want to express my appreciation for the coffees, lunches, pints of wine and all the precious moments that our group of “guiris” has shared. Thank you also Adam and Erik.

Thank you my friends back in Finland: my “business partners” Marja, Heli and Mari, and my loyal companions Veera, Reeta, Iida and Janika, I miss you very dearly and value you for receiving me with opens arms even after long silences.

I want to thank Montse and Jaume for welcoming me warmly into their family and further making me feel like home in Barcelona.

Finally, a big thank you to my family, to my brother Tuomas for putting up with me and my sunny personality all these years, for our long talks and for listening to me when I've been having difficult times, and to my parents Riitta and Kai for providing me such a wonderful start for life, for believing in me and supporting me in every single step of my life. You made me the person I am. Thank you Joan for sharing my ups and downs, for teaching me to appreciate new places and experiences, for everything we have shared and for showing me what happiness is.

Kiitos

The experimental work of this thesis has been executed in the laboratory of Endor Nanotechnologies, S.L. in Parc Científic de Barcelona (C/ Baldiri Reixac 15; 08028 Barcelona).

The work has been financed by Ajuts Talent Empresa (TEM DGR: 2009 TEM 00023), Agència de Gestió d'Ajuts Universitaris i de Recerca (AGAUR: Generalitat de Catalunya).

PUBLICATIONS

Parkkola H., Vivero L., Ramis M., Querol J., Sendra J. 2012. Proceed with caution? Concept and application of the precautionary principle in nanobiotechnology: Gold Nanoparticles and Cell Viability Evaluation.

Editors: Ach J.S., Lüttenberg B., Paslack R., Weltring K-M. LIT Verlag

Vivero L., Parkkola H., Sendra J., Querol J., Cambero J.P.G., Ramis M. 2012. Proceed with caution? Concept and application of the precautionary principle in nanobiotechnology: Gold Nanoparticle Stability Studies in Physiological Media.

Editors: Ach J.S., Lüttenberg B., Paslack R., Weltring K-M. LIT Verlag

Sobrevals L., Parkkola H., Vivero L., Miñana R., Sendra J. 2014. Nanotechnology: Recent Trends, Emerging Issues and Future Directions. Chapter: Nanomedicine: The New Age of Therapeutics.

Editor: Islam N. Nova Science Publishers, Inc.

Posters:

Parkkola H., Vivero L., Vega M., Ramis M., Querol J., Sendra J. 2010. Metallic Nanoparticles and Cytotoxicity Assessment. *International Congress of Toxicology.*

Patents:

Ramis Castelltort M., Querol Sastre J., Vivero Sanchez L., Sendra Cuadal J., Parkkola H. System for the release of a therapeutic agent, pharmaceutical composition containing it, the preparation and medical use thereof. International Publication number WO 2012/089768A1. Applicant: Endor Nanotechnologies, S.L.

Table of contents

ABBREVIATIONS

AuNP	Gold nanoparticle
CD44	Principal receptor for hyaluronic acid
CFA	Colony formation assay
CIS	Cisplatin
CSC	Cancer stem cell
DLS	Dynamic light scattering
EA	Elemental analysis
ECM	Extracellular matrix
EDS	Endor Delivery System
EDS-drug	Endor Delivery System conjugated with an anticancer drug
EGFR	Epidermal growth factor receptor
EMT	Epithelial to mesenchymal transition
EPR	Enhanced permeability and retention
ErbB2	Human epidermal growth factor receptor 2
ERK	Extracellular signal-regulated kinase
ERM	ERM protein family: ezrin, radixin, moesin
ESF	European Science Foundation
FAK	Focal adhesion kinase
FDA	US Food and Drug Administration
HA	Hyaluronic acid/Hyaluronan
HARE	Hyaluronan receptor for endocytosis
HAS	Hyaluronan synthase
H&E	Hematoxylin & eosin
HER2	(see ErbB2)
HEX	Hexosaminidase
HMW	High molecular weight
HYAL	Hyaluronidase
ICP-MS	Inductively coupled plasma mass spectrometry
ID	Initial dose
IF	Immunofluorescence
JNK	c-Jun N-terminal kinase

LMW	Low molecular weight
LYVE-1	Lymphatic vessel endothelial hyaluronan receptor 1
MAPK	Mitogen-activated protein kinase
MPS	Mononuclear phagocyte system
mTOR	Mechanistic target of rapamycin (serine/threonine kinase)
NCL	Nanotechnology Characterization Laboratory
oHA	HA oligosaccharide
PDGF/PDGFR	Platelet-derived growth factor/receptor
PDT	Photodynamic therapy
PEG	Polyethylene glycol
PI3K	Phosphoinositide 3-kinase
PKC	Protein kinase C
Pt	Platinum
RHAMM	Receptor for hyaluronan-mediated motility
ROS	Reactive oxygen species
RTK	Receptor tyrosine kinase
SPR	Surface plasmon resonance
TEM	Transmission electron microscopy
TLR	Toll-like receptor
UV-VIS	Ultraviolet-visible spectroscopy
VEGF/VEGFR	Vascular endothelial growth factor/receptor

ABSTRACT/RESUM

ABSTRACT

Novel stategies are needed to improve the limited efficacy of current cancer therapies. High expectations are directed towards nanotechnology-based applications in cancer medicine. We have developed a drug delivery system based on hyaluronic acid (HA) - coated gold nanoparticles (AuNPs) that targets CD44, a cell surface glycoprotein overexpressed by various cancer cells. This nanocarrier (EDS: Endor Drug Delivery System) provides a platform for the conjugation of anticancer agents for a more efficient cancer treatment.

We show that the unique characteristics of AuNPs remain unchanged when the targeting ligand and a chemotherapeutic agent are conjugated. HA-coating stabilizes AuNPs and improves their biocompatibility. EDS is shown to target CD44 and is internalized through this receptor. The nanocarrier does not cause toxic effects *in vitro* or *in vivo*. After conjugating an anticancer agent (CIS: cisplatin) to the nanocarrier, EDS shows gradual drug release in physiological media due to changes in pH and hyaluronidase activity, and the drug reaches its target cells in its active form. *In vivo* efficacy of EDS-CIS conjugate is higher than that of free cisplatin. However, more safety and toxicological studies must be conducted. New drug candidates are being tested in order to validate EDS as a platform for antitumoral drugs.

RESUM

Els actuals tractaments oncòlogics presentan una eficàcia limitada que forcen la recerca de noves teràpies mes eficients. En aquest sentit, la nanotecnologia ha generat moltes expectatives. Durant aquesta tesi, hem desenvolupat un sistema d'alliberació de fàrmacs formats per nanopartícules d'or (AuNP) recobertes amb àcid hialurònic (HA), dirigit a CD44, una glicoproteïna que es sobreexpresa a la superfície cel.lular de diferents tipus de tumor. Aquest sistema (EDS: Endor Delivery System) proporciona una plataforma per a la conjugació de diferents fàrmacs antitumorals per tal de tractar el càncer d'una manera més eficient.

Aquesta tesi demostra que les propietats úniques que aporten les AuNP es mantenen quan la molècula que dirigeix al tumor (HA) i l'agent antitumoral són conjugats. El recobriment d'HA estabilitza les AuNP, millorant la seva biocompatibilitat. A més, també es demostra que l'EDS va dirigit a CD44, al qual s'uneix i és internalitzat a les cèl.lules. El nanotransportador no presenta efectes tòxics ni *in vitro* ni *in vivo*. Quan el nanotransportador s'uneix a un agent antitumoral (Cisplatí, CIS), es va alliberant de manera gradual en medis fisiològics, a través de l'acció de les hialuronidases i del canvi de pH, alliberant el fàrmac amb la seva forma activa. L'eficàcia in vivo del CIS conjugat a l'EDS ha mostrat ser superior a la del fàrmac lliure. No obstant això, són necessaris més estudis de seguretat y toxicitat. Nous fàrmacs antitumorals estan sent estudiats per tal de validar l'EDS com una plataforma per a l'alliberació de fàrmacs antitumorals.

INTRODUCTION

1. INTRODUCTION

1.1 Cancer

1.1.1 Cancer – an introduction

According to the World Health Organization, approximately 14,1 million new cancer cases were diagnosed in 2012, and by the year 2030 the cancer burden is expected to increase to 23,6 million new cases per year. Cancer is also a leading cause of death and led to 8,2 million mortalities in 2012 (*International Agency for Research on Cancer and Cancer Research UK*, 2014).

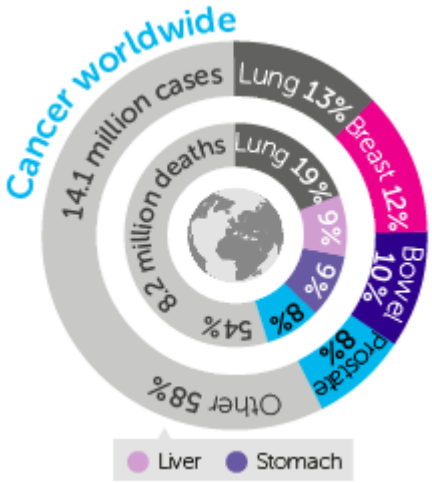

Figure 1. Worldwide cancer statistics in the year 2012. Source: Cancer Research UK.

The creation of cancer, i.e. tumorigenesis, is a complex multistep process, with multiple genetic alterations that leads to progressive transformation of healthy cells into malignant derivatives. The dynamic changes in the cancer cell genome can occur through gain of function mutations in oncogenes and loss of function mutations in tumor suppressor genes that result in growth advantage. In 2000, Hanahan & Weinberg described six essential alterations in cancer cell phenotype compared to normal cells, acquired during tumor development. These alterations are: self-sufficiency in growth signals, evasion of apoptosis, insensitivity to anti-growth signals, limitless replicative

potential, sustained angiogenesis, and tissue invasion and metastasis. The alterations occur when genetic reprogramming in various extensively interconnected signaling cascades (such as PI3K, different MAPKs and SMAD among others) takes place, leading to cancer progression (Hanahan & Weinberg, 2000).

In 2011, Hanahan & Weinberg broadened the cancer hallmark concept by introducing two new emerging hallmarks: reprogrammation of energy metabolism and evasion of immune destruction; and two enabling characteristics of neoplasia: genome instability and tumor-promoting inflammation (Figure 2). They also highlighted the importance of the tumor microenvironment with its normal tissue derived cells – endothelial cells, immune inflammatory cells and cancer-associated fibroblasts – and the dynamic extracellular matrix (ECM) that they collectively remodel in cancer progression (Hanahan & Weinberg, 2011).

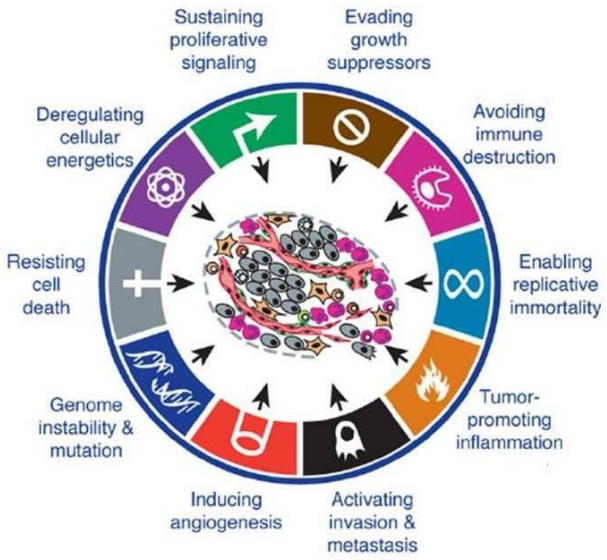

Figure 2. Hallmarks and enabling characteristics of cancer. Modified from Hanahan & Weinberg, 2011.

To tackle the global cancer burden, treatment strategies including medical, surgical, radiation, physical therapies and pain and palliative care should be designed. Thorough screening and preventive protocols should be developed and awareness increased, especially in the less developed world, where the cancer occurrence rate is growing and where there are limited resources and lack of access to quality health care. The state-of-

the-art of technology should be employed to create new innovative techniques and cost-efficient approaches tailored to the variable biology of the disease (Are et al., 2013).

1.1.2 Treatment

Cancer can be locally treated by radiation, hyperthermia, laser or removing the tumor surgically. Radiation therapy uses high energy radiation to kill cancer cells by damaging their DNA, while hyperthermia exposes tissues to high temperatures to kill or damage cancer cells. Systemic cancer treatments include chemotherapy, hormone therapy that uses drugs to inhibit the growth of hormone-dependent tumors (breast, ovarian and prostate cancer among others), and biological therapies which include gene therapy, antibodies and cytokines (American Cancer Society, National Cancer Institute, Cancer Research UK).

1.1.2.1 Cancer chemotherapy

Cancer chemotherapeutics are divided into alkylating agents (including platinum compunds), antibiotics, antimetabolites, topoisomerase inhibitors, mitotic inhibitors and others, depending on their chemical structure and mechanism of action (American Cancer Society, Table 1).

Most classical chemotherapeutic agents mediate their antitumoral effects through interactions with DNA. They act on DNA by breaking the helix itself or interfering with DNA-related proteins. Alkylating agents and some antibiotics (bleomycin and mitomycin C) form DNA adducts through strand crosslinking. Topoisomerase inhibitors, anthracycline antiobiotics and antimetabolites interfere with DNA synthesis by inhibiting different enzymes involved in DNA replication. Mitotic inhibitors act on tubulin in different ways: vinca alkaloids prevent polymerization of tubulin dimers while taxane binding stabilizes microtubules inhibiting the normal reorganization of the tubule network (Espinosa et al., 2003).

Family	Mechanism of action	Drugs	Indications
Alkylating agents (Platinum compounds)	Non-phase spesific direct DNA damage	Nitrogen mustards, nitrosoureas, alkyl sulfonates, triazines, ethylenimines (Cisplatin, carboplatin, oxalaplatin)	Leukemia, lymphoma, Hodgkin's disease, multiple myeloma, lung, breast & ovarian cancer
Antimetabolites	Substitution of nucleotides in RNA & DNA synthesis during S-phase	5-fluorouracil, 6-mercaptopurine, gemcitabine, hydroxyurea, methotrexate, pentostatin, thioguanine	Leukemia, breast, ovarian & gastrointestinal tract cancers
Antibiotics	Non-phase spesific interference with DNA replication enzymes	Actinomycin D, bleomycin, mitomycin C & anthracyclines: daunorubicin, doxorubicin, epirubicin, idarubicin	Various cancers
Topoisomerase inhibitors	Interference with DNA replication	Isomerase I: topotecan & irinotecan Isomerase II: etoposide, teniposide	Leukemia, lung, ovarian & gastrointestinal tract cancers
Mitotic inhibitors	Microtubule disruption during M-phase	Taxanes, epothilones, vinca alkaloids, estramustine	Lymphoma, leukemia, myeloma, breast & lung cancer

Table 1. Chemoterapeutic agent families. Source: American Cancer Society.

1.1.2.1.1 Platinum-based drugs

The accidental discovery of the biological properties of cisplatin in 1965 initiated the development of platinum drugs for anticancer therapy. Cisplatin rapidly proceeded into clinical trials and was approved by FDA in 1978 for the treatment of bladder and testicular cancer. After that, platinum-based agents have been used to treat ovarian, colorectal, prostate and non-small cell lung cancer among others (Kelland, 2007).

Cisplatin is a neutral complex that in order to execute its cytostatic effects, needs to be activated by replacement of the cis-chloro ligands with water molecules. The monoaquated form of cisplatin is a highly reactive species that interacts with DNA - primarily purine bases (adenosine and guanine) - and proteins and forms DNA adducts (Figure 3) (Kelland, 2000). This intra- and interstrand crosslinking leads to physical contortions in the DNA structure that is recognized by various damage recognition proteins which transduce DNA damage signals to their downstream effectors. The activated signaling pathways include p53 and MAPK (ERK, JNK & p38) among others, and through crosstalk between the different pathways involved, cisplatin-caused DNA damage leads to apoptosis (Siddik, 2003).

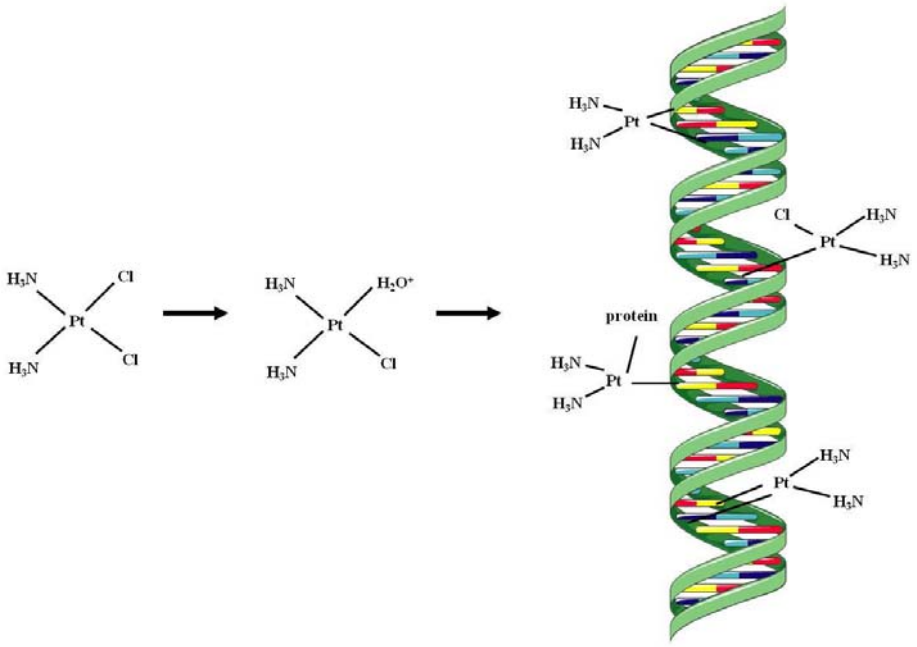

Figure 3. The mechanism of action of cisplatin.

Besides cisplatin, the other two world-wide approved platinum-based anticancer drugs are carboplatin and oxaliplatin. Since toxicity of platinum-based drugs is directly related to the facility of the replacement of the ligands, and chloride as a leaving group is highly labile, these compounds with less reactive groups were developed (Figure 4).

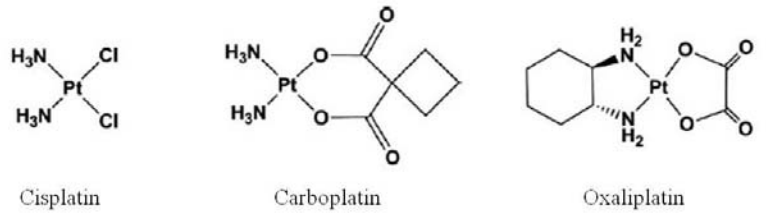

Figure 4. The structure of world-wide approved Pt-based anticancer drugs.

Nevertheless, all Pt-based drugs though express severe dose-limiting side-effects, such as neurotoxicity and myelosuppression, due to uptake into all rapidly dividing cells, not just tumors. Besides, Pt-based drugs are secreted through the kidneys, which causes rigorous nephrotoxicity. For this toxicity, big effort has been directed to development of less toxic Pt-derivatives, but many of them have been discontinued in clinical trials. In order to reduce this toxicity, during the past decade the focus has shifted towards design of delivery vehicles for the already approved Pt drugs (Wheate et al., 2010).

1.1.2.2 Personalized medicine

The aim of personalized medicine is the treatment of a disease based on the genetic characteristics of a population. This means individualized treatments of patients based on their gene and proteome expression analysis. Patients with cancers that show expression of validated cancer biomarkers can receive a treatment tailored to target their oncologic signaling profile instead of receiving classical chemotherapy that does not distinct cancer cells from normal cells.

According to Cancer Research UK, there are over 200 different types of cancer. The clinical outcome depends on traditional clinico-pathological variables (patient's age, tumor stage, grade and e.g. in the case of breast cancer, estrogen-receptor status), but also on the genetic heterogeneity of the tumors. Besides, cancer is a dynamic disease and tumor cells go through clonal evolution and changes in mutation signatures over time, which further complicates the discovery of the proper treatment. During the past 30 years, gene expression profiling has enabled definition of molecular subgroups of cancer that respond to treatment differently, which has contributed to the emergence of personalized medicine (Baird & Caldas, 2013).

In order to optimize the efficacy of personalized cancer therapy, new diagnostic and predictive biomarkers and therapeutic targets need to be discovered and validated. Personalized cancer medicine may be the answer for treating cancers with limited chemotherapeutic efficacy and decreasing chemoresistance of certain tumors. Finding the correct treatment for each patient could improve clinical outcomes greatly.

1.1.3 Cancer biomarkers

As the molecular understanding of cancer increases – owing largely to genome sequencing – the rational development of targeted cancer drugs is gaining ground. An example of biomarker-targeted cancer treatment are small molecule kinase inhibitors, with a total of 17 approved inhibitors used as anticancer therapeutics in 2013 and an estimate of nearly 400 in clinical development. The most common kinases targeted in oncology include the growth factors and/or their receptors: VEGF/VEGFR, HER2 (ErbB2), EGFR and PDGF/PDGFR; and regulators of altered metabolism: PI3K and mTOR. Probably the most known example of biomarker-targeted cancer therapy is trastuzumab, a HER2-targeting antibody, the pioneer of targeted therapy that is now widely used in the treatment of breast cancer (Gonzalez de Castro et al., 2013).

Besides kinases, other potential cancer cell biomarkers include epithelial-mesenchymal transition-associated (EMT) molecules: vimentin, N-cadherin, snail and twist; multidrug resistance proteins; pluripotency-associated transcription factors and cancer stem cell (CSC) markers CD133, ALDH, CD21 and CD44 (Mimeault & Batra, 2014).

1.1.3.1 CD44

CD44 is a transmembrane glycoprotein that mediates the response of cells to the microenvironment that surrounds them. CD44 is the main receptor of hyaluronic acid (HA) but can interact also with other lingands such as osteopontin, collagens, fibronectin and laminin. The interactions between CD44 and its ligands mediate intercellular and cell-matrix interactions, cell migration – by modulating secretion and activation of proteolytic enzymes – and migration of lymphocytes to inflammatory sites (Isacke & Yarwood, 2002).

Furthermore CD44 has a broad function in cellular signaling cascades. Through ligand binding and interactions with other cell surface receptors, it can regulate cellular growth, survival, and differentiation.

1.1.3.1.1 CD44 structure

CD44 interacts with various components of the extracellular matrix, including glycosaminoglycans (GAGs), collagen, laminin and fibronectin. CD44 consists of an amino-terminal domain that binds its ligands, a stem structure, a transmembrane region and a cytoplasmic tail region (Figure 5).

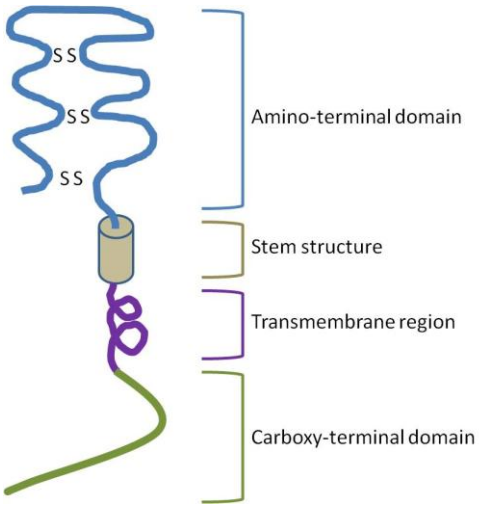

Figure 5. The structure of CD44 receptor. Modified from Ponta et al., 2003.

The amino-terminal globular domain contains motifs in its link domain (amino acids 32-123) that bind HA and other glycosaminoglycans. The link domain contains four highly conserved cysteine residues that form interchain disulphide links that account for stability of the module. Outside the link motif there are two additional cysteine residues thought necessary for correct folding and GAG binding. The stem structure separates the amino-terminal domain from the transmembrane region and is consisted of 46 amino acids. It contains alleged proteolytic cleavage sites. The transmembrane region of CD44 consists of 23 hydrophobic amino acids and is thought to have a role in the grouping of CD44 in lipid rafts. The carboxy-terminal cytoplasmic domain binds proteins associated to signaling and cytoskeletal organization, such as ankyrin and ERM family proteins (ERM: ezrin, radixin and moesin). The cytoplasmic tail contains two serine residues the phosphorylation of which, and therefore binding of the proteins, is controlled by various kinases, including protein kinase C (PKC) and Rho kinase (Ponta et al., 2003).

The human CD44 gene consists of 20 exons. The standard isoform (CD44s) expresses 10 exons being the smallest of the isoforms. The remaining 10 exons give rise to multiple CD44 variants (CD44v) formed through alternative splicing of the pre-mRNA (Figure 6).

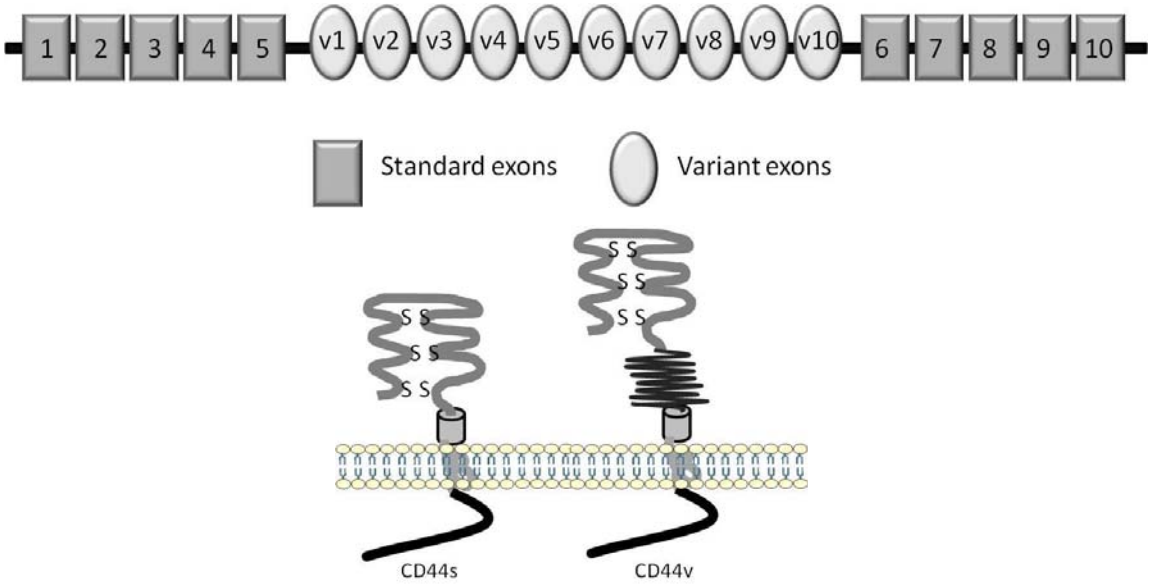

Figure 6. CD44 pre-mRNA structure (above) and CD44 standard and variant structures (below). Modified from Goodison et al., 1999.

Alternative splicing of CD44 pre-mRNA and addition of different combinations of variant exons in the extracellular structure of the receptor can alter the binding of its ligands. Besides alternative splicing, post translational modifications, such as glycosylation, addition of heparan and keratin sulphate and sialic acid residues on the standard region and variant sites further modifies ligand binding characteristics and affects the function of the receptor (Goodison et al., 1999).

1.1.3.1.2 CD44 functions

CD44 has various important roles in physiological and pathophysiological conditions (Figure 7). The functions of CD44 include cell aggregation and migration, proliferation, repair and regeneration, uptake and degradation of HA, lymphocyte activation and lymph node homing, myelopoiesis, lymphopoiesis, angiogenesis and cytokine release. CD44 shows high expression levels especially in proliferating cells, such as cells involved in tissue repair, morphogenesis, organogenesis and angiogenesis. The expression patterns and distributions of CD44s and CD44v in different tissues suggest differing functions for the standard and variant isoforms (Sneath & Mangham, 1998; Underhill, 1992).

CD44 mediates cell aggregation through anchoring HA/proteoglycan rich pericellular matrices. Being a transmembrane receptor, CD44 can communicate cell-matrix interactions into the cell, but may also conversely alter the associated matrix in response to intracellular signals. Thus CD44 provides means for interaction and communication between cells and the surrounding matrix. Besides, CD44 can serve as a co-receptor with other classical signaling receptors, physically linking to receptors such as c-Met and ErbB family of receptor tyrosine kinases, hence mediating the activation of various signaling pathways (Knudson & Knudson, 1999; Knudson & Knudson, 2004).

CD44 participates in cytoskeletal organization, binding directly to ankyrin, an adaptor protein that is attached to cytoskeletal actin. Binding of ligands promotes CD44 interactions with ankyrin as well as small GTP-binding proteins – such as RhoA that mediates phosphorylation of various cytoskeletal proteins – leading to their activation and producing changes in actin assembly and reorganization of the cytoskeleton (Bourguignon, 2008).

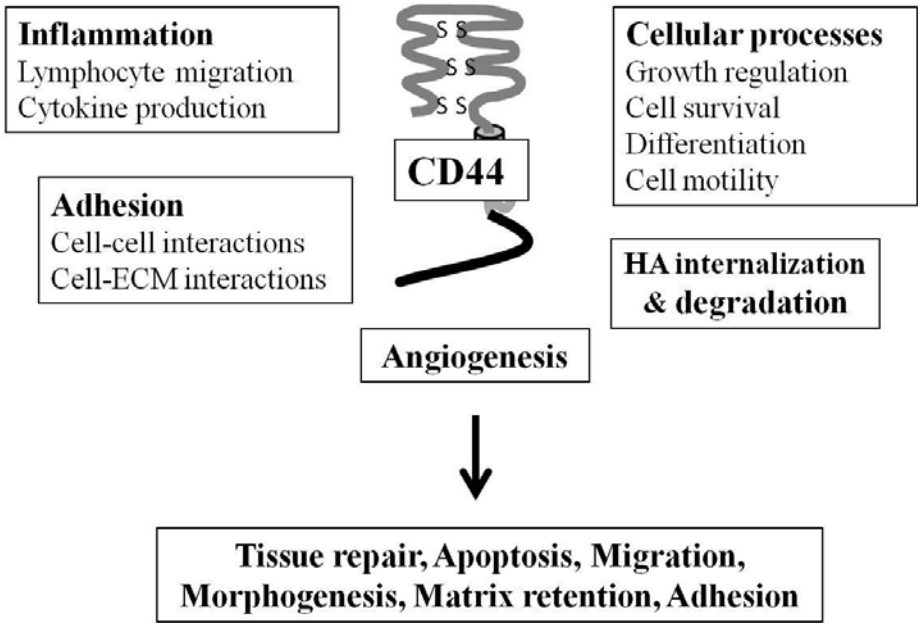

Figure 7. Some of the various processes in which CD44 participates.

CD44 has also been shown to be expressed in high levels in embryonic, hematopoietic, mesenchymal and epithelial stem cells as well as cancer stem cells (CSC) (Williams et al., 2013).

1.1.3.1.2.1 CD44 in cancer

CD44 has been shown to contribute to neoplasia. High CD44 levels are associated with various types of malignant tumors and the invasiveness of certain tumors. Due to its functions in normal tissues, CD44 can contribute to different stages of cancer. The functions involved in tumorigenesis, invasion and metastasis are:

- Cell growth promoting activity
- Production of autocrine factors caused by CD44-ligand interactions
- Locomotory signaling
- Mitogenic signaling
- Contributing to invasion via adherence to ECM through its ligands
- Invasion to HA-rich tissues by degradation of HA
- Tumor angiogenesis (Sneath & Mangham, 1998)

CD44 has also been established a CSC marker and used to isolate and enrich CSCs from different types of tumors (Al-Hajj et al., 2003; Chu et al., 2009). Cancer stem cells are characterized as stem cell-like cells within a tumor, capable of self-renewal, differentiation and able to form tumors when transplanted into a host. They are defined by asymmetric cell division, in which one progeny maintains the stem cell properties and the other one undergoes further cell division and differentiation. CSCs are believed to be more resistant to chemo- and radiation therapy than other cancer cells and are associated to metastasis (Yu et al., 2012).

1.1.3.2 Hyaluronic acid

Hyaluronic acid is the main ligand for the cell surface receptor CD44. HA is a sugar-chain macromolecule that displays different properties depending on its size; high molecular weight (HMW) HA of the ECM links its binding molecules into aggregates and regulates cell adhesion, motility, and growth while HA oligosaccharides (low molecular weight: LMW) influence the same cell behaviors by interacting differently

with cell surface receptors. Like its main receptor, HA levels are increased in many cancers (Itano & Kimata, 2008).

1.1.3.2.1 Structure and functions of HA

HA is a polysaccharide composed of repeating disaccharide units of glucuronic acid and *N*-acetylglucosamine (Figure 8). The size of a HA polysaccharide under normal physiological conditions is 1000 – 10 000 kDa and it consists of up to 25 000 disaccharides. HA is a negatively charged polymer and synthesized by three related hyaluronan synthases: HAS1, HAS2 and HAS3, multipass transmembrane enzymes that extrude HA into the cell surface or extracellular matrix while synthesizing it (Toole, 2004).

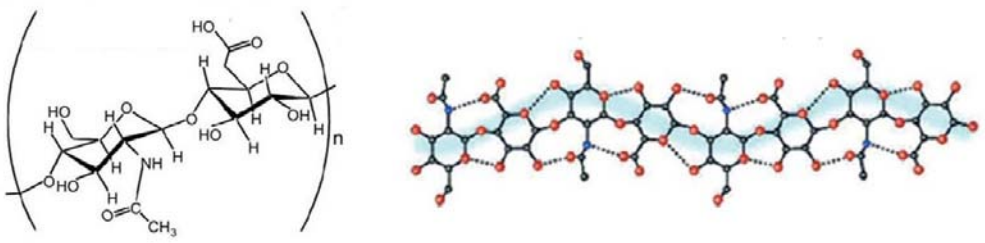

Figure 8. Structure of a HA disaccharide unit (left) and interchain hydrogen bonds within polymer consisting of 4 units (right), source: Jackson, 2009.

HA takes part in a variety of cell functions as well as in the maintenance of tissue structure. It is an important part of the ECM present in most vertebrate tissues and binds multiple proteoglycans – such as aggrecan, versican, and neurocan – that contribute to its assembly and regulate its functions. HA solutions are viscoelastic, and because of this property HA is prominent in synovial fluid and soft connective tissues. The physiological roles of HA in the ECM include water homeostasis, prevention of fluid flux through tissues and regulation of substance transport in the intercellular space, as well as lubrication and protection (Laurent et al., 1996).

Through cell surface receptors, HA also operates as a signal transducer regulating adhesion, cell motility, growth and differentiation activating various intracellular signaling cascades, such as c-Src, Ras and MAPKs. The actions of HA on the signaling

cascades are dictated by tissue concentration and size of HA molecules that interact with the receptors on cell surface. These properties are regulated by cooperating biosynthesis by HAS enzymes and the degradation of HA by hyaluronidases (HYALs) (Itano, 2008).

1.1.3.2.2 HA interactions with cell surface receptors

HA is involved in tissue homeostasis and integrity, and acts as a template for macromolecular interactions in the assembly of the extracellular matrix. For these reasons HA has been widely used in the fields of dermatology (Gold, 2009) and regenerative medicine (Diamond et al., 2012; Prestwich, 2011).

Besides CD44, HA interacts with other cell surface HA-binding proteins, hyaladherins, including:

- RHAMM/CD168 (receptor for HA-mediated motility)
- LYVE-1 (lymphatic vessel endothelial receptor 1)
- HARE/stabilin 2 (HA receptor for endocytosis)
- TLR2 & TLR4 (toll-like recpetors 2 and 4)

RHAMM is a soluble cytoplasmic HA receptor that does not contain a transmembrane domain, but still performs extracellular functions, such as forming signaling complexes with CD44 and ERK1,2 thus activating the ERK1,2 kinase pathway (Hamilton et al., 2007). RHAMM is known to bind HA, mediate HA-signaling and cell motility, but its involvement in HA-uptake has not been shown (Hall et al., 1994). This receptor promotes cell motility and invasion as a result of interaction with HA. RHAMM expression, as that of CD44, is increased in tumorigenesis. Intracellular RHAMM associates with centrosomes and mitotic spindles and through these associations has the potential to promote genomic instability and neoplastic progression. (Maxwell et al., 2008) RHAMM has also been shown to be able to compensate for CD44 in binding HA, supporting cell migration and up-regulating inflammation-related genes (Nedvetzki et al., 2004).

Systemic HA turnover is executed by the scavenger receptors LYVE-1 and HARE. LYVE-1 is expressed in lymphatic vessels and endothelia of lymph node sinuses and it binds HA, but not other glycosaminoglycans. LYVE-1 plays a role in HA homeostasis by uptaking HA to the lymph for partial degradation. HARE can be found with LYVE-1 in endothelial cells in the medullary sinuses of the lymph nodes and also in the sinusoidal epithelium of spleen and liver where HA fragments that exit lymph nodes are finally terminally degraded. Besides HA, HARE scavenges other glycosaminoglycans and takes part in their systemic clearance from the circulatory and lymphatic systems through clathrin-mediated endocytosis (Jackson, 2004, 2009).

HA also interacts with Toll-like receptors that play a role in pathogen recognition and inititation of immune responses. HA oligosaccharides have been shown to induce dendritic cell maturation and MAPK activation leading to TNF-α production. HA fragments stimulate metalloproteinase and inflammatory cytokine expression and NF-κB activation. HA-TLR interaction has as well been shown to have a protective effect against tissue injury (Black et al., 2013; Jiang et al., 2011).

1.1.3.2.3 HA degradation

HA is degraded in humans by five hyaluronidases: HYAL1, HYAL2, HYAL3, HYAL4 and PH-20/Spam1. The main hyaluronidases in charge of HA degradation in somatic tissues are HYAL1 and HYAL2. Degradation of HA is an endolytic, non-processive event where the HA fragment formed from glycosidic cleavage turns into a substrate for additional degradation. The final degradation products are tetrasaccharides, which can be further degraded intracellularly by lysosomal enzymes (Stern & Jedrzejas, 2008).

HA is degraded locally in tissues by the same cells that synthesize it. HA is internalized in a CD44-dependent mechanism that is associated with neither clathrin-coated vesicles, caveolae nor pinocytosis. The uptake of HA has been shown to depend on CD44 expression and partially degraded HA-oligosaccharides have been shown to be internalized faster than HMW HA. CD44-bound HA is degraded by HYAL2 to LMW fragments and endocytosed. After internalization, HA is delivered to lysosomes for further degradation by lysosomal HYAL1. The mechanism for CD44-mediated HA

uptake is possibly due to CD44 interactions with the actin cytoskeleton or regulated by partial ECM degradation and CD44 turnover (Knudson et al., 2002; Sironen et al., 2011).

1.1.3.2.4 HA in cancer

HA is associated with carcinogenesis and it has been shown to be produced in excess by tumor cells as well as the surrounding stromal cells. The levels of HA are elevated in many different types of tumors and high HA levels have been linked to malignant progression. Through binding its primary receptor, CD44, HA has been shown to induce various intracellular signal transduction pathways, generally associated with tumorigenesis and the disruption of the CD44-HA connection has been found to alter the activities of these pathways. The various different tumor types in which high HA concentrations have been related to malignancy include:

- Breast carcinoma
- Ovarian carcinoma
- Lung adenocarcinoma
- Prostate cancer
- Gastric and colorectal cancers
- Bladder cancer
- Head and neck cancer (Toole, 2004)

HA has various roles in the initiation and progression of cancer. HA forms part of the tumor extracellular matrix linking together macromolecules and creating a meshwork favorable for tumorigenesis, allowing crosstalk between tumor cells and the stroma. This tumor microenvironment rich with HA can also act in recruiting inflammatory cells and in activation of cancer-related signaling pathways, accelerating through these mechanisms of action angiogenesis, lymphangiogenesis and inflammation. Aberrant HA production has been shown to increase cell growth and migration by decreasing contact inhibition, and over expression of HA synthase genes enhances tumorigenic abilities of some cancer cells (Itano et al., 2008).

1.1.3.2.5 HA signaling

CD44-meadiated HA signaling differs between malignant cells and normal tissue cells. In normal tissues, where HA can be found in abundance, endogenous HMW HA binds CD44 receptors multivalently causing a quiescent state. When this binding is disrupted, signaling cascades are activated (Figure 9, A & B). In migrating cells – such as embryonic, endothelial and malignant cells – signaling is induced by the binding of the endogenous HA and inactivated by disruption of this binding (Figure 9, C & D) (Knudson & Knudson, 2004).

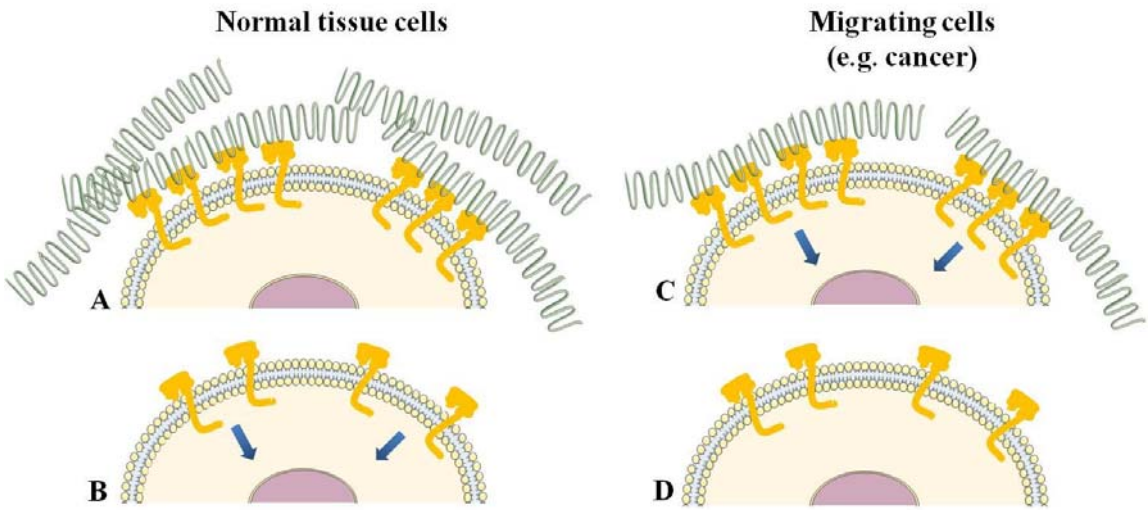

Figure 9. Normal tissue HA signaling through CD44 is induced by disruption of HA binding (A & B) while in malignant cells the situation is the opposite (C & D). Modified from Knudson & Knudson, 2004.

Besides CD44, HA has been shown to interact with other tumorigenesis-related signal-transducing receptors, including RHAMM. The binding of HA causes the cytoplasmic tail of CD44 to interact with various molecules – such as SRC kinases, RHO GTPases, VAV2, GAB1, ankyrin and ezrin – having regulatory roles in various intracellular signaling pathways. RHAMM, as well as CD44, binds HA on the cell surface and transduces signals related to malignant behavior. Interactions of HA with CD44 and RHAMM lead to alterations in the activities of tyrosine kinases, protein kinase C, focal adhesion kinase (FAK), phosphatidylinositol 3-kinase (PI3K) and various components

of the cytoskeleton (Figure 10). The effects of HA involved in tumorigenesis through CD44 regulate especially cell survival through ErbB-signaling (Toole, 2004).

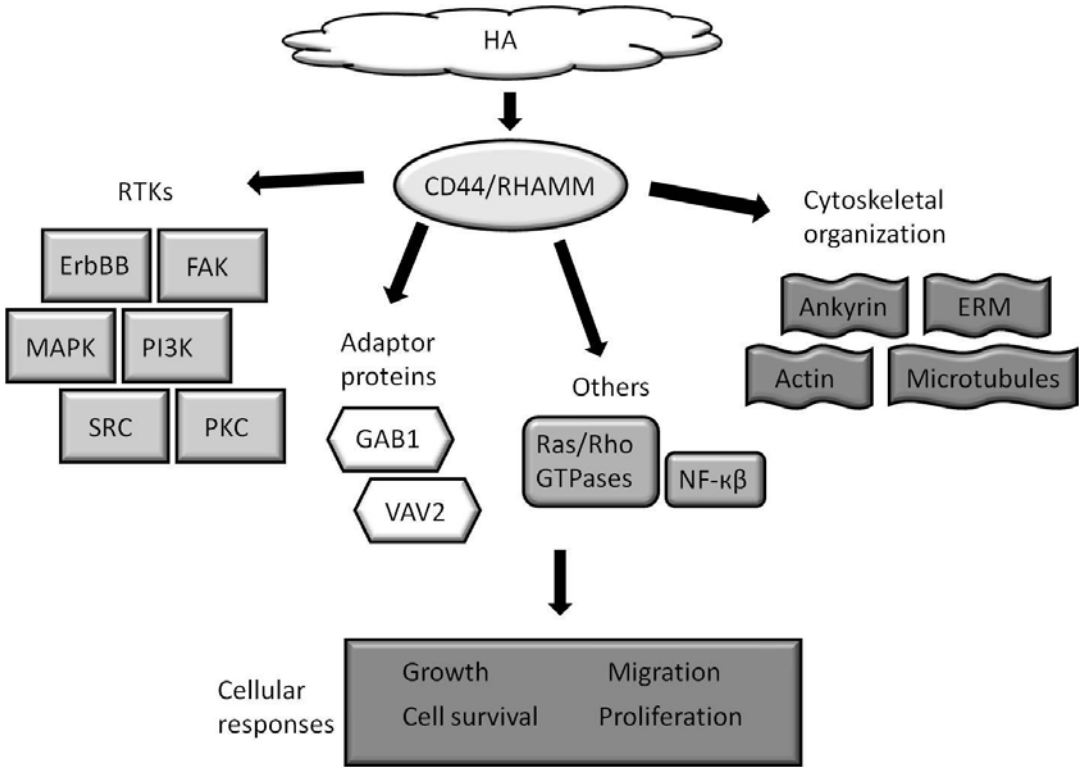

Figure 10. Cellular responses resulting from HA-CD44/RHAMM interactions and the intracellular components involved .

When native, HMW HA starts oncogenic signaling through CD44, it is thought to happen through multivalent binding of an individual HA polysaccharide to multiple receptors. Small oligosaccharides of HA (oHA) on the other hand can bind CD44 monovalently and they have been shown to have the opposite effects on CD44-signaling and tumor progression compared to the endogenous HA. oHA has been described to act as an antagonist of the native HA competing for CD44 and replacing the multivalent, cooperative binding thus interfering with tumorigenesis (Figure 11) (Toole et al., 2008).

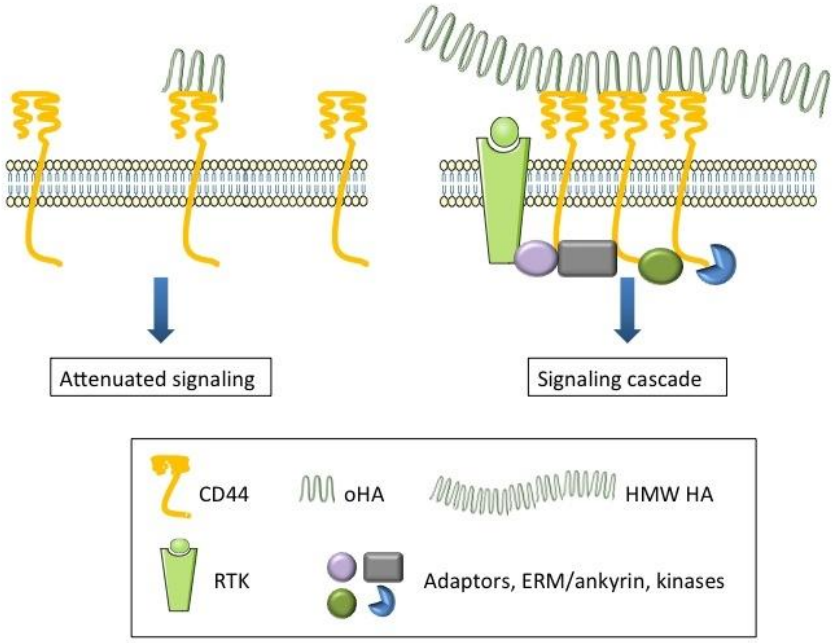

Figure 11. oHA binding compared to HMW HA binding to CD44 and the cellular response. Modified from Toole et al., 2008.

Besides exhibiting antitumoral effects, HA oligosaccharides have been shown to produce opposite effects as well (Dang et al., 2013; Sugahara et al., 2006). There is a considerable amount of literature regarding cellular responses to HA and plenty of controversy in results of studies. In some cases the size of the HA or the signaling molecules involved have not been monitored. Different sizes of HA fragments can cause diverse and often contrary effects.

In general elevated HA production by cells can promote oncogenic characteristics leading to increased tumor growth and metastasis, while reduction in HA production inhibit these processes. Variance can also occur due to deviations in HA turnover that produces low molecular weight fragments that can induce angiogenesis, as studied extensively by Professor Mark Slevin (Gaffney et al., 2009; Slevin, Kumar, & Gaffney, 2002), but detailed understanding of HA turnover and its effects on cancer cell behavior remain unclear (Toole et al., 2008).

1.1.3.3 HA-CD44-targeted therapies

HA and the entire complex system associated to its synthesis, binding and degradation offers a variety of targets for cancer therapy. Both CD44 and HA are expressed in normal tissues, not only in the tumor microenvironment, but carrier molecules extravasate and localize primarily into tumor tissue.

Strategies for HA-CD44-targeted cancer therapy include:

- Targeting drugs to CD44
- Targeting drugs to ECM HA
- Interfering with matrix HA-CD44 interactions
- Interfering with HA synthesizing or degrading enzymes

Antibody-based anticancer therapies rely on overexpression of the epitope on the target cells and the access of the carrier into the tumor tissue is facilitated by the enhanced permeability and retention (EPR) effect that results from the abnormal, leaky vasculature of the tumor compared to normal tissue. The lack of lymphatic clearance further favors localization of carriers in the tumor. Various CD44-antibodies conjugated to cytotoxic agents (for cancer therapy) and radioisotopes (for cancer detection) have reached clinical trials. Some of these anti-CD44 conjugates have shown promising results, but some have resulted in dose-limiting toxicity (Colnot et al., 2002, 2003; Rupp et al., 2007).

HA is a water soluble polysaccharide with various functional groups for conjugation, features required from a successful drug carrier. Anticancer agent-loaded HA-carriers have been widely studied *in vitro* and they show both CD44-specific uptake by cancer cells and anticancer effect (Platt & Szoka, 2008).

Professor Bryan P. Toole, one of the most respected authorities on HA, has conducted extensive research on oHA, showing that these oligosaccharides can interfere with matrix HA-CD44 interactions, inhibiting tumorigenic behavior of cancer cells. His studies have also shown that disrupting the CD44-HA interaction by oHA can even

suppress drug resistance and that oHA is a noteworthy candidate in fighting cancer (Slomiany et al., 2009a, 2009b).

Yet another target for HA-focused therapy are the HA synthases, overexpressed in many highly malignant cells. Inhibition of HAS1, HAS2 and HAS3 has been shown to decrease tumor cell growth and affect motility *in vitro* and *in vivo* (Teng et al., 2011; Wang et al., 2013). These studies prove that HASs may be valuable potential targets for anticancer therapy.

There is also evidence that HA degrading enzymes, HYALs, can act as tumor suppressors; their overexpression leads to reduction of tumorigenicity and HYAL administration *in vivo* has resulted in decreased tumor volumes (Shuster et al., 2002). On the other hand, data contrary to HYALs exhibiting tumor suppressing effects exists (Bouga et al., 2010; Franzmann et al., 2003; Tan et al., 2011). HYALs have been found overexpressed in many cancers. Their knockdown can result in decreased cell malignancy while forced overexpression can promote tumor growth. These opposite results suggest HYALs to have roles as both tumor suppressors and promoters. This dual role of HYALs seems to be a concentration-dependent phenomenon, naturally occurring levels in tumor environment acting as a promoter and exceeding levels causing tumor suppression (Karbownik & Nowak, 2013).

Studies have shown that HA can be used to target tissue microenvironments, such as those of a tumor, where an increase in HA synthesis, cellular uptake and metabolism occur. HA coupled to a variety of imaging contrast agents targeted sites of elevated HA metabolism, which shows that HA-based imaging probes could be used as diagnostic as well as therapeutic tools (Veiseh et al., 2012).

Conventional cancer therapy is starting to develop towards personalized medicine that exploits various cancer biomarkers. Special interest is directed to targeted therapies. This approach still requires validation of therapy targets, but there are already various that have been extensively studied, such as HA and the complex system associated to its synthesis and catabolism.

1.2 Nanomaterials in biomedicine

Nanomaterial (NM) – as defined by the European Comission Recommendation in 2011 – is a *natural, incidental or manufactured material containing particles of which one or more dimensions is in the size range of 1 nm - 100 nm*. Various national and international standardization bodies, organizations and authorities have pursued on developing a definition for nanomaterials, but many of the released non-normative definitions can be conflicting and we still lack a comprehensive global or an agreed EU definition.

Despite the controversy of the correct nanomaterial definition, during the recent years there has been a rapid growth in the number of products containing nanomaterials, introduced to the market in different sectors, such as the pharmaceutical, biotechnology and energy among others (Lövestam, 2010).

Engineered nanomaterials consist of various different materials, shapes and sizes. At nanoscale, their physical, chemical and biological properties can differ greatly from the corresponding bulk material. These unique size-dependent characteristics make NM very attractive for biomedical applications. Besides size, properties that contribute to NM activity include shape, hydrophobicity and electronic configuration. NM can also be easily derivatized through surface modifications to further adjust them to serve their purpose in pharmaceutical applications (Liang et al., 2008).

Nanomedicine uses nanosized tools for the prevention, diagnosis and treatment of disease. Nanomedicine aims to achieve medical benefit and to improve quality-of-life through monitoring, control, construction, repair, defense and improvement of human biological systems, as defined by the European Science Foundation's (ESF) Forward Look in Nanomedicine in 2005. The opportunities that nanomedicine offers are improved diagnostics, biosensors and imaging agents on molecular as well as *in vivo* level, and new advanced therapeutics and technologies for disease and tissue regeneration and repair (ESF Forward Look on *Nanomedicine* 2005).

Nanomedicine is a relatively young concept, even though medical applications of colloids have a long history. The birth of the nanomedicines on the second half of the 20th century was enabled by the discovery of synthetic polymer chemistry a few decades earlier. The pioneers of nanomaterials include Faraday and his studies with colloidal gold in the 19th century and Mechnikov and Ehrlich who received the Nobel Prize in 1908 for their work on phagocytosis and cell-targeted therapies. The main classes of nanomedicines today in the market or clinical development include liposomes, polymer conjugates, block copolymer micelles, dendrimers, nanocrystals, nanoparticles (NPs) and nanocapsules, that can act as drug carriers, imaging agents or have therapeutic activity on their own (Figure 12). Emerging nanomedicines encompass fullerenes, carbon nanotubes, metallic NPs, metal oxides, quantum dots and silicone-based NPs. New innovative nanomedicines arise from rational design and require the coordination of various different disciplines, such as chemists, biologists, pharmacologists, toxicologists and clinicians (Duncan & Gaspar, 2011).

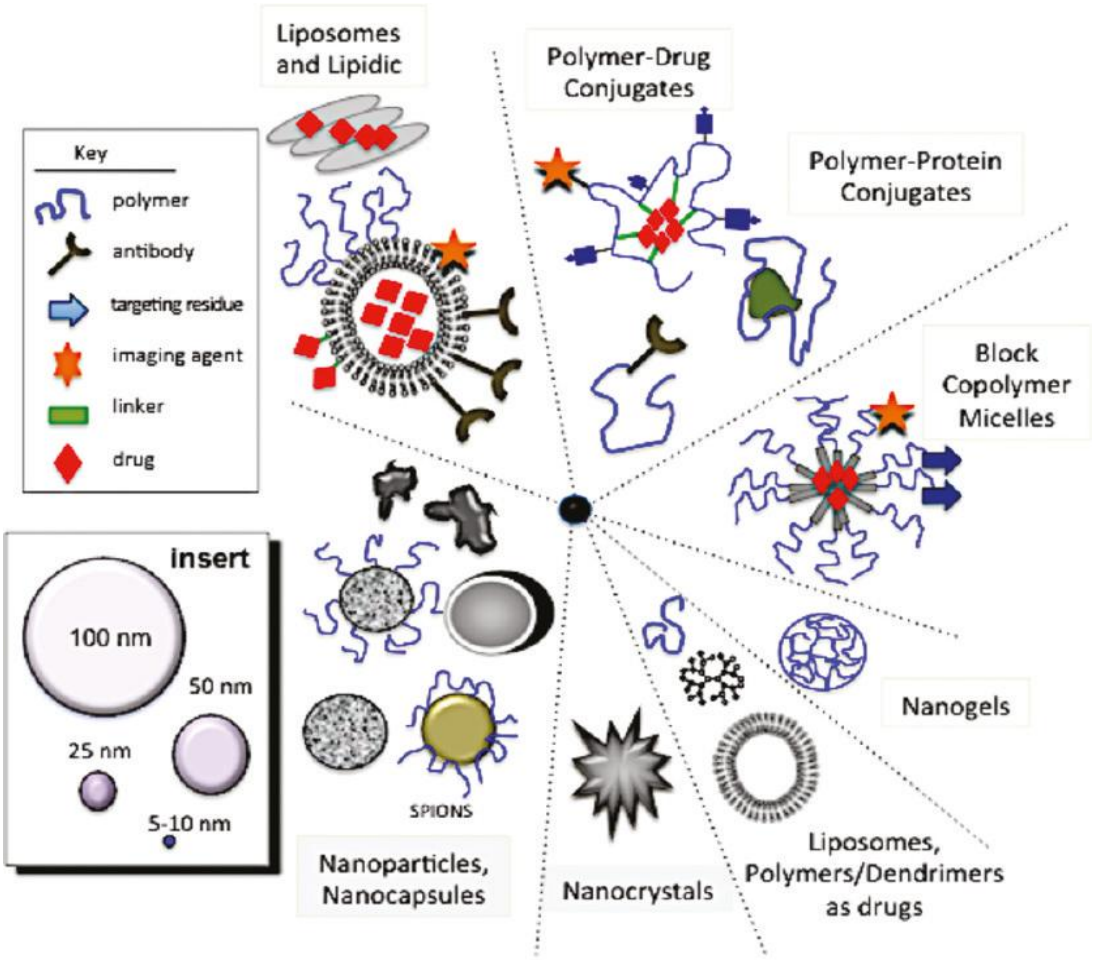

Figure 12. Main classes of nanomedicines in clinical trials or clinical use. Source: Duncan & Gaspar, 2011.

1.2.1 Cancer nanomedicine

Nanomaterials offer new strategies to diagnoe and treate cancer owing to their unique properties. Their multiple promising characteristics make them a desirable target for investigation in cancer biomedicine. NMs can be localized and detected in specific sites of diseases. Due to their small size they can evade clearance through the kidneys and exploit the EPR effect. The blood circulation time of NMs can be increased by modifying their size, composition and surface coating. Besides, the high surface-area-to-volume ratio of NMs results in a high loading capacity of ligands such as imaging and therapeutic agents (Wang et al., 2012).

Cancer nanomedicine includes applications in imaging, diagnostics and drug delivery and NMs may be used as drugs on their own or in enhancement of the efficacy of existing drugs.

1.2.1.1 Imaging and drug delivery

The unique features of NMs make them an intriguing platform for optimized therapy. NMs possess a large surface area that permits loading substantial amounts of agents or drugs. They can be targeted to disease sites by functionalizing their surface with targeting molecules. In addition, multiple different agents can be integrated on the NM surface creating multifunctional platforms. Besides, NM blood circulation time can be enhanced and escape from the mononuclear phagocyte system (MPS) ensured by modifying their size and surface. All these advantageous properties make NMs attractive for drug delivery as well as biomedical imaging (Lee et al., 2012).

NMs can reach tumors in two ways; through passive or active targeting, that can be improved by optimizing size and surface characteristics. Passive targeting exploits the EPR effect to achieve tumor accumulation while active targeting reaches the tumor owing to NM surface-integrated ligands for cell surface receptors. Probably the most utilized surface coating for passive targeting is polyethyleneglycol (PEG), which decreases blood protein interactions and increases stability. The coating for actively targeting NMs can vary from antibodies to nucleic acid ligands (Sultana et al., 2013). Specific tumor characteristics, such as genetic expression patterns, altered protein expression, uncontrolled growth, invasion and tumor microenvironment can be targeted and exploited (Shin et al., 2013).

The most innovative NMs do not function only as imaging or therapeutic agents, but are combinations of these two, acting simultaneously as therapeutic and diagnostic tools, known as theranostics. These theranostic applications can exploit among others gold NPs or quantum dots, that can be optically imaged without any modifications, and allow a high drug load. Besides, NMs that do not possess the optical features for imaging can be functionalized using fluorescent ligands among others (Doane & Burda, 2012).

Theranostic nanoplatforms hold great promise of developing cancer therapy towards personalized medicine. Imaging probes combined with therapeutic NMs or NM-based drug delivery systems are expected to simultaneously diagnose, deliver drugs and monitor therapeutic effect (Kelkar & Reineke, 2011). However, theranostic NMs have not yet reached clinical settings: safety and efficacy still need great attention.

1.2.1.2 *In vitro* diagnostics

The unique electrical, magnetic, luminescent and catalytic properties of various different NMs can be exploited in diagnostic devices. NMs can improve sensitivity and enable measurement of previously undetectable analytes. They can be used to analyze complex media samples (e.g. blood and urine) in user friendly assays reducing sample preparation and long read-out times. NM use in diagnostic assays can lead to device miniaturization and thus reduction of production costs. NM-based diagnostic devices can also allow multiple signal detection simultaneously, which can improve detection of complex diseases, such as cancer (Kurkina & Balasubramanian, 2012; Minelli et al., 2010; Shinde et al., 2012).

Inorganic metallic NPs are a class of nanomaterials that has been widely employed by *in vitro* cancer diagnostics due to their plasmon surface resonance and magnetic, photothermal and optical properties. Metallic NP-based strategies in cancer diagnostics include detection of enzyme activity, SNPs (single nucleotide polymorphisms) and tumor-related antigens. An example of a successful clinical application of NP-based diagnostic tool is an FDA-approved technology (Mirkin group, commercialized with the Verigene system from Nanosphere, Inc.) that utilizes magnetic and gold nanoparticles in a sandwich assay for multiplex detection of cancer markers. Briefly, antibody-functionalized magnetic microparticles (MMPs) are incubated with sample. Antibody- and ssDNA-functionalized gold NP-probes are added to MMPs and MMP-target-gold sandwiches are formed and separated from unbound gold with a magnetic field. ssDNA is then released from the gold NPs and this barcode DNA that corresponds to specific antibodies on the NP surfaces is analyzed by DNA array (Minelli et al., 2010).

1.2.1.3 Drugs and therapy

NMs used in medicine most often have an enabling function, i.e. they are used to enhance the characteristics of a traditional drug. However, there are NMs that convey the therapeutic effect themselves. These NMs have unique medical effects compared to conventional small molecule drugs due to their structure. An example of a therapeutic nanomedicine is NP-based magnetic hyperthermia developed by Magforce, to treat cancer. This treatment uses magnetic nanoparticles that are injected into the tumor and subjected to a magnetic field that causes the NPs to oscillate developing heat that destroys the tumor cells that have internalized the NPs (Wagner et al., 2006).

In addition to hyperthermia, metallic NPs have been reported in anti-tumorigenic applications using photodynamic therapy (PDT). An existing cancer treatment that could exploit the features of metallic NPs is ionizing radiation: for example X-ray irradiated gold NPs have been shown to induce apoptosis. Because the NPs are targeted to the tumor, damage of healthy tissue by radiation and elevated temperatures can be minimized. These techniques provide noninvasive treatment possibilities against cancer (Arvizo et al., 2013).

Nanotechnology applied to medicine can enhance greatly existing cancer drugs or create new ones with superior efficacy. It can also facilitate diagnosis due to its versatility and multifunctionality. Even though nanomedicines currently constitute only a fraction of the pharmaceutical market, they have the potential to revolutionize the industry.

1.3 Gold nanoparticles

1.3.1 History of medicinal gold

Gold has a long history of therapeutic use. The late medieval alchemists introduced the concept of the "Elixir of life", a solution containing gold that had been considered a magico-religious substance since the era of classical antiquity. Variations of this potable gold however often contained no gold, since aqua regia, needed to dissolve gold, was unknown to some of the supporters of medicinal gold. Nevertheless, potable gold was claimed to have salubrious effects on the heart and one of its most famous advocates was Paracelsus. In the 17th century potable gold entered pharmacopeias and the most common method of preparation was dissolving elemental gold in aqua regia, followed by heating to remove the solvent. The 19th century saw the development of double chloride of gold: a mixture of sodium chloride and gold chloride that was used to treat syphilis in a pill form. Double chloride injections were also used to treat alcoholism and experimented in the treatment of various incurable diseases, such as tuberculosis, diabetes and epilepsy until the 20th century. Then colloidal gold found its use in the treatment of rheumatoid arthritis and radioisotypes of gold in cancer treatment (Higby, 1982).

In eastern cultures, including China and India, the therapeutic benefits of gold preparations have been reported since 2500 BC. Today, colloidal gold is widely used in Ayurvedic medicine in India for rejuvenation and revitalization. In western medicine, intramuscularly administered gold compound, sodium aurothiomalate and orally administered auranofin are still used for treatment of rheumatoid arthritis. They act as immunomodulators, but their precise mechanisms of action remain unknown. Besides, ^{198}Au, a radioisotype of gold has been used during the 20th century as intratumoral injections to deliver large amounts of ionizing radiation into a tumor without damaging neighboring tissues due to the low penetrating ability of beta rays, the predominant radiation from ^{198}Au (Bhattacharya & Mukherjee, 2008).

1.3.2 AuNP synthesis

AuNPs can be synthesized by various methods. They can be produced by so-called "top-down" methods, such as mechanical grinding of bulk metal or using metal vapor techniques. The "bottom-up" synthesis builds NPs from smaller entities. These chemical approaches use chemical reduction of gold salts, electrochemical pathways or controlled decomposition of metastable organometallic compounds. To prevent agglomeration, a variety of stabilizing agents are used. Protection can be achieved through electrostatic stabilization, based on repulsion between particles, or steric stabilization, that uses bulky organic molecules to protect the surface of the NPs. The main classes of protective groups are:

- Polymers
- P, N and S donors (e.g. phosphanes, amines, thioethers)
- Solvents (e.g. THF, THF/MetOH)
- Long chain alcohols
- Surfactants
- Organometals (Zhou et al., 2009)

Two of the most popular methods for spherical AuNP synthesis were introduced by Turkevich in 1951 and by Brust and Schiffrin in 1994. The Turkevich method uses citrate reduction of $HAuCl_4$ in water. The size of the resulting AuNPs can be controlled by varying the proportion of the reducing agent compared to the gold salt. Besides reducing agent, citrate acts as a capping agent as well, stabilizing the NPs after synthesis. The Brust-Schiffrin method produces AuNPs of low size distribution. This method allows synthesis of AuNPs in organic solutions. It involves a reaction of $HAuCl_4$ with toluene in the presence of tetraoctylammonium bromide as the phase-transfer reagent and sodium borohydride as the reducing agent. Dodecanethiol is used as stabilizer in this reaction (Daniel & Astruc, 2004).

Besides chemical syntheses, greener biosynthetic approaches have been described. These approaches rely on bioreduction of gold salts using either cell-free extracts from

plants, micro-organisms and macrofungi, and algae, or whole organisms such as plants, mushrooms, seaweed and microbial cells (Mittal et al., 2013).

The methods described above are used for the synthesis of spherical AuNPs. Besides nanospheres, AuNPs can also be synthesized in various other forms, including nanorods (rod-shaped AuNPs), nanoshells (Au-coated e.g. silica beads) and nanocages (hollow porous AuNPs) (Figure 13) (Cai et al., 2008b).

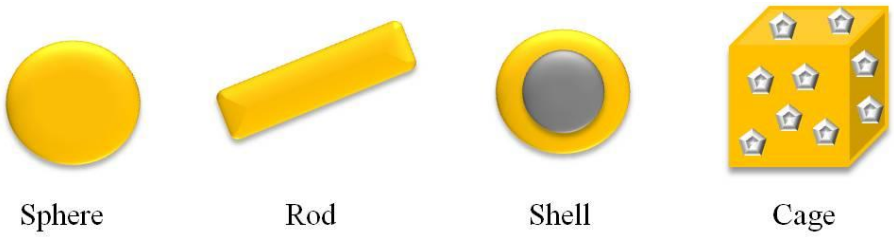

Figure 13. Different types of AuNPs. Modified from Cai et al., 2008b.

1.3.3 Properties of AuNPs

The physico-chemical properties of AuNPs depend on their size, shape, the distance between particles and their surface coating. A very interesting feature of AuNPs regarding their biomedical applications is the surface plasmon resonance (SPR). SPR is the collective oscillations of the electrons on the NP surface that match the electromagnetic field of incoming light. The SPR effect results in the deep red color of the AuNP solution and to their broad absorption band at 520 nm, when the size of the NPs is between 10 and 20 nm. The absorption band decreases when the size of the AuNPs decreases. The SPR effect also depends on the shape of the NPs, and the absorbance peak widens and shifts to blue when the NPs aggregate or agglomerate. Due to the SPR effect, AuNPs can be used in biological applications that exploit the sensitivity of the band position (Daniel & Astruc, 2004).

AuNPs absorb and scatter light. Their interactions with light can be exploited in many ways in order to visualize them by techniques such as phase contrast and differential interference contrast microscopy (direct imaging) and dark field microscopy (detecting scattered light). The color of the scattered light depends on the size and shape of the

NPs, which enables labeling with different colors. The light absorbed by the NPs leads to generation of heat, which can be detected by photothermal imaging that detects intensity fluctuations of the liquid around the NPs and by photoacoustic imaging that detects the sound wave created by heating-induced liquid expansion. AuNPs also interact with electron waves and X-rays providing high contrast in transmission electron microscopy (TEM) and X-ray imaging. Other interesting features of AuNPs are fluorescence quenching (when fluorophores are in close vicinity of the NPs), their specific Raman scattering spectrum and their capability of electron transfer (Sperling et al., 2008).

Besides possessing these unique physicochemical properties, another feature that makes AuNPs so attractive for biomedicine is the ease of modification and functionalization of the surface. The most popular AuNPs synthesis methods use thiolate ligands to stabilize the NPs, and these thiols can be easily substituted by other thiolated molecules in order to functionalize the NPs and produce surface-modified AuNPs for a variety of applications (Daniel & Astruc, 2004).

AuNPs have been confirmed biocompatible by various *in vitro* and *in vivo* studies (Bhattacharya & Mukherjee, 2008), but biocompatibility depends always on the surface modifications, that can alter the biological properties of the NPs. Functionalization of NPs with different agents finally determines how the NPs interact with their environment (Sperling & Parak, 2010). Due to the vast variety of the shapes, sizes and surface chemistry of NPs – that can all affect their fate in the body – a thorough toxicological assessment should always be conducted for AuNPs as well as other NM intended for human use.

1.3.4 Biomedical AuNP-applications in cancer

The past few decades have witnessed a growing interest in the use of inorganic NPs in biomedical research. Cancer is one of the main causes of mortality worldwide and traditional cancer therapy has its limitations. Surgery can only remove accessible tumors and chemotherapy provokes severe side effects due to lack of targeting.

Therefore nanotechnology and within it AuNPs are of high interest in the field of oncology both in diagnosis and therapy of cancer.

AuNPs have the potential to aid in the development of novel cancer nanomedicines and personalized oncology. Areas in which AuNPs have been investigated include:

- *In vitro* assays
- *In vitro* and *in vivo* imaging
- Therapy
- Drug delivery

1.3.4.1 In vitro assays

AuNPs have been reported in *in vitro* cancer diagnosis in various ways. As mentioned earlier, applications for DNA arrays have even reached the clinic. Nucleotide recognition by AuNPs can be studied by utilizing multiple techniques, such as atomic force microscopy (Jin et al., 2007), gel electrophoresis (Qin & Yung, 2007), scanometric assay (Son & Lee, 2007), SPR imaging (Li et al., 2006) and Raman spectroscopy (Cao et al., 2002) among others, due to the characteristics of AuNPs. AuNPs have also been studied in immunoassays (Liu et al., 2008), protein assays (Tang et al., 2007) and cancer cell detection when coated with different cancer-related molecules (Kah et al., 2007; Medley et al., 2008).

1.3.4.2 Imaging

AuNPs have been used for immunostaining long before the emergence of nanomedicines. Gold-labeled antibodies against the target of interest are added to fixed cell or tissue samples and gold provides excellent contrast for microscopy. AuNPs are more stable compared to fluorescence labeling and do not suffer from photobleaching. Single-particle tracking uses only a few ligand-conjugated AuNPs that bind their targets on cell surface and allow the observation of their movement on the membranes of living cells (Sperling et al., 2008).

AuNPs with controlled optical properties have been extensively studied as X-ray contrast agents. This is based on their high atomic weight compared to the surrounding tissues. Traditionally X-ray imaging using conventional contrast agents is capable of targeting specific tissues, but the facility of AuNP functionalization enables molecular imaging of tumors. Other features that give AuNPs advantage compared to the conventional contrast agent iodine are lower toxicity, osmolality and viscosity and higher blood circulation time (Ahn et al., 2013).

1.3.4.3 Therapy

AuNPs may display intrinsic antitumoral activity. AuNPs have been shown to exhibit anti-angiogenic properties, especially through inhibition of vascular endothelial growth factor (VEGF) expression – one of the main pro-angiogenic factors – by absorbing these heparin-binding proteins onto their surface and denaturizing them (Mukherjee et al., 2005). Non-functionalized AuNPs have also shown antitumoral effects *in vivo* by abrogating MAPK-signaling as well as by reversing epithelial-mesenchymal transition (EMT) through reducing the expression of EMT-related proteins (Arvizo et al., 2013).

AuNPs have the potential for non-invasive tumor treatment also through photothermal therapy (PTT). AuNPs absorb light with high efficiency in the near infrared region (NIR: 630-900 nm), where attenuation by tissues is minimal. Instead of singlet oxygen upon irradiation as the conventional photosensitizers used for photodynamic therapy (PDT), AuNPs generate heat that destroys the cancer tissue. The ease of modification by e.g. cancer cell-targeting ligands gives AuNPs an advantage as efficient candidates for PTT. Local hyperthermia results in loss of membrane integrity, DNA damage, apoptosis and even necrosis and by targeting AuNPs to cancer cells, damage to healthy tissues can be minimized. Especially gold nanorods have shown potential in photothermal therapy (Arvizo et al., 2012; Dreaden et al., 2012). An interesting example of AuNP-based cancer therapy is AUROLASE® by Nanospectra Biosciences, Inc. It consists of gold-covered silica nanoshells that accumulate in the tumor after intravenous injection due to the EPR effect. The tumor is then irradiated with a near infrared laser, and the AuNPs absorb the light converting it to heat which destroys the cancer tissue (Day et al., 2012;

Morton et al., 2010; Schwartz et al., 2011). AUROLASE® is currently in Phase 1 clinical studies for refractory head and neck cancer.

1.3.4.4 Drug delivery

Drug delivery vehicles can enhance the solubility, stability, biodistribution and pharmacokinetics of free drugs or create drug reservoirs that aim at maintaining the plasma levels constant. AuNPs possess many qualities that make them an interesting platform for drug delivery (Kumar et al., 2013).

AuNPs have been studied for the delivery of different chemotherapeutics. Paclitaxel-functionalized AuNP synthesis has been reported (Gibson et al., 2007) and 5-fluorouracil (5-FU) has been caged in AuNPs and photocontrollably released by UV-radiation (Agasti et al., 2009).

The examples above are likely to take advantage of the EPR effect to reach the tumor. For active targeting the AuNPs need to be conjugated with targeting moieties, such as antibodies or ligands for receptors expressed by cancer cells. Targeting has been studied by conjugating AuNPs for example with folic acid that targets folate receptors on the surface of rapidly proliferating cancer cells and transferrin that targets transferrin receptors on cancer cells with fast division rate. These studies have shown that functionalized AuNPs are easily internalized by cancer cells that express their target receptors and suggest better drug delivery with functionalized AuNPs compared to non-targeted (Llevot & Astruc, 2012).

A very interesting example of targeted drug delivery is CYT-6091, AuNPs conjugated to PEG (to improve blood circulation time and reduce clearance by macrophages) and to tumor necrosis factor alpha (TNF-α, a cytokine that recognizes cancer cells and causes necrosis as well). TNF-α as a free drug shows high dose-limiting toxicity, but when administered as PEG-AuNP-TNF complex, it targets tumors and can be administered systemically in higher doses. CYT-6091 was developed by CytImmune Inc. and has reached Phase 2 clinical trials (Libutti et al., 2010; Paciotti et al., 2004).

The main advantage that AuNPs offer to cancer nanomedicine is multifunctionality. Due to their unique characteristics, they can be the foundation for a variety of applications in oncology. Gold also has a long history in medical use and has been shown biocompatible and non-toxic, depending on the surface chemistry, naturally. The near future may even witness clinical applications of theranostic Au-based applications, which both monitor and treat the disease simultaneously.

OBJECTIVES

OBJECTIVES

Current systemic cancer therapies suffer from dose-limiting side effects of conventional chemotherapeutics and a lack of specific targeting to the tumor, since most cancer drugs take advantage of the EPR effect and use passive targeting to reach the tumor. Given the promise that nanotechnology holds for oncology and the recent development of cancer medicine towards personalized medicine – that takes into consideration the specific cancer biomarkers of a patient – we decided to design a tumor cell-targeting nanocarrier for the delivery of traditional chemotherapeutics.

The aim of this project has been the development and characterization of EDS (Endor Delivery System). EDS is a 2-part drug delivery system consisting of a AuNP and a targeting ligand. The gold core is coated by HA oligosaccharides which act as a targeting agent that guides the system to solid tumors, and simultaneously protect the nanosystem from rapid clearance. EDS can be further modified to carry different small molecule drugs (EDS-Drug). After reaching the tumor environment the delivery system is meant to release the chemotherapeutic drug.

The specific objectives for this thesis have been:

1. Characterization of EDS

    a. Chemical characterization to assure that the bare AuNPs resulting from the synthesis are disperse, uniform and of low size-distribution, and that conjugating the bare AuNPs to HA in order to generate EDS does not change the characteristics greatly.
    b. Biological characterization to demonstrate biocompatibility, tumor-targeting and safety of EDS.
        i. Internalization studies in cell lines expressing differing amounts of CD44 to show that EDS targets the HA receptor CD44.
        ii. Toxicity studies to study *in vitro* and *in vivo* if EDS can be safe for human use.

2. Characterization of EDS-Drug

a. Chemical characterization to assure that the addition of the drug does not change the characteristics of the nanocarrier.
b. Biological characterization to demonstrate efficacy besides tumor-targeting and safety of EDS-Drug.
    i. Internalization studies to demonstrate that the anticancer agent reaches the tumor environment and cancer cells and that CD44-targeting remains unchanged.
    ii. Toxicity studies to show that while performing its action, the drug does not cause redundant toxicity when conjugated to the nanosystem.
    iii. Efficacy studies. Efficacy *in vitro* to demonstrate that conjugation to EDS does not inhibit the drug from performing its function. *In vivo* antitumoral effect study of EDS-Drug in a mouse xenograft model in order to discover whether the effect of the drug can be enhanced with the nanocarrier.

MATERIALS AND METHODS

2. MATERIALS AND METHODS

The materials and methods section of this thesis is divided into four parts.

Part 1 consists of nanomaterial synthesis, including the synthesis of AuNPs, EDS, fluorescently labeled EDS (EDS^{fl}) and PEGNPs that were used as NP control in some of the studies. Part 1 also describes three different strategies that were used to generate the double conjugates EDS-drug, and procedures to concentrate and remove the excess of unconjugated material from the solution.

Part 2 presents the techniques used in the chemical characterization of the nanomaterials to study their shape, size, state and stability. Chemical characterization also included defining the concentrations of the different components (NPs, HA, drug) in the solutions after the purification and concentration processes following synthesis.

Part 3 describes the *in vitro* characterization of EDS and EDS-drug. This part includes basic cell culture methods, cell line characterization for CD44, toxicity, internalization and *in vitro* efficacy studies.

Part 4 focuses on the effects of EDS and EDS-Drug *in vivo*. The studies of this part consist of blood circulation time and *in vivo* efficacy studies. Biodistribution and tumor accumulation of gold and platinum were quantified and histology for CD44 expression in different tissues was performed to rationalize our findings. *In vivo* toxicity was studied besides biodistribution by monitoring animal weight and blood biochemical analysis.

2.1 Nanosystem synthesis

Nanomaterials used in this study are:

- EDS: 12 nm gold nanoparticles coated with hyaluronic acid
- EDS^{fl}: 12 nm gold nanoparticles coated with fluorescently labeled hyaluronic acid
- PEGNPs: 12 nm gold nanoparticles coated with polyethylene glycol
- EDS-L1-CIS: 12 nm gold nanoparticles coated with hyaluronic acid and linked to cisplatin through linker 1 (L1)
- EDS-Mua-CIS: 12 nm gold nanoparticles coated with hyaluronic acid and linked to cisplatin through linker 2 (Mua)
- EDS-CIS: 12 nm gold nanoparticles coated with hyaluronic acid with cisplatin encapsulated in the coating

The synthesis of each nanomaterial started with the synthesis and characterization of AuNPs, followed by conjugation to HA, HA^{fl}, PEG and/or chemotherapeutic agent. After each conjugation the excess material, that had not been conjugated, was removed in order to achieve a homogenous solution.

2.1.1 AuNP synthesis

A variety of different methods for AuNP synthesis, using different reductive agents and stabilizers, exist and they display different characteristics (size and shape) of the final products. We chose to utilize the Turkevich method – described by Turkevich in 1951 and refined by Frens in 1973 (Kimling et al., 2006) – that uses trisodium citrate ($Na_3C_6H_5O_7$: Sigma-Aldrich) as the reductive agent. Briefly, to obtain a solution of 100 ppm of gold, 150 mL dH_2O with 7,6 mM $Na_3C_6H_5O_7$ was brought to boil with agitation. 3 mL 25 mM $HAuCl_4$ (Sigma-Aldrich) was rapidly injected into the solution. The reaction was let boil for 3 min and stopped. The colour of the solution changed from clear to rich red/burgundy.

2.1.2 AuNP conjugation

An EDS molecule consists of a AuNP coated with HA. To obtain this product, the first step was thiolation of HA, followed by dialysis to eliminate excess of the reaction reagents. The resulted thiolated HA (HA-SH) was lyophilized and conjugated to AuNPs.

2.1.2.1 HA thiolation

30-50 kDa sodium hyaluronate was purchased from Contipro Group. Thiolation of HA was performed dissolving 0,35 mM sodium hyaluronate and 10,12 mM cystamine dihydrochloride (Sigma-Aldrich) in a buffer consisting of 0,1 M H_3BO_3 and 0,4 M HCl at pH 8 (Sigma-Aldrich). The solution was heated to 45 ºC with constant stirring and 0,2 M sodium cyanoborohydrate (Sigma-Aldrich) was added. The reaction was executed during 5 days in an air-free atmosphere using argon. 0,13 M D-L-dithiothreitol (DTT, Sigma-Aldrich) was added and after 1 h, dialysis was performed using 3,5 kDa membranes (Spectrum Laboratories, Inc.) in 5 L dH2O with 0,3 mM HCl and 3 g NaCl (Sigma-Aldrich). The buffer was changed three times per day and the final product was lyophilized.

2.1.2.2 AuNP-HA conjugation

225 mg of lyophilized HA-SH was added to 150 mL AuNPs (100 ppm) and the solution was stirred for 30 min. The resulting EDS solution was then filtered through PES filters with 2 µm pores.

2.1.2.3 EDS^{fl} synthesis

Gold nanoparticles have been shown to quench fluorescence depending on the distance of the fluorochrome from the NP core and the maximum quenching occurs with fluorochromes emitting near the wavelength of the plasmon peak of the NPs (Reineck et

al., 2013). We conjugated the gold nanoparticles with fluorescently labeled HA using HiLyte Fluor dye that emits at 647 nm, which differs substantially from the AuNPs absorbance maximum (520 nm) to study internalization of the nanosystem with confocal microscopy.

AuNPs and HA-SH were prepared as described earlier. 10 mg of HA-SH, 2 mg of 1-ethyl-3-(3-dimethylaminopropyl)carbodiimide (EDC) and 1 mg of Hylite 647 fluorophore (Anaspec) were dissolved in 3 mL of PBS and stirred for 2 hours. The solution was dialyzed with 3,5 kDa membranes for 24 h to remove the excess of reagents and lyophilized. The resulting HA-SH^{fl} was conjugated AuNPs as described earlier with HA-SH to produce the fluorescently labeled EDS: EDS^{fl}.

2.1.2.4 PEGNP synthesis

Bare gold nanoparticles could not be used as a control in the biological studies due to agglomeration in biological media. In some of the experiments, we found it necessary to include a nanoparticle control; PEG (polyethylene glycol) -coated gold NPs were used since they have been proven to be stable and biocompatible. PEG is probably the most used coating to render different types of NPs biocompatible and it is widely used in the pharmaceutical industry to slow clearance of various pharmaceutical agents (Fishburn, 2008), but it may also negatively influence the nanoparticle drug carrier performance. The disadvantages of PEG-coating include interference with NP-cell interactions and immune reactions to pegylated NPs (Amoozgar & Yeo, 2012).

AuNPs were synthesized as described earlier. 200 mg PEG (*O*-[2-(3-Mercaptopropionylamino)ethyl]-*O′*-methylpolyethylene glycol; Sigma-Aldrich) was added to 133,3 mL of AuNPs (100 ppm) and left to react for 30 min.

2.1.3 EDS-CIS conjugation

Different approaches to conjugate the drug to the nanosystem were explored in the development process of the nanosystem-drug double conjugates. Three different strategies were tested:

A. EDS+ L1 + Cis (Linker 1)

B. EDS + Mua + Cis (Linker 2)

C. EDS + CIS (drugs encapsulated into the HA coating of the nanoparticles)

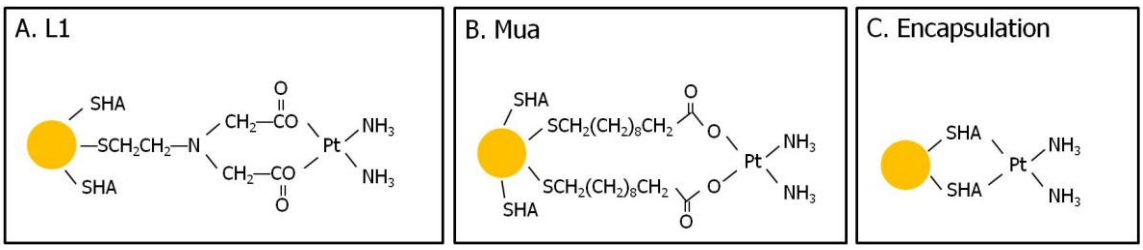

Figure 14. Linking strategies A, B and C for conjugating the drug to the nanocarrier.

Different concentrations of the drugs were tested in the double conjugate synthesis to determine the most effective synthesis approach in order to achieve the highest drug load for the nanocarrier. Cisplatin for the studies was purchased from Sigma-Aldrich.

2.1.3.1 L1

To synthesize linker L1, we mixed 2,25g cystamine hydrochloride in 200 mL EtOH and 20 mL triethylamine with 6,6 mL ethyl bromoacetate and 1,04 mg potassium iodide (all reagents from Sigma-Aldrich). After 6h in agitation at RT, the solution was filtered to remove the insoluble reagents. The filtered solution was concentrated by a rotary evaporator and subjected to flash chromatography (1:1 CH_2Cl_2:EtOAc).

To remove the carboxyl group (and to enable conjugations to cisplatin) the resulting product from flash chromatography was dissolved in MetOH (10 mL Sigma-Aldrich) and NaOH (5 mL Sigma-Aldrich) overnight with agitation. 5 mL of dH_2O was added

and the pH was adjusted to 3. In low temperature L1 precipitated, and was washed with EtOH/H_2O.

To synthesize EDS-L1-CIS, 322 ppm AuNP solution was conjugated with 0,4 mM L1 in MetOH for 4h with constant agitation. The pH was adjusted to 10 and 825 μM cisplatin and 12,5 μM HA-SH were added. To synthesize EDS-L1-Cis with a lower drug load, 4,9 μM L1 and 9,95 μM Cis were used.

2.1.3.2 Mua

322 ppm AuNP solution was conjugated to 1,65 mM of the ligand Mua (Sigma-Aldrich) during 4h with constant agitation. The pH of the solution was adjusted to 10 and 825 μM cisplatin and 12,5 μM HA-SH were added. To synthesize EDS-Mua-Cis with a lower drug load, 2 μM Mua and 9,95 μM Cis were used.

2.1.3.3 Encapsulation

EDS was prepared as described earlier. To a solution of 100 ppm AuNPs 20, 500 or 2000 μM cisplatin was added. The solution was stirred overnight at 40 ºC. The resulting EDS-Cis was concentrated to a theoretical concentration of 1000 ppm Au and 200, 5000 or 20 000 μM Cis after purification. Final concentrations were determined by ICP-MS.

2.1.4 Purification and concentration of NM

In order to be sure that the EDS, EDS^{fl}, PEGNP and EDS-drug solutions did not contain an excess of unconjugated HA, fluorophore, PEG or drug (respectively), we purified them using the Stirred Cell (Millipore) that applies pressure for macromolecule concentration.

After conjugation, non-conjugated HA, PEG and drug excess was removed from the double conjugate solution carefully through cellulose ultrafiltration membranes with

pore sizes of 100 kDa (Millipore) that allow the free HA, PEG and drug to pass, but prevent conjugated nanosystems from passing. Every 150 mL of nanosystems was washed with 1 L dH_2O and finally concentrated to a volume of 15 mL resulting in a concentration of 1000 ppm of Au. In some experiments EDS was concentrated up to a concentration of 3200 ppm.

2.2 Chemical characterization of the nanosystems

2.2.1 TEM

Transmission electron microscopy (TEM) is based on a beam of electrons passing through an ultra-thin sample in a vacuum and an image is formed from the interactions of the electrons with the sample. Depending on the density of the sample, electrons pass through or are scattered and disappear from the beam. The unscattered electrons hit a fluorescent screen and an image of the sample is formed. Samples with high electron density, such as AuNPs, can be directly detected by TEM, while organic samples need to be previously processed.

10 µl of NPs was placed on a copper grid (formvar coated 200-mesh copper grid, Ted Pella, INC.) and air-dried. The NPs were visualized by JEOL 1010 of the CCiTUB, at 80 kv with A CCD Megaview III camera and the image acquisition software AnalySIS. From each sample 200 NPs were measured for size-distribution analysis by ImageJ.

2.2.2 DLS

Dynamic light scattering (DLS) can measure the mean size (hydrodynamic diameter) not only of the NP core, but also the organic coating that envelops the particles. Besides the diameter of the sample, DLS provides information about its dispersity. DLS measures the time-dependent fluctuation (the Brownian motion) in the scattering intensity of a monochromatic laser light directed to the sample suspension.

NP-samples were analyzed in plastic cuvettes (BrandTech Scientific, Inc.) with an optical path length of 1 cm. The DLS analysis was performed using Malvern Nano ZS Zetasizer (Malvern Instrument) at 532 nm wavelength with a fixed-angle dispersion of 173º.

2.2.3 Z-potential

Zeta potential is a tool used for determining the state of NP surface and predicting the stability of the NP solution. NPs exhibit a surface charge that gathers a thin layer of ions with an opposite charge to the NP surface. Zeta potential is the electric potential at the boundary of this double layer. NPs with values between -25 and +25 mV are usually considered to show instability and values from -100 to -25 and from +25 to +100 stable.

Zeta potential was measured Malvern Nano ZS Zetasizer (Malvern Instrument) using U-shaped capillary cuvettes (Disposable capillary cell, Malvern Instrument).

2.2.4 ICP-MS for Au & Pt quantification

Inductively-coupled plasma mass spectrometry (ICP-MS) is capable of detecting metals at concentrations as low as one part in 10^{12} by ionizing the sample and then using a mass spectrometer to separate and quantify these ions. Besides quantifying the amount of gold in solutions, ICP-MS can be used to detect and quantify AuNPs in cells and animal tissues with a previous digesting process. We employed ICP-MS to quantify the amounts of Au (and Pt) in the solutions of AuNP, EDS, PEGNPs and EDS-drug in:

- Solutions resulting from synthesis (batch characterization)
- Solutions used in *in vitro* and *in vivo* studies
- Cell pellets to study NP internalization
- Blood/plasma of animals after injection
- Various organs of animals after injection

The amount of gold in solution was analyzed by ICP-MS and knowing the weight of one single nanoparticle, the number of NPs was calculated with the following formula:

$$\text{Nº NPs} = V_{Au}/V_{NP} = (\text{mass}_{Au}/\delta_{Au})/(\pi * D^3/6)$$

To determine the Au and/or Pt concentration in organic solutions and tissues, the samples were digested with nitric acid and hydrochloric acid (some samples required also H_2O_2), which together form aqua regia to degrade the organic material in the sample. Digestion was performed overnight at 90 ºC. After digestion, samples were made up to a defined volume with thiourea (Sigma-Aldrich) in 1 % HCl (depending on sample weight). The ICP-MS analysis was performed by the CCiTUB using a PerkinElmer Optima 3200RL ICP-MS (Waltham, MS) in standard conditions. HNO_3, H_2O_2 and HCl used in digestion for ICP-MS analysis were Instra-analyzed grade (Baker) and Supra-analyzed grade (Merck).

The organs were weighed at the moment of extraction, and the fraction subjected to ICP-MS was weighed again. The amount of Au/Pt in the fraction was normalized to the weight of the extracted organ to correspond to accumulation in the whole organ. To study accumulation in the whole skin level of the animal, we used the following formula to determine the whole skin area (cm^2):

$$10{,}5 * \text{weight (g)} * 2/3$$

The area of the skin fraction subjected to ICP-MS analysis was measured upon extraction and the accumulation of Au/Pt was normalized to account to the quantity in the whole skin.

2.2.5 EA

Elemental analysis (EA) quantifies the amount (typically a weight percent) of an element in a compound, most commonly carbon, hydrogen, nitrogen and sulphur. The combustion of the sample with an excess of oxygen results in products such as CO_2, H_2O and N_2 that are collected by traps using He through a reduction tube and separated by using thermal conductivity. EA was used to quantify the amount of HA in EDS after synthesis followed by purification.

Samples were lyophilized prior to analysis. The analysis was performed by the CCiTUB using an organic element analyzer Thermo EA 1108 (Thermo Scientific) in standard conditions recommended by the manufacturer (helium flux at 120 ml/min, combustion oven at 1000 ºC, chromatographic column oven at 60 ºC, oxygen inside the loop: 10 ml, 100 kPa). Thermo EA Flash 2000 (Thermo Scientific) analyzer was also employed (helium flux at 140 ml/min, combustion oven at 950 º C, chromatographic column oven at 65 º C, oxygen inside the loop: 10 ml, 250 kPa).

All the HA chains are expected to be conjugated to the surface of NPs, so furthermore we were able to calculate the number of HA chains per NP using the data from ICP-MS analysis (Au quantity) and the calculated number of AuNPs in solution.

2.2.6 Stability studies

2.2.6.1 Visual examination

Aggregation of gold nanoparticles in solution is easily visualized by naked eye due to color change from rich red to blue. The surface plasmon resonance (SPR) of gold NPs of size up to 20 nm causes absorption of light in the blue-green spectrum while red is reflected, yielding in a red color. As particle size increases, e.g. due to aggregation, the wavelength of surface plasmon resonance related to absorption shifts to longer wavelengths, resulting in absorption of red light and reflection of blue. This phenomenon yields in blue/purple color (Figure 15).

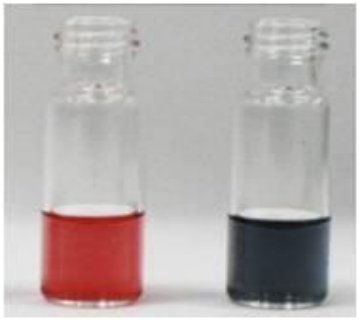

Figure 15. Stable (left) and aggregated (right) AuNPs.

Bare AuNPs and EDS were diluted in a saline solution (PBS) 1:1 and the color change from red to blue was inspected visually.

2.2.6.2 UV-VIS

The phenomenon of SPR shifting when AuNPs aggregate can be examined by using ultraviolet-visible spectroscopy besides visual inspection. The characteristic absorbance peak shifts to the right and widens according to the degree of aggregation of the AuNPs.

The spectra of AuNPs and EDS in synthesis solution and in PBS were measured with the spectrophotometer Biotek PowerWave XS using Gen5 software. Readings were executed using 96-well plates and the minimum volume of 150 µl of the nanomaterials.

2.3 *In vitro*-characterization of the nanosystems

2.3.1 Cell line characterization

In order to demonstrate that our nanocarrier targets CD44, we needed to study the responses of cells with varying expression levels of the receptor to EDS. For this we started the *in vitro* studies by examining the expression levels of the receptor in various cancer cell lines established from different cancer tissues.

CD44 levels in various cell lines were examined by quantitative real-time PCR (RNA level), western blot (membrane-bound and intracellular protein) and FACS (membrane-bound protein) analysis. Western blot was also employed to study levels of CD44 and RHAMM down regulation after siRNA-treatments.

2.3.1.1 Cell culture

Cells were routinely cultured in DMEM (Lonza) supplemented with 10 % FBS, 100 units penicillin/ml, 100 ug streptomycin/ ml, and an additional 2 mM glutamine (Lonza). The cell lines were kept in a humidified incubator at 37 °C, 5 % CO2 and passed every 3-4 days. In most studies the cell culture medium used was free of phenol red in order to be able to monitor possible aggregation of the nanoparticles. Used cell lines were are listed in Table 2.

Name	Description
A549	Human epithelial lung carcinoma
BxPC3	Human epithelial pancreatic adenocarcinoma
HCT116	Human epithelial colorectal carcinoma
HEPG2	Human hepatocellular carcinoma
HT1080	Human epithelial fibrosarcoma
HT29	Human epithelial colorectal adenocarcinoma
MCF-7	Human epithelial breast adenocarcinoma
MDA231	Human epithelial breast adenocarcinoma
OVCAR-3	Human epithelial ovarian adenocarcinoma
Panc-1	Human epithelial pancreatic ductal carcinoma

Table 2. Cell lines used in this study.

Cells were routinely tested for mycoplasma using the EZ-PCR Mycoplasma Test Kit (Biological Industries).

2.3.1.2 Cell line characterization by qPCR

Gene expression of the main receptor (CD44) for hyaluronic acid was examined on RNA-level by quantititative real-time PCR. Cells were seeded on 6-well plates and let reach 80 % confluency. Cells were then washed with PBS and scraped in Tri Reagent (Sigma-Aldrich). Total RNA was extracted according to the manufacturer's instructions and quantified using a NanoDrop ND-1000 spectrophotometer (Thermo Scientific). 1,5 µg of total RNA from each sample was converted into cDNA with High Capacity cDNA Reverse Transcription kit (Applied Biosystems) and cDNA was used for quantitative real-time PCR performed using TaqMan® assays from Applied Biosystems. Assays included CD44 and 18S as an internal control (Table 3: used assays, Table 4: cycling conditions). Data was analyzed in terms of cycle threshold number (C(T)) and normalized relative to endogenous 18S rRNA.

Assay	Amplicon length	Catalog number
CD44	70 bp	Hs01075861_m1
18S	187 bp	Hs99999901_s1

Table 3. TaqMan® assays used in cell line characterization.

Step	Conditions	Cycle repeats
UDG incubation	2 min; 50ºC	Hold
Enzyme activation	10 min; 95ºC	Hold
Denaturation	15 s; 95ºC	40 cycles
Annealing / Extension	1 min; 60ºC	

Table 4. Cycling conditions for qPCR.

2.3.1.3 Cell line characterization by Western blot

Western blotting to detect CD44 and RHAMM levels in cell lines on protein level was performed with a SDS-PAGE Electrophoresis System under reducing conditions. 80% confluent cells were solubilized in RIPA buffer (Sigma-Aldrich) that included protease and phosphatase inhibitors (Sigma-Aldrich). Total protein in the lysates was quantified by BCA Protein Assay kit (Thermo Scientific Pierce) and 50 µg of total protein was denaturalized by heating to 95ºC for 5 min in reducing conditions (with β-mercaptoethanol). Lysates were then electrophoresed on 7,5 % acryl amide gel with Tris running buffer and protein bands were transferred to nitrocellulose membrane. The expression of CD44 (and RHAMM for siRNA-internalization studies) was identified by using specific antibodies (Table 5). Membranes were blocked with 5 % milk in TBS-tween (0,05%) in RT for 1h; probed with primary antibodies in blocking buffer O/N at 4°C; washed and exposed to secondary HRP-conjugated antibodies in blocking buffer at RT for 1h. Protein bands were detected through autoradiography using enhanced chemiluminescence ECL Western Blotting Substrate (Thermo Scientific Pierce). β-actin was used as a protein loading control.

Antibody	Host species	Dilution	Supplier
anti-CD44	Mouse	1:1000	Cell Signaling Technology
anti-RHAMM	Rabbit	1:1000	Epitomics
anti-β-actin	Mouse	1:10 000	Abcam
anti-mouse	Goat	1:1000	Abcam
anti-rabbit	Goat	1:1000	Abcam

Table 5. Antibodies used for WB.

2.3.1.4 Cell line characterization by flow cytometry

Cells were trypsinized and counted. 1 x 10^5 cells were incubated with PE-Cy™5 Rat Anti-Mouse CD44 (0,4 ug / 1 x 10^5 cells, BD Biosciences) in PBS-BSA (2%), shaking in the dark, RT, for 1h, in the presence of 20% fetal bovine serum. Cells were washed by centrifugation at 1500 rpm for 5 min and resuspended in PBS-BSA (2%) and DAPI stained to exclude dead cells. The cells were analyzed using Gallios Flow Cytometer (Beckman Coulter). Data collected from the experiments were analyzed using Gallios 1.2 (analysis software from Beckman Coulter).

2.3.2 Internalization studies

After studying the expression levels of CD44 in different cell lines, we started EDS and EDS-CIS uptake studies. We chose cell lines that express different levels of CD44 (Panc-1: high; MDA231: intermediate; MCF-7: low; HEPG2: not detected), exposed them to the nanosystems and quantified the amount of gold inside the cells, visually by TEM and immunofluorescence (IF) quantitatively by ICP-MS. We also studied internalization in a highly expressing cell line (Panc-1) with down regulated expression achieved by siRNA transfections.

2.3.2.1 TEM for cells

TEM enables the resolution and visualization of details that are not covered by optical microscopy; tissues, cells and microorganisms can be studied ultrastructurally. TEM

can be employed in studying the morphology of cells and organelles and to characterize viruses and bacteria. Since TEM works in vacuum and biological samples contain large quantities of water, they must be dehydrated while preserving the structure with different fixatives. After this, the specimen is embedded in resin that polymerizes into a hard solid block and cut into thin sections before placing it into a copper grid and heavy metal staining. Then the samples can be studied under the electron beam of the microscope.

MDA231 were seeded on 60 mm plates, 200 000 cells/plate and let grow for 48h. Cells were then treated with 100 ppm EDS for 3 and 24 h. When time points were reached, cells were incubated twice with fixing solution (30 min, agitation, on ice). 1/3 of the fixing solution was removed and cells were carefully collected by scraping. Cells were pelleted, washed and stored at 4 ºC until post-fixation. Post-fixation was performed with OsO_4 (Sigma-Aldrich) solution carefully not disrupting the pellet, in the dark, on ice for 2h. Pellets were then washed repeatedly with dH_2O and dehydrated in increasing concentrations of acetone (Table 6).

Acetone %	Time	Nº changes
50%	10 min	1
70%	10 min	2
90%	10 min	3
96%	10 min	3
100%	15 min	3

Table 6. Dehydration procedure of post-fixed cells for TEM analysis.

After dehydration, the cells were embedded in resin using dilutions of EPON (Sigma-Aldrich) mixes (Table 7) at RT. Finally cells were embedded in embedding moulds containing fresh resin and polymerized at 60 ºC for 24h. The sectioning, heavy metal staining and grid preparation were executed by the CCiTUB.

Solution	Dilution	Time
EPON 1/acetone	1/3	1h
EPON 1/acetone	1/1	1h
EPON 1/acetone	3/1	1h
EPON 1	-	2h to O/N
EPON 1	-	O/N (or 5h if last incubation was O/N)
EPON 2	-	2h to O/N
EPON 2	-	2h

Table 7. Resin embedding procedure of dehydrated cells for TEM analysis.

The NPs internalized by MDA231 were visualized by JEOL 1010 microscope of the CCiTUB, at 80 kV with A CCD Megaview III camera and the image acquisition software AnalySIS.

2.3.2.2 Immunofluorescence

We used immunofluorescence to study the internalization of EDS, conjugating AuNPs with fluorescently labeled HA, this way permitting visualization of the internalized HA, since the NP internalization had already been executed by TEM. Cell lines with differing CD44 expression levels were treated with this EDS^{fl}, and before visualizing the intracellular fluorescent signal, cells were fluorescently stained with anti-CD44 to reveal the cell surface receptor.

MCF-7, MDA231 and Panc-1 were seeded on sterile glass coverslips on 6-well plates (200 000 cells/well) and let attach and grow until the following day. Cells were treated with 100 ppm EDS^{fl} for 24h. Coverslips were then fixed with 10% formalin for 15 min (Sigma-Aldrich). The samples were then washed with PBS and blocked with 1% BSA (Sigma-Aldrich) in PBS for 30 min. Coverslips were then incubated with anti-CD44 (Cell Signaling Technology) in the blocking solution in a humidified chamber at RT for 1h, followed by incubation with FITC-conjugated anti-mouse IgG (Sigma-Aldrich) for 1h in the dark. Cells on coverslips were counterstained with 1 ug/ml DAPI (Sigma-Aldrich) in PBS and mounted on glass slides with DPX mounting medium (Sigma-Aldrich). Slides were analyzed by Leica AF7000 confocal microscope.

2.3.2.3 Internalization by ICP-MS

Panc-1 (100 000 cells/well) and HEPG2 (300 000 cells/well) were seeded on 6-well plates and let grow for 48 hours. Cells were treated with EDS (100 ppm) or EDS (18,9 ppm) and EDS-CIS (172 μM CIS, 18,9 ppm Au) for 24 h. Cells were washed four times with 0,01 % TWEEN-PBS in order to remove NPs attached on the cell surface. Cells were then collected by careful scraping, and pelleted by centrifugation. Pellets were stored at -80˚C until ICP-MS analysis. The quantity of Au/Pt was normalized to the number of cells; two wells of each treatment were counted at the moment of collecting the cells.

2.3.2.4 siRNA transfection and ICP-MS

Besides detecting NPs in cell lines expressing differing levels of CD44, we considered it essential to study their uptake in cells, where naturally occurring CD44 expression has been knocked down. The silencing was executed by small interfering RNA (siRNA), short sequences of double stranded RNA that bind to and promote the degradation of mRNA at specific sequences and in doing so, prevent the production of the corresponding proteins.

Panc-1 were transfected with the Cell Line Nucleofector® Kit R (Lonza) according to the manufacturer's protocol. Shortly, cells were trypsinized and 1 x 10^6 cells were pelleted and resuspended in 100 μl room-temperature Nucleofector® Solution. Cell suspension was combined with 60 nM Silencer® Select siRNA (Table 8) and subjected to Program X-005 (Nucleofector® Device 2, Lonza). Transfected cells were moved onto 6-well plates (1 x 10^6 cells divided into three wells). Cells were incubated at 37˚C for 48 hours, treated with EDS (100 ppm) or EDS (18,9 ppm) and EDS-CIS (172 μM Cis, 18,9 ppm Au) for 30 minutes. Cells were washed four times with 0,01 % TWEEN-PBS in order to remove NPs attached on the cell surface. Cells were then collected by careful scraping, and pelleted. Pellets were stored at -80˚C until ICP-MS analysis.

Non-transfected cells were used as controls and cells were counted from two wells of the non-transfected and each siRNA-transfected cells in order to normalize gold

accumulation to cell number. Transfection efficiency was verified by western blot before analyzing the cell pellets by ICP-MS.

Target	Cat. Nº	Supplier
Non-target	4390846	Ambion
CD44	4390824, ID: s2682	Ambion
RHAMM	4390824, ID: s6672	Ambion

Table 8. siRNAs used in EDS internalization sudies.

2.3.3 Toxicity studies

2.3.3.1 Cell viability assays & IC50

In vitro cytotoxicity testing is commonly used in defining the toxicological profile of chemicals and pharmaceuticals. Compared to animal studies, it is ethically more acceptable and less expensive to conduct. Cellular testing is also easier to control and reproduce. The most employed assays for nanomaterial cytotoxicity evaluation measure toxicity by colorimetric methods. However, questions of suitability of different methods have been raised and used tests should be determined valid for the materials being tested (Lewinski et al., 2008).

We tested different commonly used commercially available cell viability assays while searching the most suitable assay to use with our nanosystem. The cell preparation, treatment and incubation time procedures were equal for all the assays, only incubation time with assay reagents, solubilizers/developers and wavelength for absorbance quantification changed according to the assay.

Cells were seeded on 96-well plates, 3×10^3 – 11×10^3 cells/well (depending on the cell line, Table 9). Cells were let to attach and grow for a minimum of 24 hours to reach the logarithmic phase of cell growth and then nanosystems were added to each well. A dilution series of 1/4 was used, starting from theoretical 1000 ppm (Au). After 72 hours of incubation cells were visualized by light microscopy (Nikon E600) and pictures were taken. Treatment was removed and cells were washed with PBS three times. The

appropriate cell viability assay reagents, reconstituted according to manufacturer's instructions, and possible solubilizers/developers were added (Table 10). Absorbance was measured at the recommended wavelengths by the spectrophotometer Biotek PowerWave XS and relative cell viability was analyzed.

Cell line	Cells / well
A549	3000
BxPC3	9000
HEPG2	11 000
Panc-1	8000

Table 9. Number of cells seeded per well for cytotoxicity assays.

Assay	Supplier	Incubation T	Solubilizer / Developer	Absorbance
MTT	Sigma-Aldrich	3h	70% 2-propanol	570 nm
NR	Sigma-Aldrich	2 - 3h	50% EtOH / 1% acetic acid	550 nm
WST-1	Roche	30 min - 2h	-	450 & 650 nm
HEX	Sigma-Aldrich	15 min - 2h	EDTA-glycine	410 nm

Table 10. Cell viability assays used in the study.

Complete cell culture medium, to which all EDS dilutions were compared, was used as the negative control. Cytotoxicity experiments were performed with 6 parallel repeats and at least three times with all cell lines.

The nanosystems used for cytotoxicity studies were analyzed by ICP-MS (after change of buffer to medium by the Stirred Cell and sterile-filtration) for exact Au/Pt concentrations and this information was used for IC50 determination. Cell viability curves were constructed from the data that resulted from the cell viability assays and the IC50 values were calculated using the viability curves generated by GraphPad Prism.

2.3.3.2 Ames test

An important part of safety assessment is the identification of substances capable of inducing mutations. Chemicals that can induce mutations can probably cause damage in the germ line and are even capable of inducing cancer. Ames mutagenicity assay is a

bacterial mutation assay designed to detect a wide range of chemical agents capable of causing genetic damage. This assay employs various histidine dependent *Salmonella typhimurium* strains carrying different mutations in the histidine operon and tryptophan dependent *Escherichia coli* strains that carry mutations in the trpE gene that codes for anthranilate synthase component I, an enzyme needed in tryptophan synthesis. When these test strains are grown on minimal media agar plates containing a trace of histidine/tryptophan, only bacteria that revert to histidine/tryptophan-independent can form colonies. There is always a relatively constant number of spontaneous revertants, that increases when a mutagen is added (Mortelmans & Riccio, 2000; Mortelmans & Zeiger, 2000).

Bacteria strains used for Ames mutagenicity assay were: *Salmonella typhimurium* strains TA98, TA100 and TA1535 and *Escherichia coli* strain WP2 uvrA pKM101 (Table 11). Strains were purchased from CECT (Colección Española de Cultivos Tipo, University of Valencia).

Bacteria strain	Mutation	Reverse event	Limiting factor
S. typhimurium TA98	-1 frameshift mutation	Frameshift	Histidine
S. typhimurium TA100	GAG/CTC to GGG/CCC	Base-pair substitution	Histidine
S. typhimurium TA1535	GAG/CTC to GGG/CCC	Base-pair substitution	Histidine
E. coli WP2 uvrA (pKM101)	Ochre mutation	Transition/transversion	Tryptophan

Table 11. The bacteria strains employed in mutagenicity testing of EDS and their characteristics.

Lyophilized bacteria were resuspended in liquid nutrient broth and incubated O/N at 37 ºC with agitation. The next day cultures were streaked on glucose minimal (GM) agar plates with excess of biotin and histidine (TA98, TA100 and TA1535), ampicillin (TA98, TA100 and WP2 uvrA pKM101) and tryptophan (WP2 uvrA pKM101) to create individual clones. This purification process was repeated twice. Clones from the second purification plate were placed on a fresh GM agar plate (supplemented with appropriate nutrients) to create a master plate. When growth was observed, clones were inoculated in nutrient broth and genetic analysis to ensure the maintenance of genetic integrity of the clones was performed. The studied parameters were biotin-, histidine- and tryptophan-dependence, ampicillin resistance (strains including pKM101 plasmid), uvrA marker (extreme sensitivity to ultraviolet light irradiation) and rfa mutation

(defective lipopolysaccharide coating, permeability to bulky chemicals) (Table 12 & Table 13).

Bacteria strain	Biotin	Histidine	Biotin & histidine	Tryptophan
S. typhimurium TA98	+	+	+	-
S. typhimurium TA100	+	+	+	-
S. typhimurium TA1535	+	+	+	-
E. coli WP2 uvrA (pKM101)	-	-	-	+

Table 12. The dependency of the different bacteria strains used on biotin, histidine and tryptophan verified by genetic analysis.

Bacteria strain	Ampicillin resistance	uvrA marker	rfa mutation
S. typhimurium TA98	+	-	+
S. typhimurium TA100	+	-	+
S. typhimurium TA1535	-	-	+
E. coli WP2 uvrA (pKM101)	+	+	-

Table 13. Characteristics of the different bacteria strains employed.

To start the mutagenicity assay an O/N culture was prepared of the clones that had passed the genetic analysis. The next day EDS and PEGNP dilutions starting from 100 ppm were prepared and pre-incubated with the O/N bacteria cultures (1-2 x 10^8 bacteria) and PBS at 37 ºC for 20 min with agitation in sterile glass tubes. 2 mL melted top agar containing either biotin and a trace of histidine (*S. typhimurium*) or tryptophan (*E. coli*) was added to each tube after pre-incubation and the mixes were poured on GM agar plates. After solidification of top agar plates were incubated at 37 ºC for 48 h and the colonies that had formed were counted (Figure 16). The experiment was performed with triplicate samples and strain-specific mutagenesis-inducing positive controls were used (Table 14).

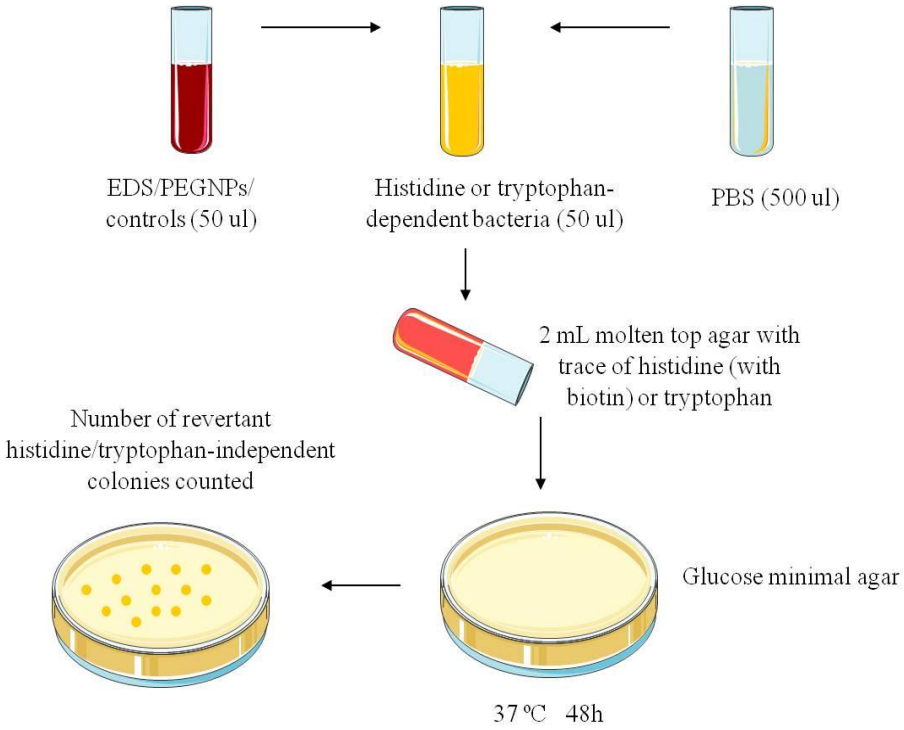

Figure 16. Ames mutagenicity testing pre-incubation procedure.

Bacteria strain	Positive control (/plate)	Supplier
S. typhimurium TA98	4-Nitro-o-phenylenediamine (2,5 ug)	Sigma-Aldrich
S. typhimurium TA100	Sodium azide (5 ug)	Sigma-Aldrich
S. typhimurium TA1535	Sodium azide (5 ug)	Sigma-Aldrich
E. coli WP2 uvrA (pKM101)	Mitomycin C (0,5 ug)	Sigma-Aldrich

Table 14. Strain-spesific mutagenesis-inducing controls for Ames test.

The Ames mutagenicity test was performed without metabolic activation.

2.3.3.3 Comet assay

Genotoxic chemicals can cause alterations in DNA structure or bind to DNA and cause spontaneous disintegration of DNA under physiological conditions and lead to DNA lesions harmful to the human genome. Comet assay is a widely used technique in identification of such substances. The comet assay, also known as single cell gel electrophoresis (SCGE) assay, is a quantitative technique, that measures DNA damage by quantifying migration of denatured DNA fragments out of the nucleus during electrophoresis (Liao et al., 2009).

Panc-1 were seeded on 12-well plates, 3 x 10^5 cells per well. After 24h nanosystems were added in the wells in concentrations of 100 ppm and 50 ppm. Cells were treated for 6h after which the medium was changed. 24h after the beginning of the treatment cells were harvested by trypsinization, centrifuged and resuspended in PBS. Cell suspension was then mixed with 37 °C 1% low melting point agarose (Sigma-Aldrich), and placed on glass slides previously precoated with 1% normal melting point agarose (Sigma-Aldrich) and spread with cover glass. Slides were left at 4 °C for 10 minutes and cover glasses were removed. Slides were then immersed in lysis buffer for 1 h at 4 °C. After lysing the cells, slides were rinsed in distilled water and left in the electrophoresis buffer for alkaline unwinding for 20 minutes at 4 °C. Samples were then run in the same buffer for 20 minutes at 4 °C at 25 V. Slides were rinsed with distilled water and immersed in three lots of neutralizing buffer for 5 minutes at 4 °C. Lysis, electrophoresis and neutralization were performed in the dark. Finally slides were stained with 1 ug/ml DAPI (Sigma-Aldrich) and comets were visualized by Nikon E600 microscope. DNA damage was quantified by analyzing the tail DNA percentage of 50 cells per treatment using CaspLab - Comet Assay Software Project. As positive control we used cells treated for 20 min with 100 μM H_2O_2.

2.3.3.4 ROS production

Reactive oxygen species (ROS) are by-products of cellular metabolism of oxygen, which can generate damage to cellular structures, when their production is dramatically increased due to e.g. environmental stress and some drugs. This state of oxidative stress can lead to apoptosis and immunological responses and is implicated in many pathological conditions, such as cardiovascular diseases and cancer (Bayr, 2005).

2',7'-dichlorohydrofluorescein diacetate (H_2DCFDA) is one of the most commonly used fluorescent probes for ROS detection. It is a cell permeable ROS indicator that diffuses passively into cells and is retained inside the cells after cleavage by intracellular esterases. When oxidated by ROS, H_2DCFDA is cleaved into highly fluorescent 2',7'-dichlorofluorescein (DFC).

Panc-1 were seeded on 12-well plates, 1 x 10^5 cells per well. After 48h different concentrations of nanosystems were added in the wells. At 1h, 2h, 4h 8h, 12h and 24h cells were washed twice with PBS and 40 μM H_2DCFDA (Life Technologies) in PBS was added in an equal amount of growth medium. Cells were incubated at 37˚C for 15 minutes, washed with PBS and visualized by fluorescence microscope. Then cells were lysed with ROS lysis buffer and moved to a black clear bottom plate for reading fluorescence (FLx800 Fluorescence Microplate Reader) with excitation wavelength 485 nm and emission wavelength 528 nm. 5 mM diethyl maleate (Sigma-Aldrich) in growth medium was used as positive control.

2.3.4 Drug release

In vitro drug release from EDS-CIS was studied in PBS. EDS-CIS was incubated in RT with PBS (neutral pH) and the solution was passed through the Stirred Cell (Merck Millipore) – used to purify and concentrate nanosystems) – at time points 0, 30 min, 6 h, 24 h and 72 h. The drug that was still conjugated to the nanosystem remained in the stirrer unable to pass the 100 kDa porous cellulose ultrafiltration membrane (Millipore), while the released drug passed through and was collected. The flow through was analyzed by ICP-MS to quantify the released Pt.

2.3.5 Efficacy studies

2.3.5.1 Colony formation assay

Clonogenic assay (Colony Formation Assay, CFA) is a cell survival assay based on the ability of a single cell to grow into a colony. The assay measures every single cell for its ability to reproduce. CFA was originally described to determine effects of ionizing radiation, but is widely used to study the effectiveness of chemotherapeutic agents (Munshi et al., 2005).

Panc-1 were seeded on 6-well plates (600 cells/ well) and let attach O/N. Cells were then treated with EDS-CIS and CIS (1; 0,5; 0,25 μM CIS) for 10 d. The formed colonies were then fixed with 10% formalin (Sigma-Aldrich) and stained with 0,05 % crystal violet (Sigma-Aldrich). Colonies were counted and inhibitory percentage determined.

2.4 *In vivo*-characterization of the nanosystems

Nanocarriers hold great promise in increasing efficacy and reducing side-effects of conventional anticancer drugs, but their size may also enable them to pass various biological barriers which can lead to toxic effects. These effects may not be detected by *in vitro* studies that lack the ability to deliver information on cell-cell interactions, so in vivo studies of nanomaterials is necessary (Fadeel & Garcia-Bennett, 2010). Besides, *in vivo* studies can offer valuable information about biodistribution and tumor-targeting, that cannot be obtained by *in vitro* experiments.

Animal procedures met the guidelines of European Community Directive 86/609/EEC and were approved by the Comité Ético de Experimentación Animal (CEEA) of the PCB (Parc Científic de Barcelona) or VHIR (Vall d'Hebron Institut de Recerca).

The concentrations of the different components of the nanosystem batches used in each study are presented in the tables under each section.

2.4.1 Animals

The discovery of T-cell deficient nude athymic mice enabled transplantation of human tumor tissues (xenografts) in mice. Nude mice are genetic mutants with a dysfunctional thymus due to a mutation at Foxn1 (winged-helix/forkead transcrition factor) gene that blocks thymus-derived T cells. Due to the inhibited immune system, nude mice do not exert a rejection response to foreign cells introduced in them. During the past few decades these xenografts have become an essential part of routine screening in development of novel anticancer agents (Belizário, 2009; Flanagan, 1966; Morton & Houghton, 2007).

Animals were housed in plastic cages in controlled environmental conditions of humidity (60%), temperature (22°C ± 2°C) and light with food and water ad libitum. Immunodeficient athymic Nude-Foxn1^{nu} (Harlan Laboratories) mice were males and

females and 4-6 weeks of age at the beginning of the experiments. Animals were euthanized by CO_2 inhalation followed by cervical dislocation.

2.4.1.1 Subcutaneous xenograft models

To generate tumor xenografts, 6-week-old male or female athymic nude mice were subcutaneously injected with 6 x 10^6 cells of HT1080, Panc-1 or OVCAR-3 into the right flank. Once the tumors reached an average size of 100 mm^2 (HT1080 & Panc-1) or 150 mm^2 (OVCAR-3), treatments were initiated.

2.4.1.2 EDS studies

EDS animal studies were performed with the batch in Table 15.

C_{Au} (ppm)	C_{Au} (mg/ml)	C_{HA} (mg/ml)
976,30	0,9763	7,5

Table 15. EDS batch used in the in vivo studies.

2.4.1.2.1 EDS blood circulation

Blood levels of gold were studied after intraperitoneal EDS injection until 24 h post-injection in healthy mice. Mice received a single intraperitoneal dose of 10 mg/kg EDS and blood samples were collected from the submandibular vein at 30 min, 2 h, 4 h, 6 h, 12 h and 24 h and analyzed by ICP-MS.

2.4.1.2.2 EDS biodistribution

HT1080 and Panc-1 tumor-bearing mice received an intraperitoneal dose of 10 mg/kg (Au) EDS twice per week during one month (a total of eight doses). The mice were sacrificed and various organs were collected, snap-frozen and analyzed by ICP-MS.

2.4.1.2.3 Blood biochemical analysis after EDS administration

By performing blood biochemical analysis, we wanted to determine whether EDS could cause heart, hepatic or renal damage. The parameters studied were albumin, urea, glutamic-pyruvate transaminase (also known as alanine aminotransferase: GPT/ALT), and glutamic oxaloacetic transaminase (also known as aspartate transaminase: GOT/AST).

Albumin blood levels decreases due to pancreatic damage, nephropathy, enteropathy, hemorrhage and liver failure. Increase of urea can be an indication of catabolic states, congestive heart failure, renal failure, blocked urethra, or ruptured bladder. Both GPT and GOT can increase due to hepatocellular and muscle damage.

HT1080 and Panc-1 tumor-bearing mice received an intraperitoneal dose of 10 mg/kg (Au) EDS twice per week during four weeks (a total of eight doses). Blood was collected from the submandibular vein and the biochemical analysis was performed by the Laboratory Animal Applied Research Platform (LAARP) of PCB. Number of animals was four for the saline group and four for the EDS group.

2.4.1.3 EDS-Drug studies

2.4.1.3.1 *In vivo* stability of double conjugated candidates

The stability analysis comparing two drug-encapsulating (Table 16) candidates was performed by Leitat Technological Centre. A single dose of candidate B (EDS + Mua + CIS) and candidate C (EDS + CIS) was injected intravenously and intraperitoneally. Blood samples were collected at time points 0h, 1h and 4h, plasma separated and analyzed for Au and Pt by ICP-MS.

Treatment	C_{Au} (ppm)	C_{Au} (mg/ml)	C_{Pt} (ppm)	C_{Cis} (µM)	Pt/Au
EDS + Mua + CIS	999,07	0,999	88,60	454,19	0,09
EDS + CIS	1991,91	1,992	2404,54	12325,93	1,21

Table 16. Nanosystem batches used in the *in vivo* stability study.

2.4.1.3.2 EDS-CIS biodistribution

The biodistribution analysis was performed by CIBBIM Nanomedicine (Vall d'Hebron Institut de Recerca). EDS-CIS (Table 17) was injected into Panc-1 tumor-bearing female athymic nude mice intravenously and intraperitoneally at a single dose of 5 mg/kg. Blood (plasma), tumor, liver, lungs, spleen, kidneys and pancreas were collected from the treated mice at 4 hours, 24 hours and 48 hours post injection and analyzed by ICP-MS. At 48 h tumor, spleen, lymph nodes, pancreas, kidney, stomach, intestine, liver and heart were also formalin-fixed, embedded in paraffin and analyzed for CD44 staining by immunohistochemistry.

C_{Au} (ppm)	C_{Au} (mg/ml)	C_{Pt} (ppm)	C_{Cis} (µM)	C_{HA} (mg/ml)
3237	3,237	3225	16532	20

Table 17. EDS-Cis batch used in the blood circulation time study.

2.4.1.3.3 *In vivo* tumor growth

OVCAR-3 tumor bearing mice received intraperitoneal doses of the following treatments:

- EDS-Cis: 2 mg/kg (Cis); 0,75 mg/kg (Au) (Table 18)
- EDS-Cis: 4 mg/kg (Cis); 1,5 mg/kg (Au) (Table 18)
- Cis 2 mg/kg
- Cis 4 mg/kg
- EDS: 1,5 mg/kg (Au) (Table 18)
- PBS (saline)

The experiment was conducted by Leitat Technological Centre. Administrations took place twice per week. When the saline-treated animals were reaching tumor size of 1000 mm^3, mice were sacrificed; their livers and tumors were collected, snap-frozen and stored at -80 ºC for ICP-MS analysis. The number of animals used for the in vivo tumor growth study was a minimum of 9 per treatment group.

Treatment	C_{Au} (ppm)	C_{Au} (mg/ml)	C_{Cis} (µM)	C_{Cis} (mg/ml)	C_{HA} (mg/ml)
EDS	730	0,73	-	-	7,82
EDS- CIS	730	0,73	6640	2	6,28

Table 18. EDS & EDS-Cis batches used in the *in vivo* tumor growth study.

2.4.2 Histology

Through histological studies, we first identified organs susceptible for accumulation of the nanosystems by analyzing the CD44 expression levels in tumor and various organs. Next we visualized the NPs in the organs that showed the most accumulation by ICP-MS analysis after EDS administration. When organs were collected for histology, they were fixed in formalin and embedded in paraffin. Histologies were performed by CIBBIM Nanomedicine (Vall d'Hebron Institut de Recerca) or Unit of Experimental Toxicology and Ecotoxicology (UTOX-PCB).

2.4.2.1 Immunohistochemistry

Expression levels of CD44 in tumor, spleen, lymph nodes, pancreas, kidney, stomach, intestine, liver and heart of the animals included in the EDS-Cis blood circulation study were analyzed by CIBBIM Nanomedicine (Vall d'Hebron Institut de Recerca).

Antigen retrieval for paraffin embedded samples was executed by standard pan heating. The primary antibody (anti-mouse & anti-human CD44s, Merck-Millipore) was used at a concentration 1/200. The secondary antibody was horseradish peroxidase conjugated and developed by the DAB chromogen. Sections were counterstained with hematoxylin and mounted in DPX.

2.4.2.2 H&E

To visualize NPs accumulated in the liver, and to study tissue morphology after the EDS-CIS efficacy experiment, hematoxylin-eosin staining was performed by the Unit of Experimental Toxicology and Ecotoxicology (UTOX-PCB). The staining was executed using a Varistain^{TM} 24-4 automatic slide stainer (Thermo Fisher Scientific). Histologic evaluation was performed with a Nikon E600 microscope.

2.4.2.3 Silver staining

To visualize NPs accumulated in the skin, silver staining was performed by the Unit of Experimental Toxicology and Ecotoxicology (UTOX-PCB). Paraffin embedded samples were deparaffinated and samples were dried and silver stained using the Silver Enhancing kit for light and electron microscopy (BBInternational) according to the manufacturer's instructions. The slides were then counterstained with hematoxylin and mounted in DPX. Tissues were visualized with a Nikon E600 microscope.

2.4.3 Animal weight

Animals included in biodistribution and in vivo tumor growth studies were weighed every few days and monitored from the beginning of the study until the end of the experiment.

2.5 Statistical analysis

The statistical analyses of the *in vitro* studies were performed using the GraphPad Prism and Statgraphics softwares. Results are expressed as mean (SD) (Standard Deviation). A one-way analysis of variance (ANOVA) or Kruskal-Wallis nonparametric test were used. Differences were considered statistically significant (*) when p value ≤ 0.05.

The statistical analyses of the *in vivo* studies were performed using GraphPad Prism software and the results are expressed as mean (SD) or mean ± SEM (Standard Error of the Mean). For the in vivo efficacy study, a one-way ANOVA (followed by a Bonferroni *post-hoc* test at a significance level of $p \leq 0.05$) was employed using the tumor volumes of the day of the sacrifice.

ANNEX: solutions

Common solutions

PBS 10X

Reagent	Concentration	per 1 L	Supplier
NaCl	1,4 M	80 g	Sigma-Aldrich
KCl	27 mM	2 g	Sigma-Aldrich
Na_2HPO_4	102 Mm	14,4 g	Sigma-Aldrich
KH_2PO_4	20 mM	2,4 g	Sigma-Aldrich

dH_2O up to 1 L.
pH adjusted to 7,4.
Diluted to 1X for use.

WB buffers

4X Laemmli buffer

Reagent	Concentration	per 100 mL	Supplier
Tris-HCl (pH 6,8)	250 mM	3 g	Sigma-Aldrich
Glycerol	40 % v/v	40 mL	Sigma-Aldrich
SDS	5 % w/w	5 g	Sigma-Aldrich
Bromophenol blue	0,005 % w/v	5 mg	Sigma-Aldrich

dH_2O up to 100 mL.
5 % β-mercaptoEtOH added before use.

10X Running buffer

Reagent	Concentration	per 1 L	Supplier
Tris-HCl (pH 8,3)	250 mM	30,285 g	Sigma-Aldrich
Glycine	1920 mM	144,13 g	Sigma-Aldrich
SDS	1 % w/v	10 g	Sigma-Aldrich

dH_2O up to 1 L.
Diluted to 1X before use.

1X Transfer buffer

Reagent	Concentration	per 1 L	Supplier
Tris-HCl	25 mM	3,029 g	Sigma-Aldrich
Glycine	192 mM	14,41 g	Sigma-Aldrich
MetOH	20 % v/v	200 mL	Sigma-Aldrich

Tris & glycine dissolved in 800 mL dH_2O.
MetOH added.

10X TBS

Reagent	Concentration	per 1 L	Supplier
Tris-HCl (pH 7)	250 mM	30,285 g	Sigma-Aldrich
NaCl	1,35 M	79,478 g	Sigma-Aldrich
KCl	40 mM	2,98 g	Sigma-Aldrich

TEM for cells

PB solution 0,2M

Reagent	per 1000 mL	Supplier
NaH_2PO_4	21,8 g	Sigma-Aldrich
Na_2HPO_4	6,4 g	Sigma-Aldrich

dH_2O up to 1000 mL.
pH adjusted to 7,4.

Fixative

Reagent	Concentration	per 250 mL	Supplier
PB solution	0,12 M	150 mL	-
Glutaraldehyde 10X	2,5%	25 mL	Sigma-Aldrich

dH_2O up to 250 mL.

OsO_4 solution

Reagent	Concentration	per 5 mL	Supplier
PB solution	1 M	2,5 mL	-
OsO_4 4%	1%	1,25 mL	Sigma-Aldrich

dH_2O up to 5 mL.

EPON 1 solution

Reagent	per 50 mL	Supplier
Eponate 12	23,5 g	Ted Pella, Inc.
DDSA	12,5 g	Ted Pella, Inc.
NMA	14 g	Ted Pella, Inc.

Agitated for few minutes
avoiding bubble formation.

EPON 2 solution

Reagent	per 20 mL	Supplier
EPON 1 solution	19,63 mL	-
DMP-30	0,37 mL	Ted Pella, Inc.

Cell viability

HEX substrate

Reagent	Concentration	per 100 mL	Supplier
HEX substrate	7,5 mM	0,128 g	Sigma-Aldrich
Sodium citrate	0,1 M	1,47 g	Sigma-Aldrich
Triton-X	0,25%	250 ul	Sigma-Aldrich

Substrate & sodium citrate dissolved in 40 mL dH_2O.
pH adjusted to 5 and volume adjusted to 50 mL.
Triton-X dissolved in 50 mL dH2O.
Substrate solution & Triton-X solution mixed and sterile-filtered.
Stored at -20 ºC until use.

HEX developer

Reagent	Concentration	per 200 mL	Supplier
Glycine	50 mM	0,75 g	Sigma-Aldrich
EDTA	5 mM	0,292 g	Sigma-Aldrich

Glycine dissolved in 180 mL dH_2O.
pH adjusted to 10,4.
EDTA dissolved in glycine solution and volume adjusted to 200 mL.
Sterile-filtered and stored at -20 ºC until use.

Ames test

Nutrient broth

Reagent	per 500 mL	Supplier
Beef extract	2,5 g	Sigma-Aldrich
Peptone	5 g	Sigma-Aldrich
NaCl	2,5 g	Sigma-Aldrich
Agar (only for solid media)	7,5 g	Sigma-Aldrich

dH_2O up to 500 mL.
pH adjusted to 7,2.
Autoclaved and stored at RT in the dark.

GM agar plates

Reagent	per 1 L	Supplier
Agar (in 900 mL dH2O)	15 g	Sigma-Aldrich
VB salt solution (50X)	20 mL	-
Glucose solution (10% v/v)	50 mL	-

Agar and dH2O autoclaved.
Sterile VB salts & glucose added.
Poured on plates and stored at 4ºC.

VB salt solution (50X)

Reagent	per 100 mL	Supplier
$MgSO_4 \cdot 7H_2O$	1 g	Sigma-Aldrich
Citric acid (anhydrous)	9,14 g	Sigma-Aldrich
K_2HPO_4	50 g	Sigma-Aldrich
$NaNH_4HPO_4$	17,5 g	Sigma-Aldrich

Ingredients added in the indicated order in 65 mL dH2O.

Volume adjusted to 100 mL.

Autoclaved and stored at RT.

Glucose solution (10% v/v)

Reagent	per 100 mL	Supplier
Dextrose	10 g	Sigma-Aldrich

dH2O up to 100 mL.

Autoclaved and stored at 4ºC.

Biotin solution (0,01%, w/v)

Reagent	per 100 mL	Supplier
D-biotin	1 mg	Sigma-Aldrich

dH2O up to 100 mL.

Sterile-filtered (0,45 uM pores) and stored at 4ºC.

To create excess biotin GM agar plates, add 8 mL into GM agar solution.

Histidine solution (0,5%, w/v)

Reagent	per 100 mL	Supplier
L-histidine	50 mg	Sigma-Aldrich

dH2O up to 100 mL.

Autoclaved and stored at 4ºC.

To create excess histidine GM agar plates, add 8 mL into GM agar solution.

Ampicillin solution (0,8%, w/v)

Reagent	per 100 mL	Supplier
Ampicillin	8 mg	Sigma-Aldrich

dH2O up to 100 mL.

Sterile-filtered (0,45 uM pores) and stored at 4ºC.

To create ampicillin GM agar plates, add 3 mL into GM agar solution.

Tryptophan solution

Reagent	Concentration	Supplier
Tryptophan	0,05 mM	Sigma-Aldrich

dH2O up to 100 mL.

Sterile-filtered and stored at 4ºC.

To create excess tryptophan GM agar plates, add 3 mL into GM agar solution.

Top agar supplemented with histidine/biotin

Reagent	per 1 L	Supplier
Agar	6 g	Sigma-Aldrich
NaCl	6 g	Sigma-Aldrich
Histidine/biotin solution (0,5mM)	100 mL	-

Agar and NaCl dissoveld in 900 mL dH2O and autoclaved.
Sterile-filtered histidine/biotin solution added.

Histidine/biotin solution (0,5mM)

Reagent	per 100 mL	Supplier
D-biotin	12,4 mg	Sigma-Aldrich
L-histidine	9,6 mg	Sigma-Aldrich

Boiling dH2O up to 100 mL.
Sterile-filtered and stored at 4ºC.

Crystal violet solution (0,1% w/v)

Reagent	per 100 mL	Supplier
Crystal violet	100 mg	Sigma-Aldrich

dH2O up to 100 mL.
Sterile-filtered and stored at RT.

Comet assay

Lysis buffer

Reagent	Concentration	per 1 L	Supplier
NaCL	2,5 M	146,1 g	Sigma-Aldrich
Na_2EDTA	0,1 M	37,2 g	Sigma-Aldrich
Tris	10 mM	1,21 g	Sigma-Aldrich

dH_2O up to 1 L.
pH adjusted to 10.
Stored at 4 °C until use.
Immediately before use, add 1 mL / 100 mL Triton-X.

Alkaline electrophoresis buffer

Reagent	Concentration	per 1 L	Supplier
NaOH	0,3 M	12 g	Sigma-Aldrich
EDTA	1 mM	0,29 g	Sigma-Aldrich

dH_2O up to 1 L.
pH adjusted to > 13.
Stored at 4 °C until use.

Neutralizing buffer

Reagent	Concentration	per 1 L	Supplier
Tris	0,4 M	48,88 g	Sigma-Aldrich

dH_2O up to 1 L.

pH adjusted to 7,5.

Stored at 4 °C until use.

ROS assay

Lysis buffer

Reagent	Concentration	per 1 L	Supplier
Tris	50 mM	6,057 g	Sigma-Aldrich
EDTA	5 mM	1,461 g	Sigma-Aldrich
Triton-X	1%	10 mL	Sigma-Aldrich
NaCl	150 mM	8,766 g	Sigma-Aldrich

dH_2O up to 1 L.

pH adjusted to 7,4.

RESULTS

3. RESULTS

The experimental part of this project, as well as this results section, has been divided into two parts. We started part 1 by chemically characterizing EDS and studying its stability, targeting and toxicity *in vitro;* followed by biodistribution and toxicity of this nanocarrier *in vivo*.

Part 2 of this results section starts with studies of different conjugation methods for the drug and selection of the final candidate. This second part then describes the chemical characterization and stability of EDS-Drug, and also *in vitro* uptake and efficacy studies and preliminary *in vivo* efficacy studies as well as biodistribution.

3.1 Characterization of EDS

3.1.1 Chemical characterization

Nanomaterials used in this study were analyzed by TEM, DLS, EA and ICP-MS, all of which are techniques included in the physico-chemical characterization cascade for nanomaterials described by Nanotechnology Characterization Laboratory (NCL). A thorough stability examination, including UV-VIS analysis, was also included in our characterization process.

3.1.1.1 TEM

Bare and HA-conjugated AuNPs were visualized by TEM to analyze their size-range and dispersity. Bare NPs were of size 11,56 ± 1,2 (Figure 17) and disperse in solution. The size distribution of the NPs was determined by GraphPad Prism.

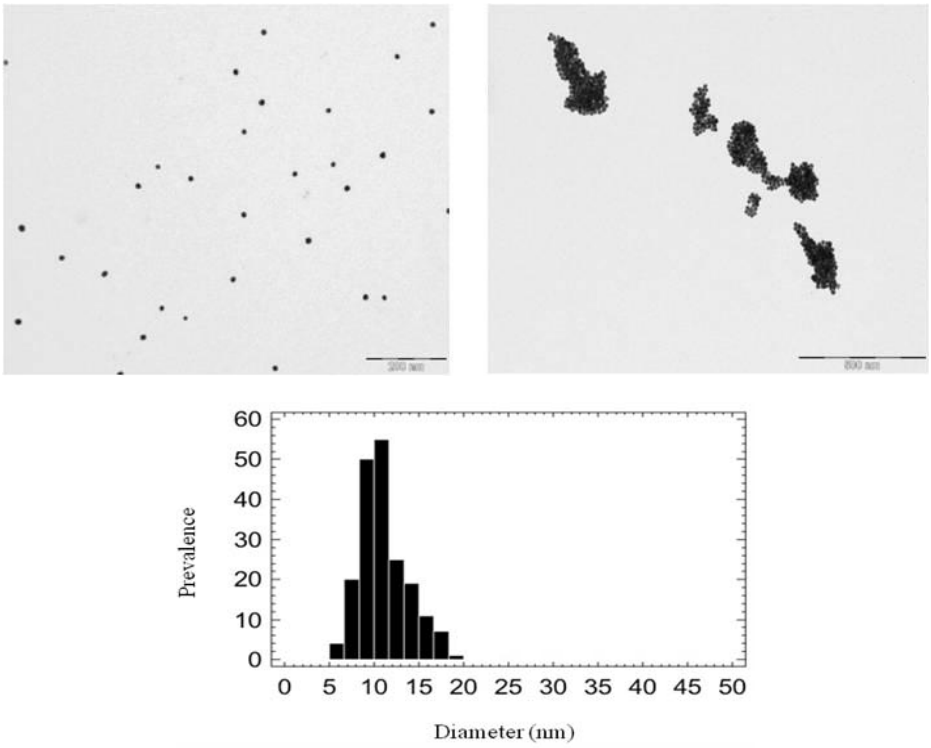

Figure 17. Above: TEM images of gold nanoparticles. Disperse AuNPs (left) and aggregated AuNPs (right). Only disperse AuNPs of the appropriate size were used for HA conjugation. Below: Size-distribution of AuNPs analyzed by GraphPad Prism.

3.1.1.2 DLS

Size distribution of bare NPs and EDS was determined by DLS in addition to TEM. The average size of unconjugated NPs was 12 nm as revealed also by TEM and when conjugated to HA, the size of the conjugates was close to 100 nm in diameter (Figure 18).

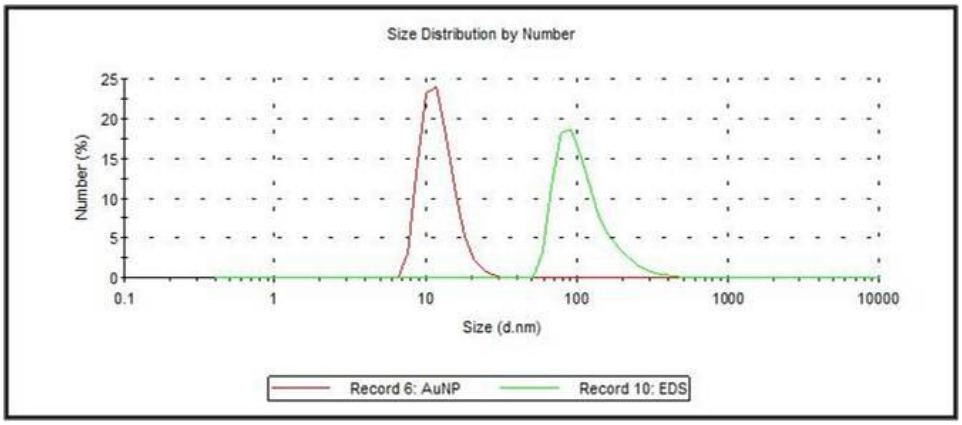

Nanosystem	Size (nm)
AuNP	11,56 ± 0,2
EDS	97,7 ± 6,9

Figure 18. The hydrodynamic radii of bare AuNPs and EDS measured by DLS (mean (SD)).

3.1.1.3 Z-potential

By studying zeta potential of the nanosystems, the surface charge of bare NPs and EDS were compared. The surface charge remained unchanged when NPs were conjugated to HA, at about -38 mV (Table 19), while the hydrodynamic radii grew.

Nanosystem	Z pot (mV)
AuNP	-38,5 ± 1,8
EDS	-38,2 ± 1,3

Table 19. The surface charge of EDS and bare AuNPs (mean (SD)).

3.1.1.4 ICP-MS

ICP-MS was used to quantify the amount of gold and therefore the number of gold nanoparticles in solution. The concentrations of NPs from 3X (100 ppm) synthesis and EDS solution concentrated up to 100X were determined in order to confirm the theoretical concentration (Table 20).

Solution	Theoretical concentration	Concentration by ICP-MS
3X (Synthesis)	100 ppm (0,1 mg/ml)	95,98 ± 2,99 ppm
31X (Concentrated)	1000 ppm (1 mg/ml)	948, 96 ± 27,76 ppm
50X (Concentrated)	1600 ppm (1,6 mg/ml)	1709,67 ± 194,62 ppm
100X (Concentrated)	3200 ppm (3,2 mg/ml)	3222,25 ± 20,71 ppm

Table 20. Gold concentrations of NP solutions that resulted from 3X synthesis and EDS concentrated up to 31X, 50X and 100X measured by ICP-MS (mean (SD)).

3.1.1.5 EA

The percentage of carbon and nitrogen in EDS solution were quantified using elemental analysis. Since all the C and N molecules in this solution belong to HA molecules, the number of HA chains in the sample could be calculated knowing the average size of the molecule (30-50 kDa) (Table 21). The percentage of C and N was quantified and normalized by the number of AuNP/ml.

Au (ppm)	AuNPs/ml	HA (mg/ml)	Nº HA chains/ NP
948, 96 ± 27,76	$5,42*10^{13} \pm 1,59*10^{12}$	7,76 mg/ml	2158,12 ± 127

Table 21. Au and HA concentrations in 31X EDS solution determined by ICP-MS and EA, respectively. Calculations of theoretical number of HA molecules surrounding each gold nanoparticle. Values are expressed in mean (SD).

3.1.1.6 Stability

Stability of bare and HA-coated NPs was studied in saline solution in order to demonstrate that HA-coating protects AuNPs from aggregation and renders them more biocompatible in physiological media.

3.1.1.6.1 Visual analysis

Bare and HA-coated nanoparticles were diluted in H2O and PBS, and color changes were studied visually. Bare NPs aggregated in the saline solution which was detected by

color change from red to blue, whereas HA-coated NPs sustained their disperse state; no color change was observed (Figure 19).

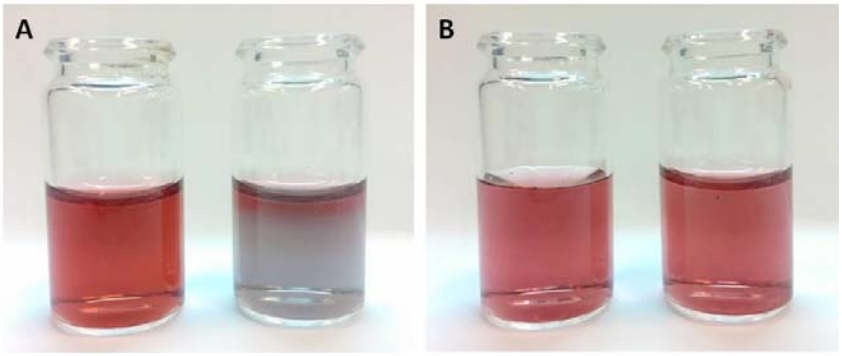

Figure 19. Bare (A) and HA-coated (B) AuNPs in aqueous solution (left) and PBS (right). Aggregated AuNPs appear blue, while the color of disperse NPs is red.

Aggregation of bare, but not HA-coated nanoparticles was also observed in cell culture by light microscope. Bare NPs aggregated on cell surface and formed aggregates big enough to be visualized by light microscope, while NPs with HA-coating remained in a disperse state and could not be seen (Figure 20).

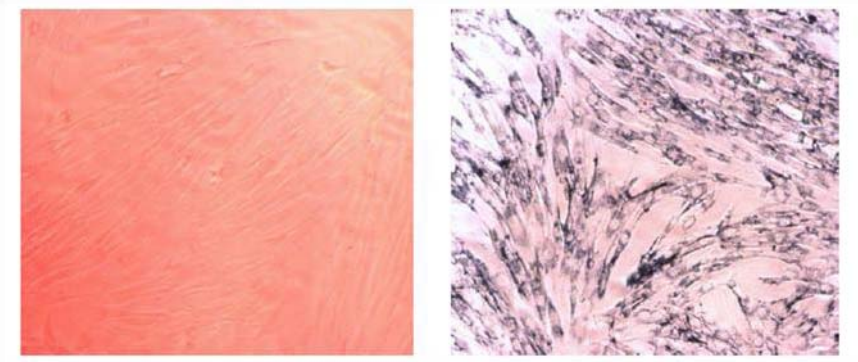

Figure 20. HA-coated (left: nor visible) and bare (right: aggregated on cell surface) AuNPs in cell culture.

3.1.1.6.2 UV-VIS

Bare AuNPs and EDS were also compared by UV-VIS in H_2O solution. AuNPs demonstrated the typical absorbance peak at 520 nm, and EDS showed a slight shift to the right, moving the peak to 524 nm (Figure 21).

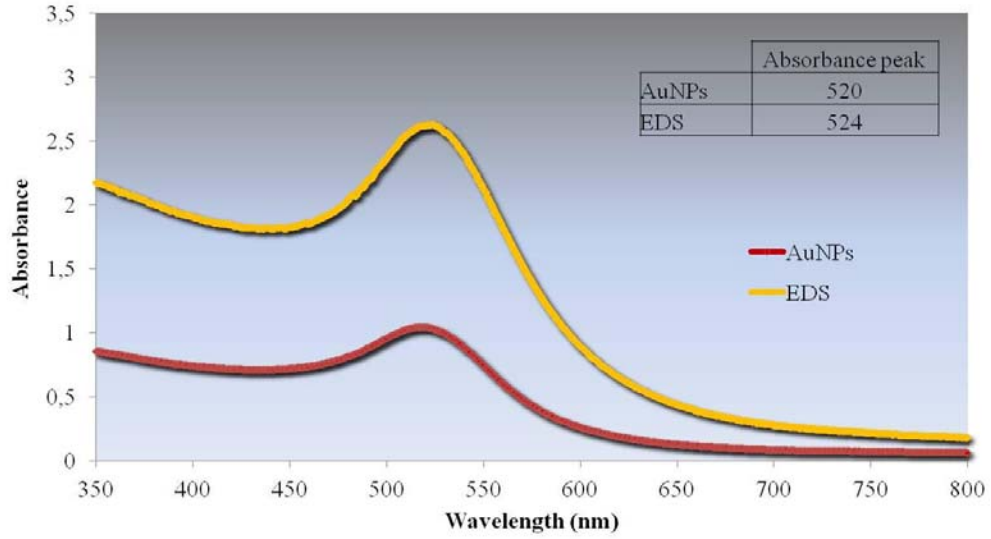

Figure 21. UV-VIS spectra of bare AuNPs and EDS in H_2O. Both show the characteristic AuNP peak, conjugation of HA causes a slight shift to the right.

When the UV-VIS spectra of bare AuNPs and EDS in PBS was studied, the absorbance peak of EDS remained unchanged while the peak of aggregated AuNPs widened and made an ample shift to the right (Figure 22).

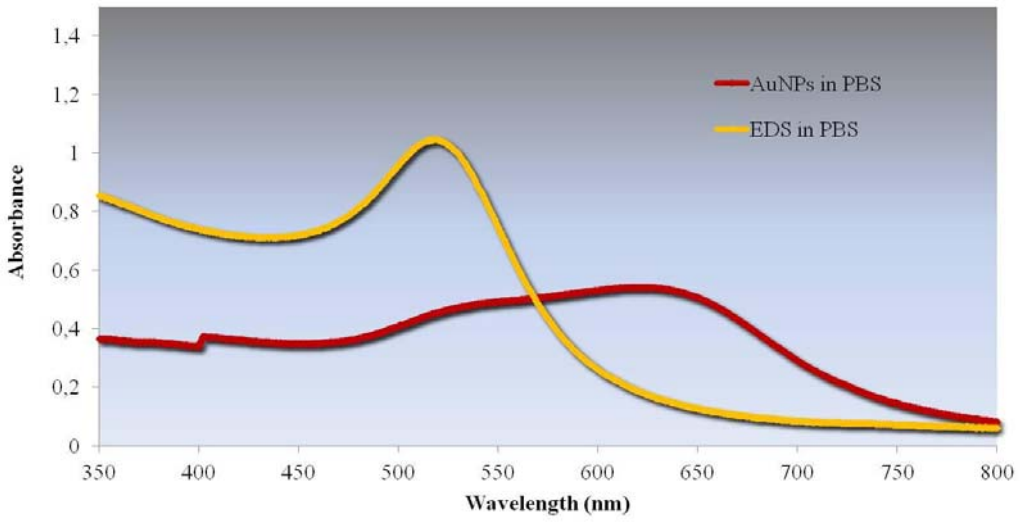

Figure 22. UV-VIS spectra of bare AuNPs and EDS in PBS solution. AuNPs aggregated and lost the characteristic peak, while the peak of EDS remained unchanged compared to H_2O solution (see Figure 21).

The chemical characterization studies proved EDS synthesis to be well controlled. Coating the NPs with HA converted the bare nanoparticles stable and biologically compatible in physiological media avoiding aggregation that bare NPs are prone to in saline solutions. Through ICP-MS we were able to quantify the number of EDS particles in solution and EA allowed us to quantify the number of HA molecules around one single AuNP.

3.1.2 Internalization of EDS

To perform its role and release the drug load that it is carrying, the nanocarrier needs to reach the target cells. In addition to demonstrate specific taregting of the delivery system to CD44, its uptake was studied in cell lines that express different levels of this receptor.

3.1.2.1 CD44 expression in different cell lines

CD44 levels were analyzed on RNA, total cellular protein and cell surface receptor level by RT-PCR, WB and FACS, respectively (Figure 23 & Figure 24).

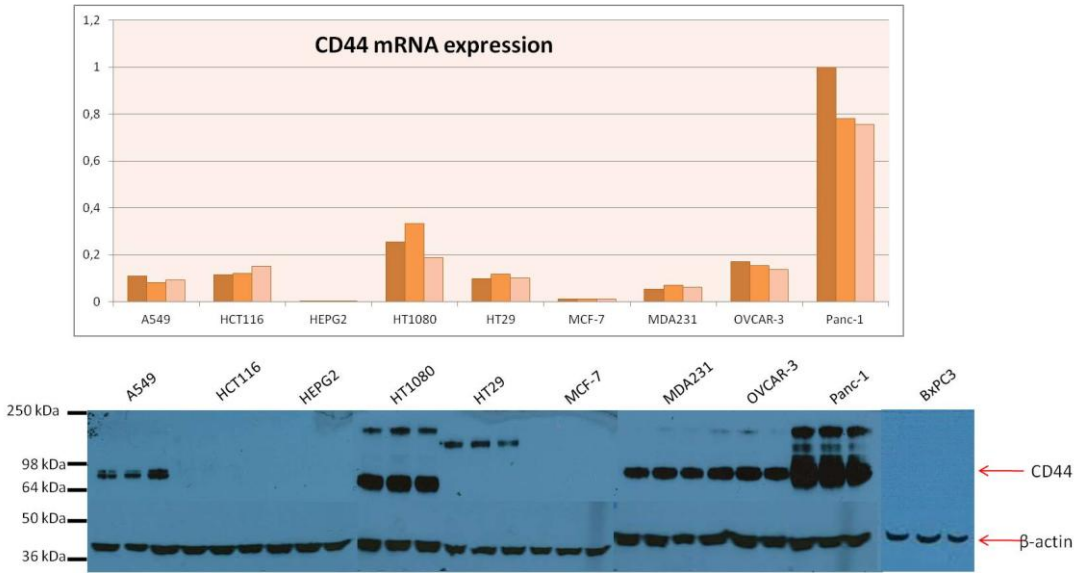

Figure 23. CD44 mRNA (above) and protein (below) levels in selected human cancer cell lines. Results are expressed as relative expression levels and the study was performed with triplicates.

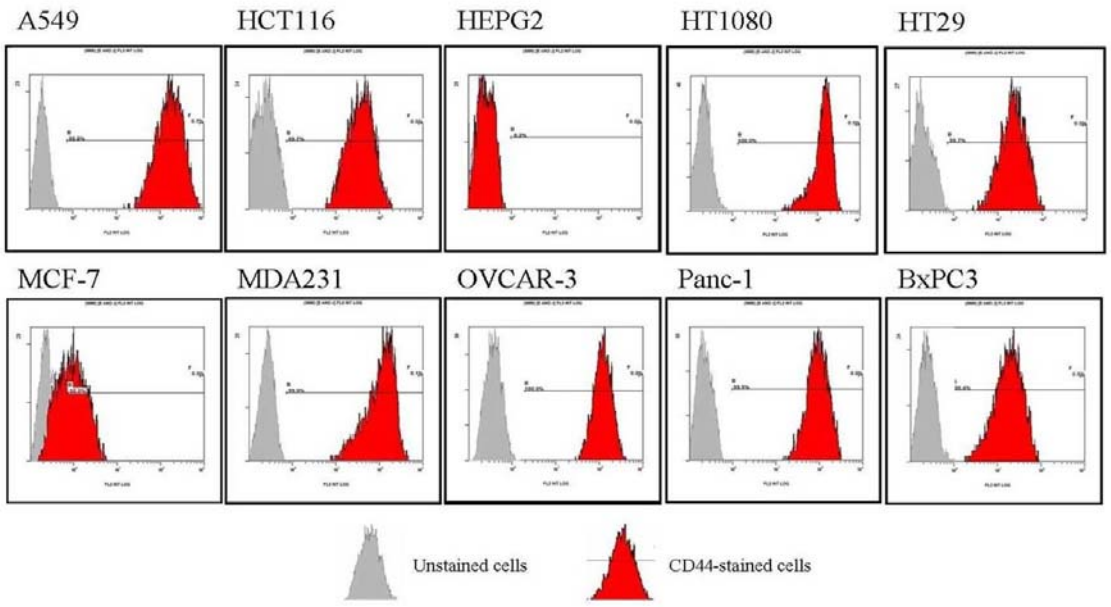

Figure 24. FACS analysis of CD44 levels in selected cell lines. Grey peaks represent the unstained control cells and red peaks the CD44-positive cells. The greater the shift to the right, the more CD44 cells express.

Based on the CD44 expression studies, we chose the following human cancer cell lines for the studies conducted in this project:

- HEPG2: hepatocellular carcinoma, undetected CD44 expression
- MCF-7: epithelial breast adenocarcinoma, low CD44 expression
- BxPC3: epithelial pancreatic adenocarcinoma, low CD44 expression
- A549: epithelial lung carcinoma, intermediate CD44 expression
- MDA231: epithelial breast adenocarcinoma, intermediate CD44 expression
- OVCAR-3: ovarian carcinoma, intermediate CD44 expression
- HT1080: fibrosarcoma, intermediate CD44 expression
- Panc-1: epithelial pancreatic ductal carcinoma, high CD44 expression

3.1.2.2 Internalization

3.1.2.2.1 TEM

To study internalization by TEM, we employed the breast cancer cell line MDA231, which expresses intermediate levels of CD44. The HA-coated nanoparticles were internalized after 3 hours' incubation time, and the nanoparticles were seen on the surface of the cells as well as inside the cells, in vesicle-like compartments (Figure 25), but were not found inside the nuclei. There were no visible differences between 3 h and 24 h incubation times (data not shown).

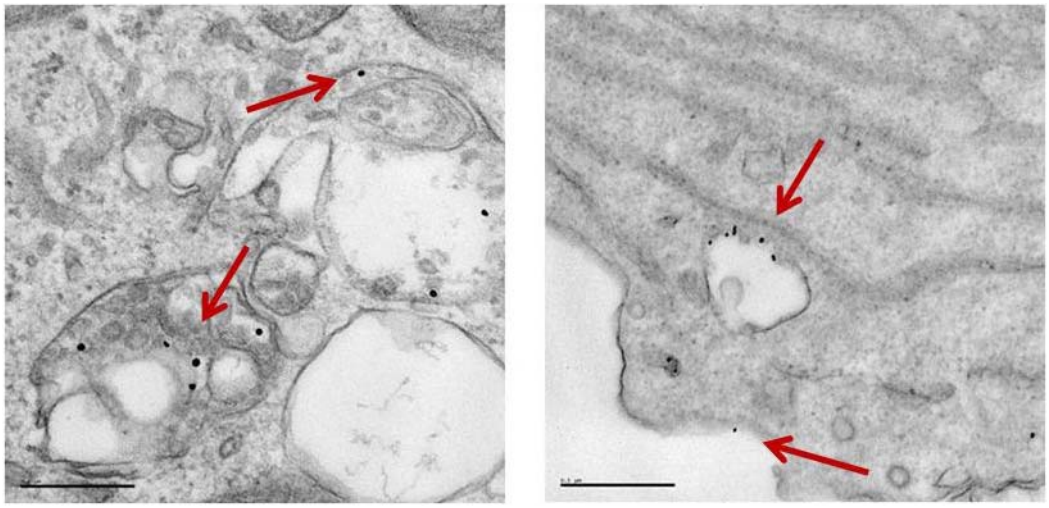

Figure 25. TEM image showing EDS internalized by MDA231 cells.

3.1.2.2.2 Immunofluorescence

MCF-7 and MDA231 were chosen for the fluorescent uptake studies; they are both breast cancer cell lines, but MCF-7 expresses very low levels of CD44 according to our cell line characterization whereas the level of CD44 expression in MDA231 is intermediate and we had already shown by TEM that EDS is internalized by these cells. Confocal microscopy studies showed that the nanosystem was internalized by MDA231, but not by MCF-7 after a 24 h treatment (Figure 26).

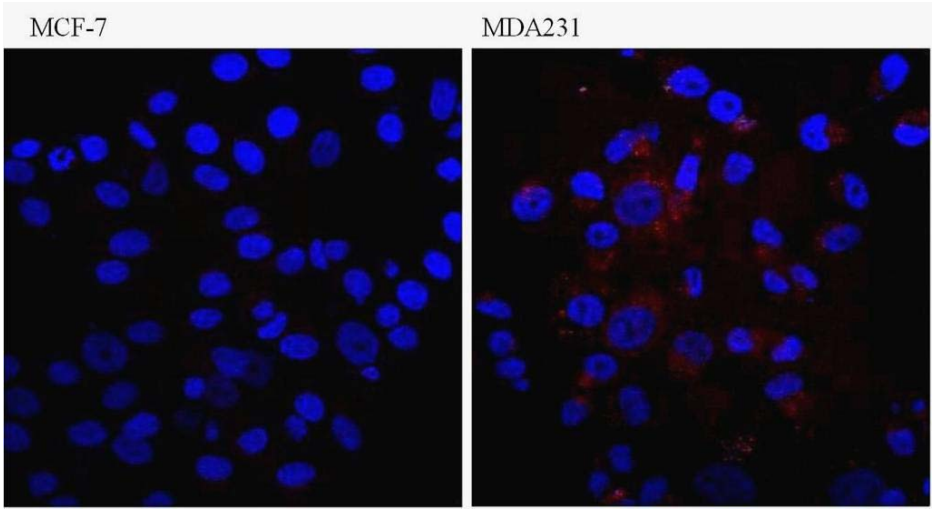

Figure 26. Fluorescently labeled EDS (red) internalized by MDA231 (right), but not by MCF-7 (left). The nuclei were counterstained by DAPI (blue).

Next we visualized fluorescently labeled EDS uptake in Panc-1, a pancreatic cancer cell line that expresses very high levels of CD44, also staining the cell surface receptor (Figure 27).

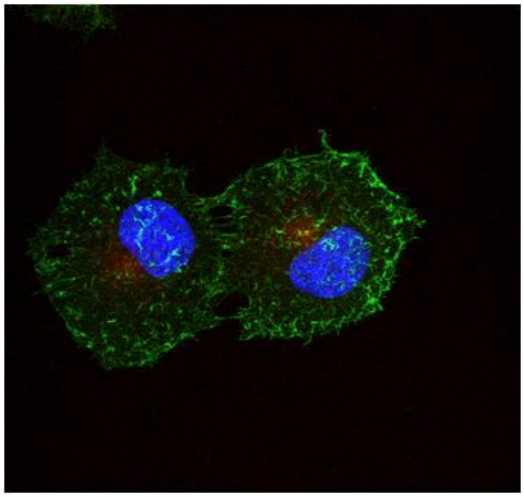

Figure 27. Fluorescently labeled EDS (red) internalized by Panc-1 that expresses very high levels of CD44 (green).

3.1.2.2.3 ICP-MS

Targeting was further studied by ICP-MS in two different cell lines with highly differing expression levels of CD44: HEPG2 (no CD44 expression) and Panc-1 (high CD44 levels). Besides EDS, these two cell lines were treated with PEGNPs as a control of AuNPs with no targeting ligand. The analysis showed that the amount of gold inside the EDS-treated cells was almost 10-fold higher in Panc-1 than HEPG2 while the PEGNP-treated cells contained low amounts of gold in both cell lines (Figure 28). The values were normalized to cell number in the studied cell lines.

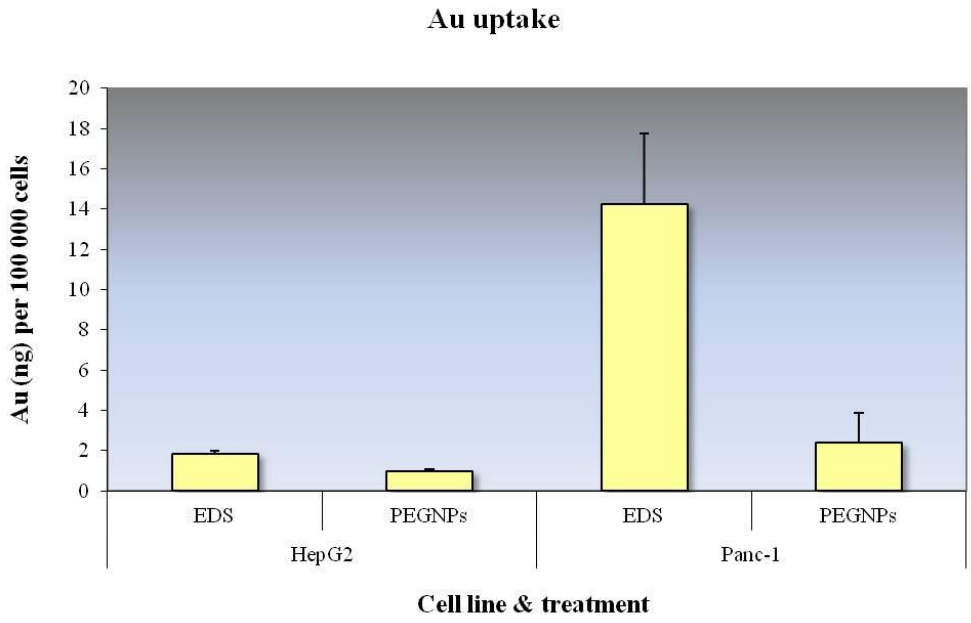

Figure 28. Gold content (ng/100.000cells) in EDS- and PEGNP-treated HEPG2 and Panc-1, analyzed by ICP-MS (mean (SD)). EDS uptake was higher in CD44-positive Panc-1 than in CD44-negative HEPG2. Uptake of non-targeted PEGNPs was low in both cell lines.

After demonstrating that internalization, and therefore targeting, of EDS in different cell lines seems to depend on the expression levels of CD44, we wanted to examine whether the same can be seen in one cell line with down-regulated CD44 compared to the normal levels. CD44 expression was knocked down on protein level with siRNA. After 30 min treatment with EDS the cells were harvested as described earlier and analyzed the uptake of gold by ICP. We found that down-regulating CD44 – but not RHAMM – reduced gold uptake substantially. The down regulation of the two receptors was confirmed by western blot (Figure 29).

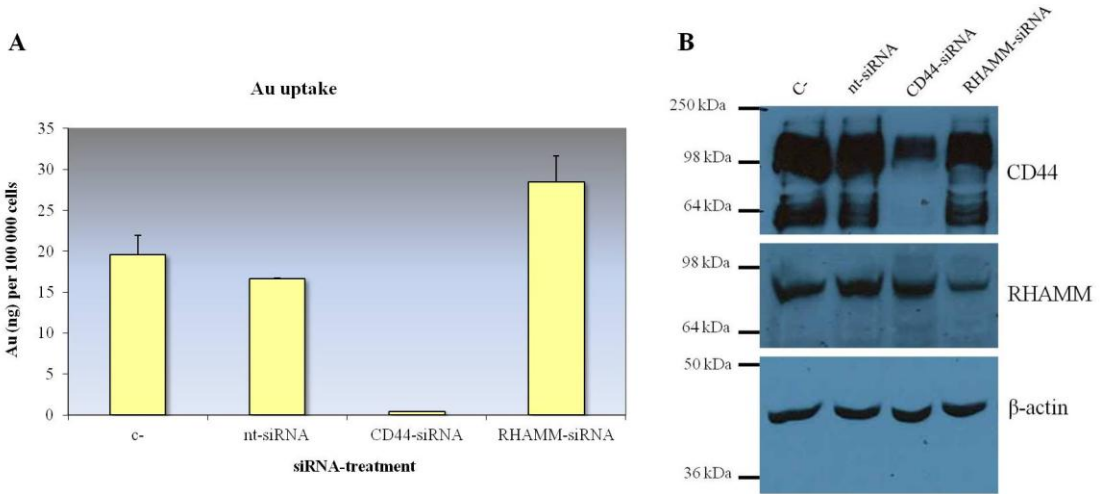

Figure 29. Gold content of CD44- and RHAMM-silenced Panc-1 (A). Only CD44 knock down resulted in a decrease of gold uptake. CD44 and RHAMM silencing were confirmed by WB (B) (mean (SD)).

The immunofluorescent uptake studies further confirmed the results of the TEM studies showing that the nanosystem targets CD44: Au was found inside the cells and internalization seemed to depend on the expression levels of the HA-receptor. We were able to visualize the nanosystems in two cell lines expressing intermediate and high levels of CD44 (MDA231 and Panc-1, respectively), but failed to see the nanosystem inside a cell line that does not express the receptor for HA (MCF-7.) By studying internalization of EDS in cells with varying CD44 expression levels by ICP-MS, we achieved information about the absolute quantities of the nanoparticles inside cells and showed that down-regulation of CD44 decreases EDS uptake.

3.1.3 Toxicity of EDS

Besides carrying the drug into its target tissue, an efficient delivery system needs to be safe and it cannot cause toxic effects itself. To ensure the safety of EDS we studied its possible toxicity *in vitro* and *in vivo*.

3.1.3.1 *In vitro* toxicity

In vitro cytotoxicity of the nanosystem was studied by cell viability assays. Genotoxicity was determined by Ames bacterial mutagenicity test and the DNA damage measuring comet assay, and the capability of EDS to produce reactive oxygen species and therefore damage to cellular structures was measured by ROS assay.

3.1.3.1.1 Cell viability

In order to find the most compatible assay with gold nanoparticles, different commonly used assays, including NR and WST-1 in addition to MTT, were tested to evaluate cell viability after NP treatment. However, they all showed interference with AuNPs. Finally, hexosaminidase assay proved to be the most suitable. This assay uses 4-Nitrophenyl N-acetyl-beta-D-glucosaminide, a substrate for an endogenous hexosaminidase, that catalyzes cleavage of 4-nitrophenol, which can be measured by spectrophotometry. Compared to the other methods, hexosaminidase assay utilizes a wavelength that differs greatly from the absorption peak of AuNPs and does not interact with them (Figure 30).

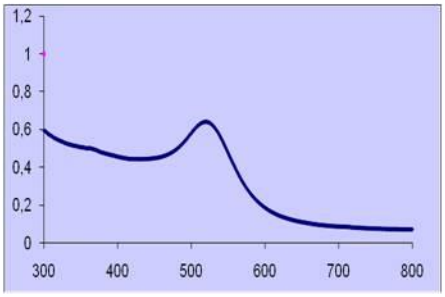

Reagent	Wavelength
MTT	570 nm
NR	550 nm
WST-1	450 nm
Hexosaminidase	410 nm

Figure 30. The absorption peak of AuNPs (left) is at 520nm. Wavelengths of different cytotoxicity assays employed to quantify cell viability (right).

3.1.3.1.2 IC50

After validating the most suitable assay, cell viability was studied in different cell lines expressing different levels of CD44. The IC50 in the chosen three cell lines expressing different levels of the HA-receptor showed that the cell lines expressing more CD44 produce a lower IC50 than cell lines with lower CD44 levels (Table 22).

	A549	Panc-1	HEPG2	BxPC3
IC50	88 ± 48 ppm	97 ± 42 ppm	286 ± 60 ppm	177 ± 24 ppm

Table 22. IC50 of EDS in cell lines expressing differing levels of CD44 (mean (SD)).

3.1.3.1.3 Ames test

Possible mutagenic properties of EDS were studied by the Ames salmonella/microsome mutagenicity assay. Three *Salmonella typhimurium* (TA98, TA100 and TA1535) strains and one *Escherichia coli* (WP2 UVrA) strain were subjected to EDS and the rate of their reverse mutation due to the treatment was measured after the characteristics of the different strains were verified by genetic analysis. EDS showed no mutagenicity with the four bacteria strains tested compared to the negative control (spontaneous mutant frequency, Table 23), not even with high concentrations (Figure 32 & Figure 33). PEGNPs were used as control.

Bacteria strain	Spontaneous mutant frequency
S. typhimurium TA98	13,5 ± 5,5
S. typhimurium TA100	190,7 ± 34,7
S. typhimurium TA1535	21,5 ± 6,4
E. coli WP2 uvrA (pKM101)	16,3 ± 3,2

Table 23. The spontaneous mutant frequency measured in the employed bacteria strains (mean (SD)).

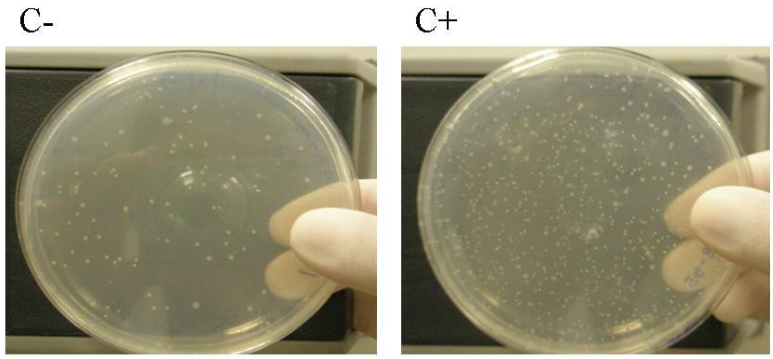

Figure 31. *S. typhimurium* TA100 c- and c+ plates.

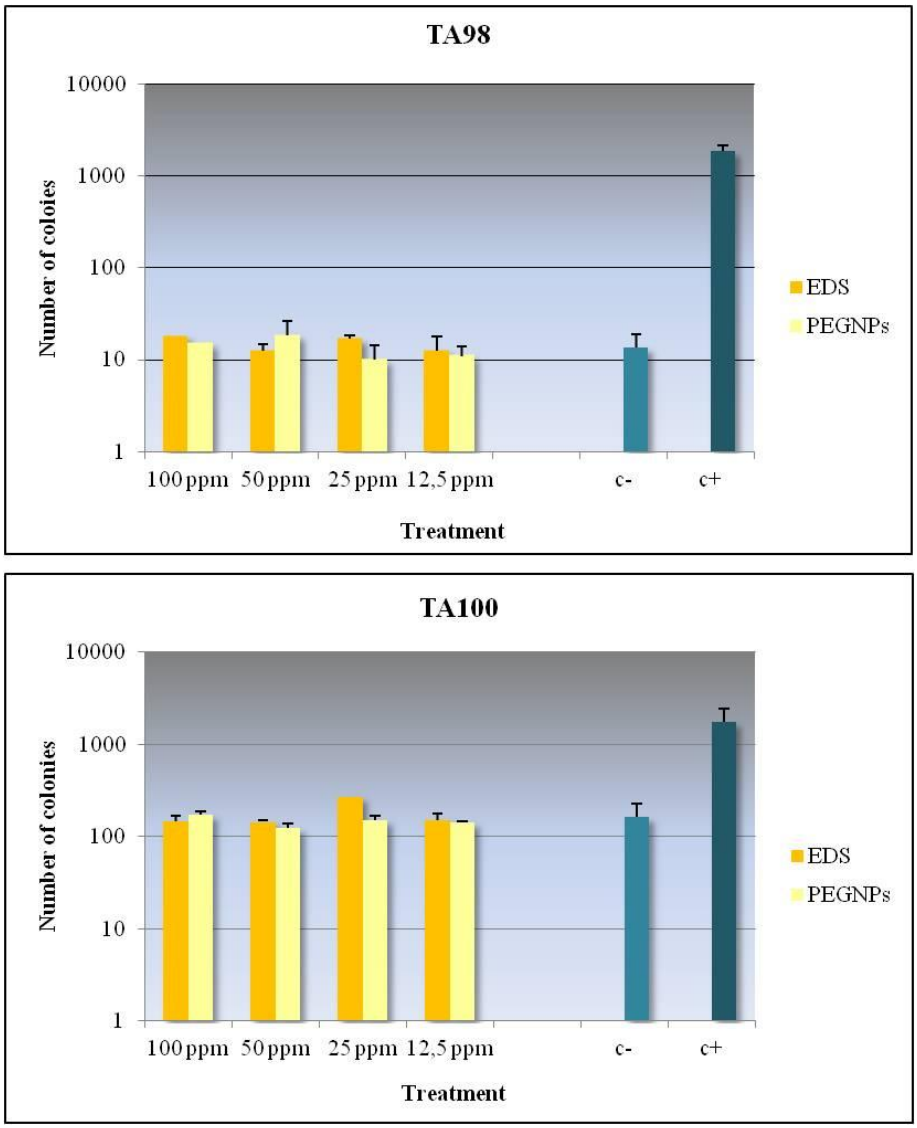

Figure 32. Ames reverse mutation test in *S. Typhimurium* TA100 and TA98, TA1535 strains (mean (SD)). EDS did not show mutagenicity in the tested strains.

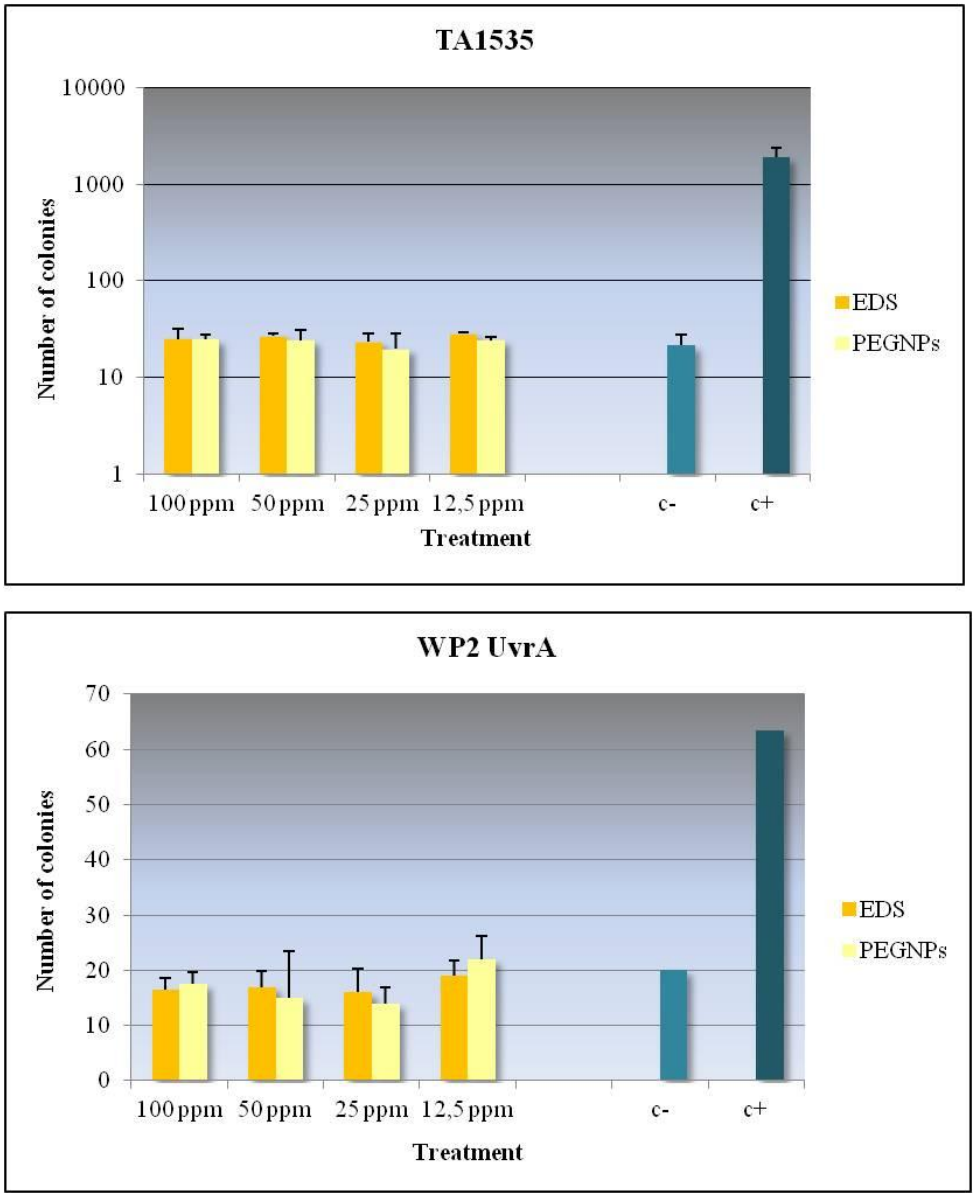

Figure 33. Ames reverse mutation test in *S. Typhimurium* TA1535 and *E. Coli WP2 UVrA* strains (mean (SD)). EDS did not show mutagenicity in the tested strains.

3.1.3.1.4 Comet assay

The effects of EDS on DNA were studied by comet assay. This assay measures DNA damage at the level of individual eukaryotic cells. Panc-1 cells were treated with EDS and subjected to alkaline comet assay. There was no evidence of DNA damage in the EDS-treated cells (Figure 34). PEGNPs were used as a NP control.

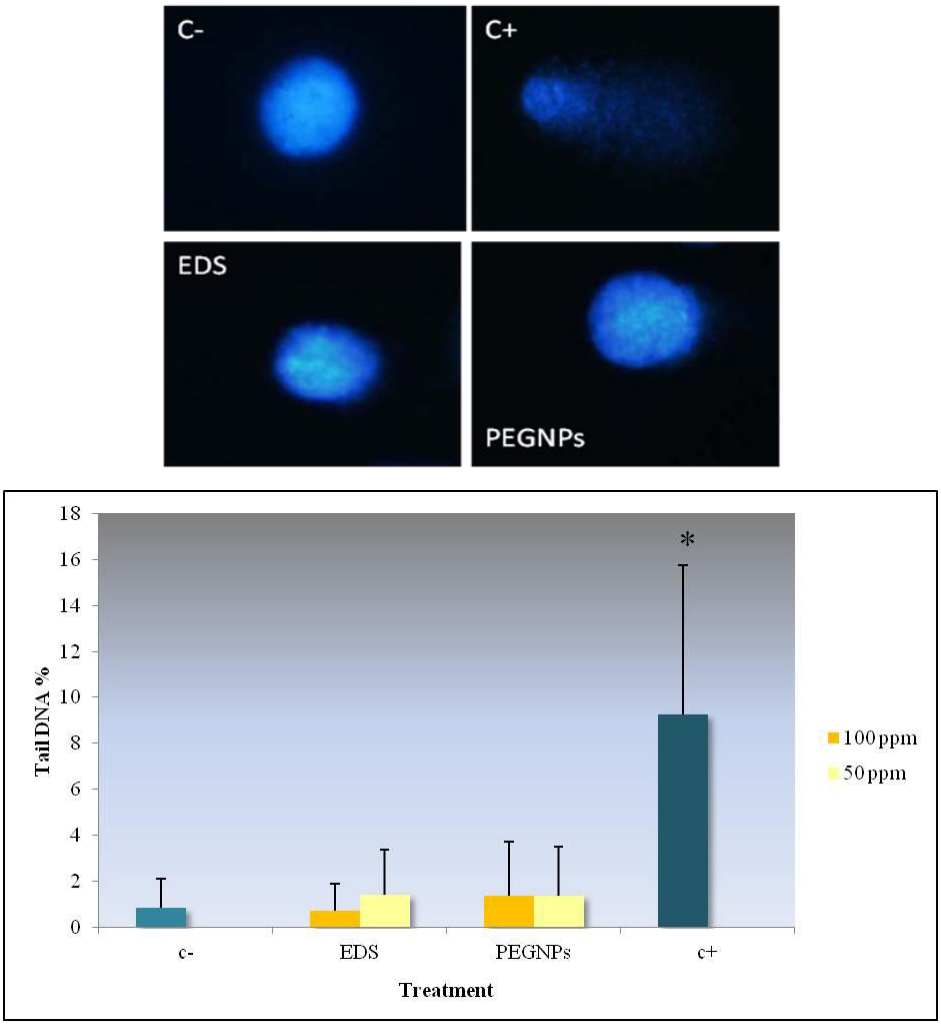

Figure 34. Panc-1 single cells subjected to comet assay (above) and the tail DNA percentage analyzed in 50 cells by the CaspLab - Comet Assay Software Project (below) (mean (SD)). EDS did not produce DNA damage.

3.1.3.1.5 ROS assay

Panc-1 cells were treated with EDS and collected for fluorometric ROS analysis at different timepoints. We found that EDS did not cause any increase in ROS production during the 24-hour timecourse (Figure 35 and Figure 36). The ROS producing effect of the positive control (diethyl maleate) was transitory due to cell death that occurred between 4 and 6 h treatment.

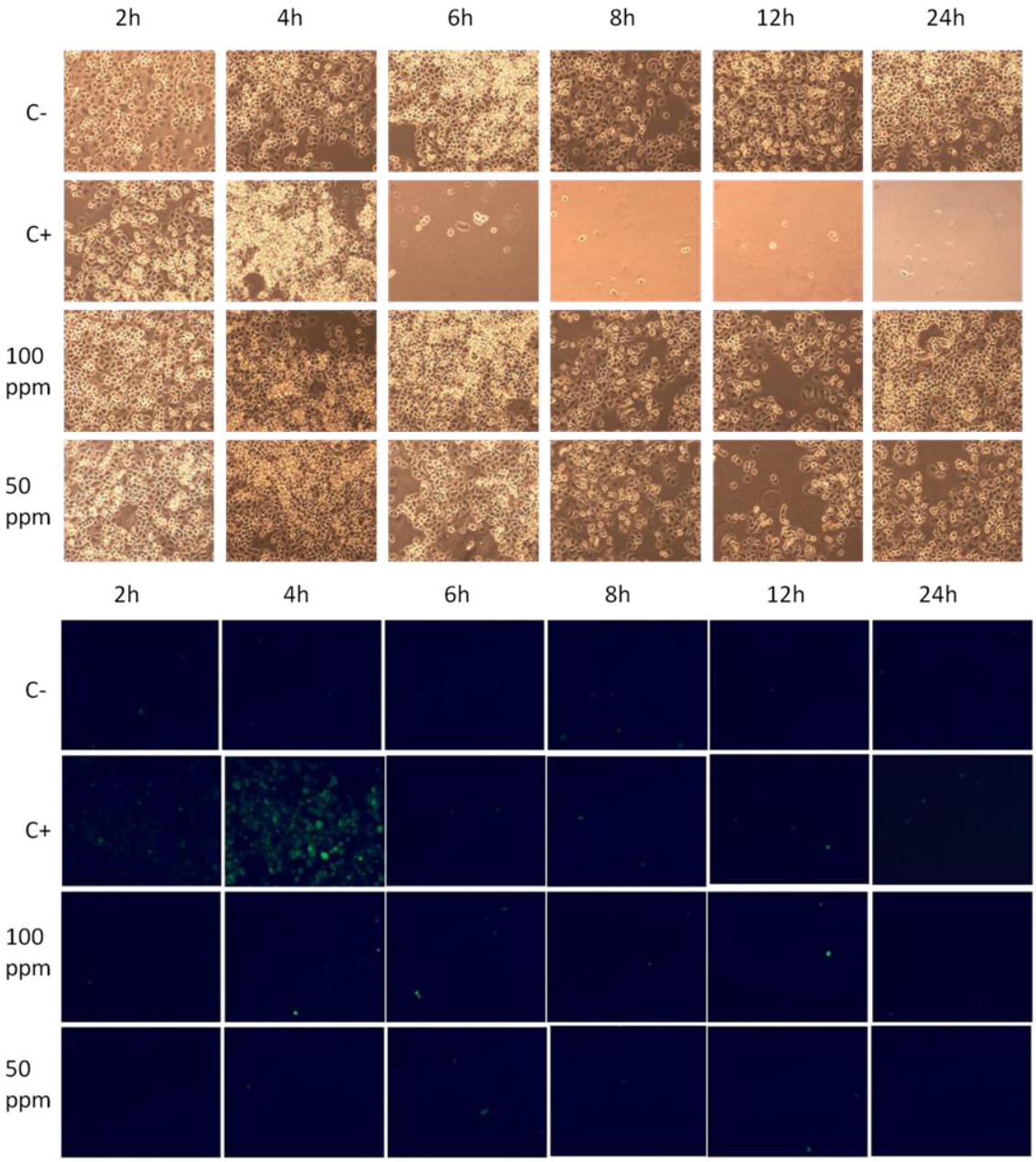

Figure 35. ROS production by EDS-treated Panc-1. Cells were visualized by light microscope (above) and fluorescent microscope (below) before reading the fluorescence to confirm results. EDS did not cause ROS production during the time course.

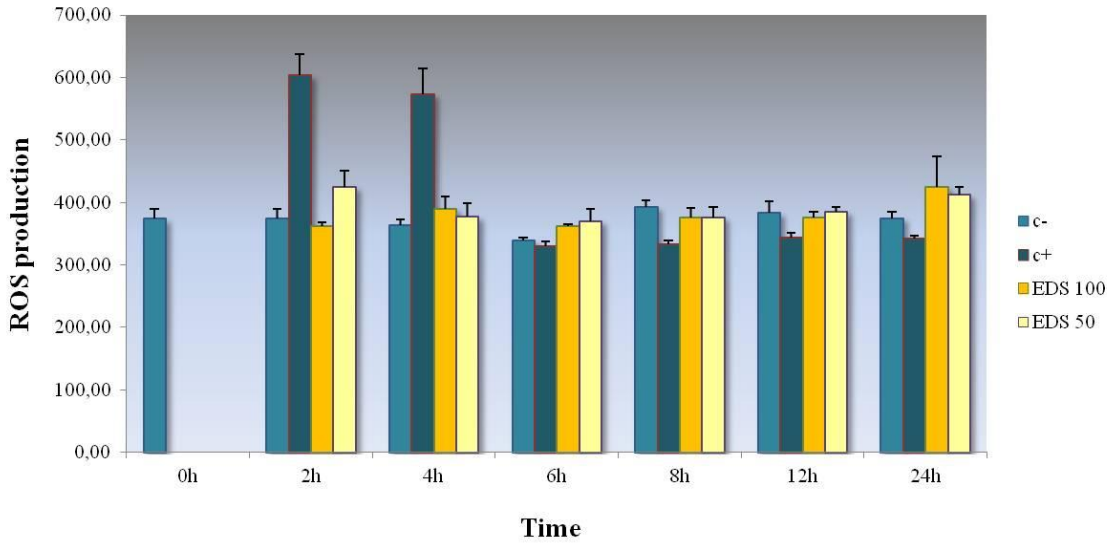

Figure 36. ROS production by EDS-treated Panc-1 measured by fluorescent plate reader. Y-axis: relative fluorescence units, X-axis: time (mean (SD)). EDS did not cause ROS production during the time course.

Even though EDS caused a slight decrease in cell viability, our studies demonstrated that it did not cause cellular damage. The nanosystem did not cause genotoxicity, which was proven by two different assays: bacterial reverse mutation test and single cell gel electrophoresis. We did not find EDS creating an increase in ROS production either.

3.1.3.2 *In vivo* toxicity

To determine the fate of our nanocarrier in the body, its biodistribution in tumor-bearing mice was studied and histology and silver staining performed for the organs that accumulated the most gold in order to study the possible toxicity caused to the organ and to visualize the accumulated NPs. The weight of the animals was monitored throughout the biodistribution experiment and possible systemic toxicity was measured by blood biochemical analysis.

3.1.3.2.1 CD44 expression in Panc-1 xenografts

CD44 expression in mouse tumor, spleen, lymph nodes, pancreas, kidney, stomach, intestine, liver and heart was characterized by immunohistochemical staining in Panc-1 xenografts by CIBBIM Nanomedicine (Vall d'Hebron Institut de Recerca).

The highest CD44 staining was found in the tumor, as expected. CD44 staining was also observed in:

- Tissues with high inflammatory cell content (spleen and lymph nodes)
- Epithelia of the intestine
- Epithelia of the stomach
- Kupffer cells in the liver

Staining was scarce in pancreas and kidneys, and absent in the heart (Figure 37).

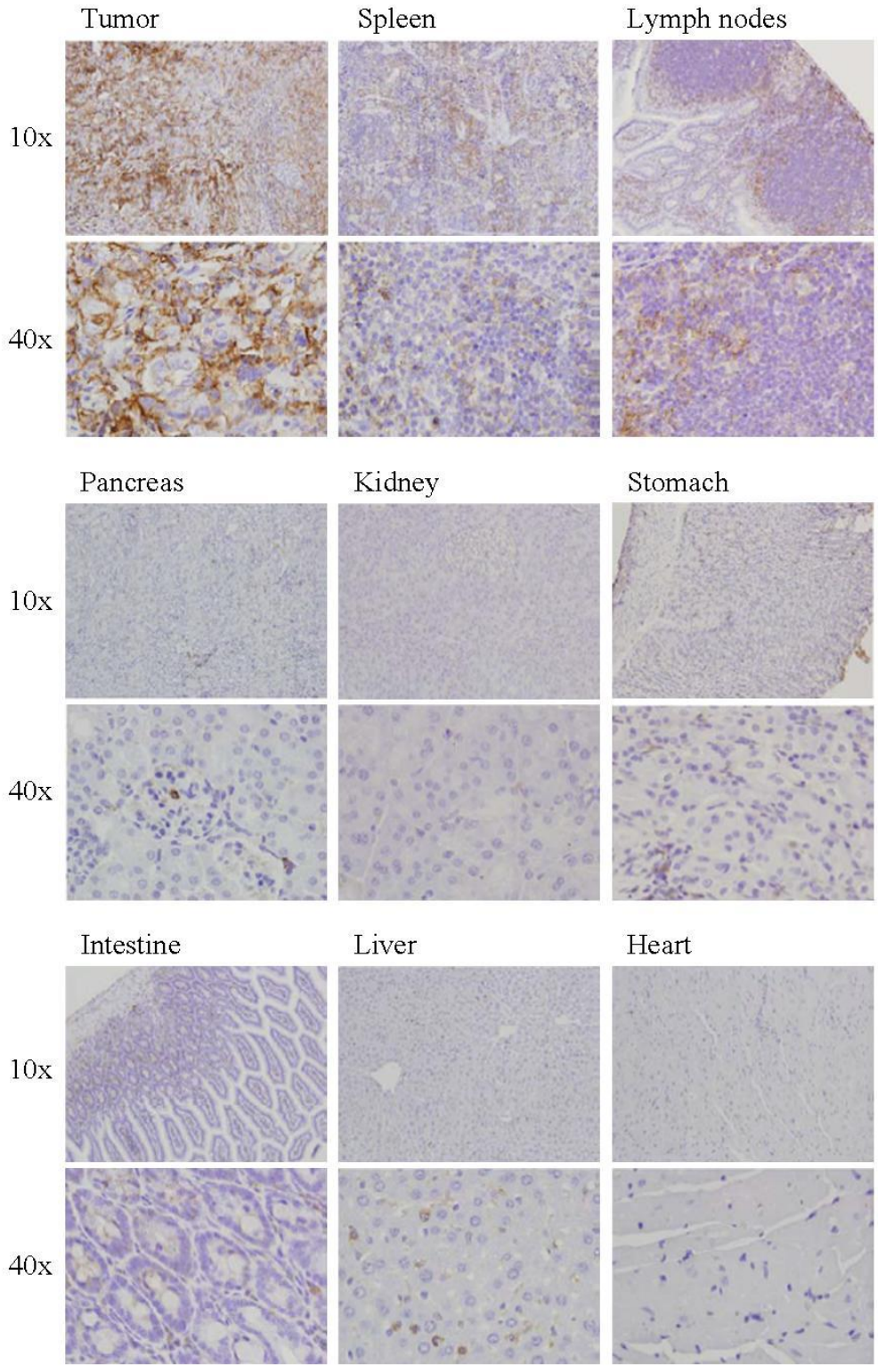

Figure 37. CD44 staining in various organs of the Panc-1 xenografts.

3.1.3.2.2 Blood circulation

Blood levels of EDS were studied in tumor-bearing mice. The quantity of Au showed an increase until 4 h, and then started a gradual decrease. After 12 h half of the Au was cleared from circulation, and at 24 h post-injection, practically all Au was cleared from circulation (Figure 38).

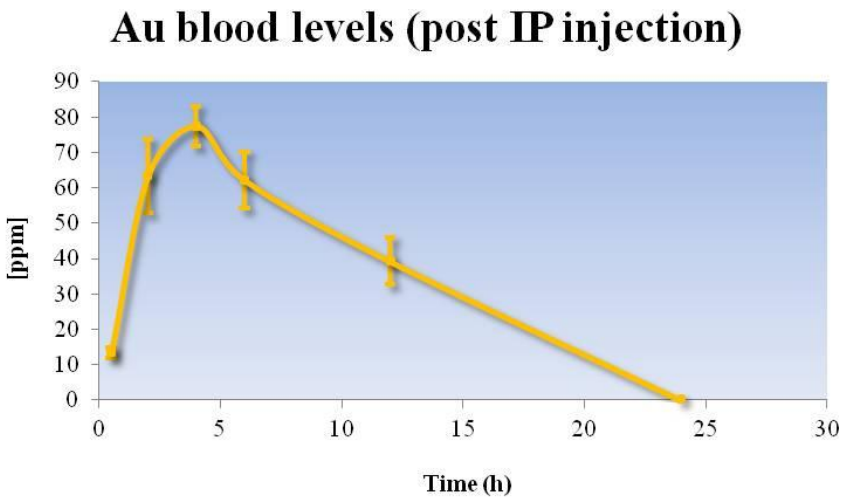

Figure 38. EDS blood levels after a single intraperitoneal injection until 24 h (mean ± SEM).

3.1.3.2.3 Biodistribution

Biodistribution of EDS was studied in two xenograft models, HT1080 (intermediate CD44 levels) and Panc-1 (high CD44 levels) that showed very similar patterns. The highest accumulation of gold after 8 doses of EDS administered during four weeks, was detected in the liver (74,06 % in HT1080 and 63,01 % in Panc-1) followed by skin (18,89 % in HT1080 and 9,52 % in Panc-1) and tumor (1,66 % in HT1080 and 0,83 % in Panc-1). Very small amounts of gold were also detected in the kidneys, lungs and bone marrow (Figure 39 & Figure 40).

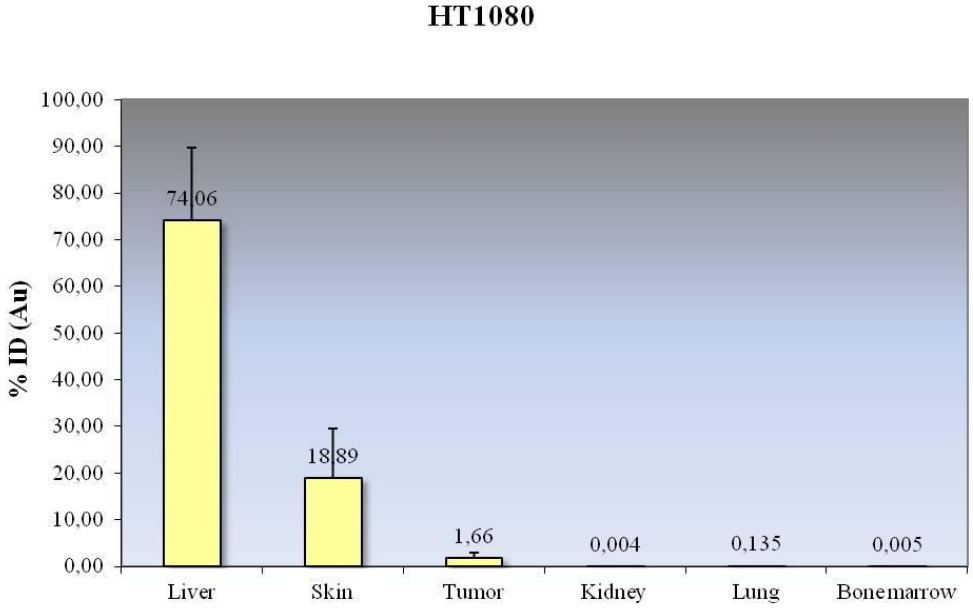

Figure 39. Biodistribution of EDS in a HT1080 xenograft model. Data is represented as percentage of the injected dose (mean (SD)).

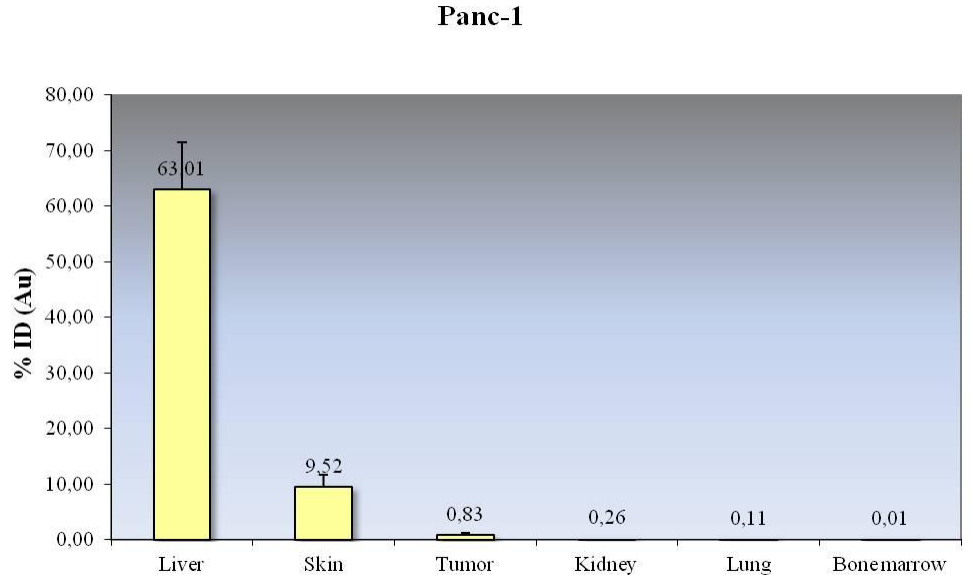

Figure 40. Biodistribution of EDS in Panc-1 xenograft model. Data is represented as percentage of the injected dose (mean (SD)).

3.1.3.2.4 Animal weight

The weight of the animals of the biodistribution studies was measured during the experiment. The animals receiving EDS did not suffer any weight loss during the experiment in either of the xenograft models (Figure 41, HT1080 presented).

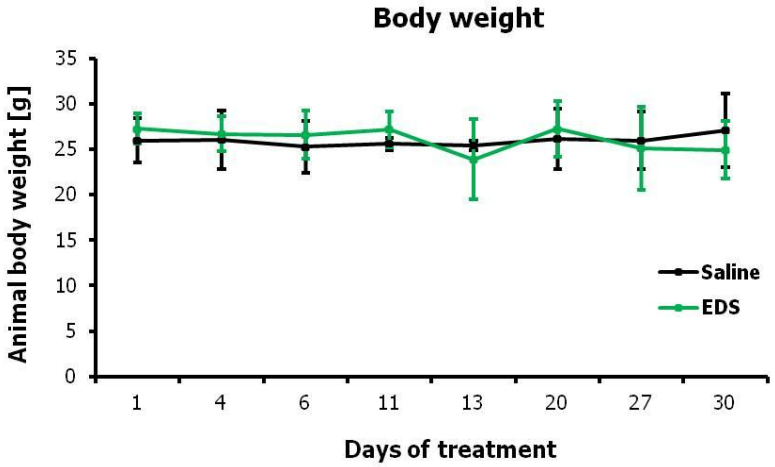

Figure 41. Animal body weight during biodistribution study (mean ± SEM).

3.1.3.2.5 Histology: tissue morphology (H&E and silver staining)

The two organs that accumulated most gold (liver and skin) in the HT1080 xenograft model were also subjected to histological analysis to visualize nanoparticles and to study possible changes in tissue morphology. The stainings were performed by the Unit of Experimental Toxicology and Ecotoxicology (UTOX-PCB).

Since the highest accumulation was seen in the liver by ICP-MS, hematoxylin and eosin staining (H&E) was enough to show the nanoparticles. The nanoparticles were found to be localized in Kupffer cells interposed between hepatocytes, but no evidence of toxicity was seen; the hepatic lobules seemed intact and we did not find signs of necrosis or inflammation (Figure 42).

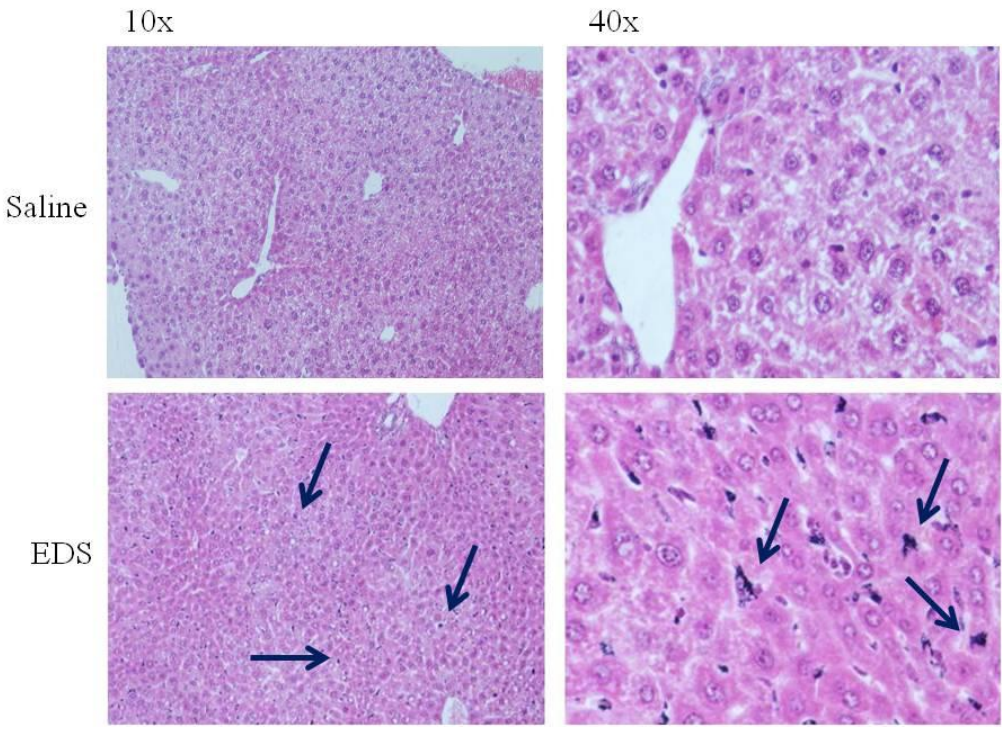

Figure 42. Liver H&E staining of athymic nude mice after EDS administration in athymic nude mice. NPs are localized in Kupffer cells between hepatocytes.

Gold accumulation levels in skin were lower than in liver, so in order to better visualize the nanoparticles in these tissues, silver enhancing was performed. Gold was found accumulated in the dermis of the skin (Figure 43) but we could not detect any morphological changes compared to the control mice.

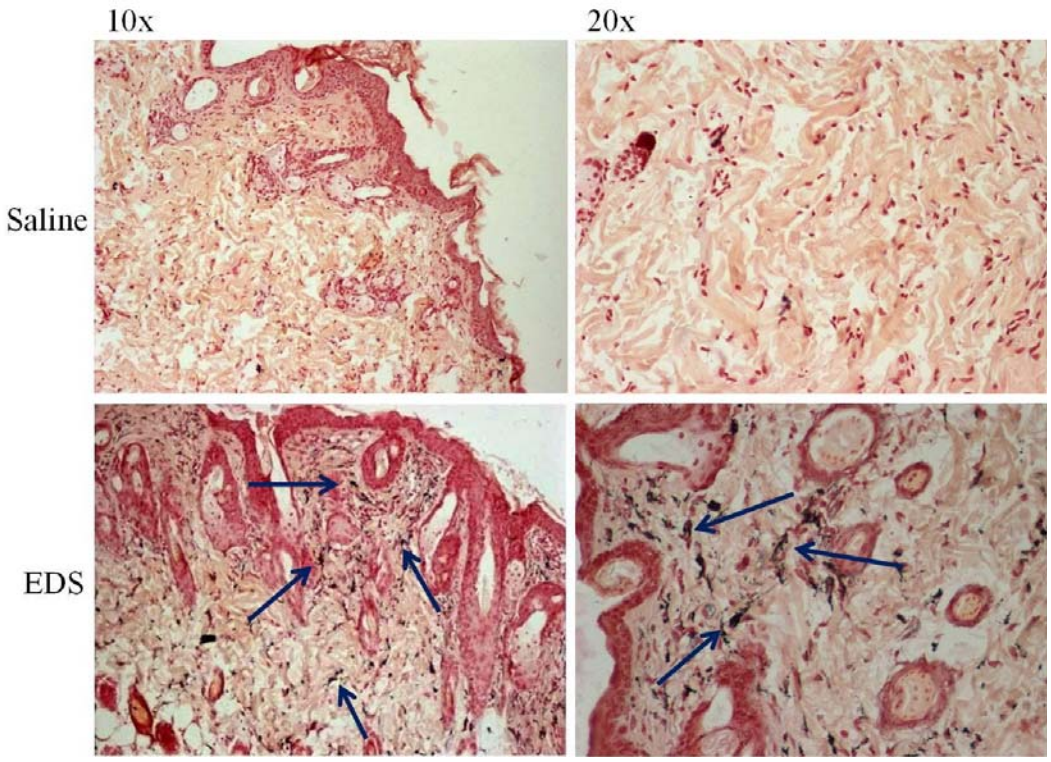

Figure 43. Skin silver staining of athymic nude mice after EDS administration. NPs were found in the dermis.

3.1.3.2.6 Blood biochemical analysis

To further study the possible toxic effects of EDS *in vivo*, a blood biochemical analysis was performed. HT1080 and Panc-1 tumor-bearing mice received 8 doses of EDS (10 mg/kg) during a time period of 4 weeks. The analysis was performed after the first week of the study to analyze acute toxicity and at the end of the experiment to study long term toxicity. We found no evidence of pancreatic (albumin), hepatic (albumin, GOT, GPT) or renal (urea) damage, none of the analyzed parameters showed an increase due to a single EDS administration or repeated injections (Table 24) despite the accumulation in liver that was found by ICP-MS and histology.

1 week	Albumin (g/dl)	Urea (mg/dl)	GPT (U/l)	GOT (U/I)
Saline HT1080	4,2 ± 0,42	43,25 ± 3,77	73,25 ± 11,87	111 ± 4,97
EDS1 HT1080	4,2 ± 0,24	36,75 ± 1,50	54,5 ± 22,16	86,25 ± 12,82
Saline Panc-1	3,98 ± 0,15	51 ± 10,10	37,5 ± 1,73	109,5 ± 14,18
EDS1 Panc-1	4 ± 0,35	49 ± 1,73	35 ± 3,46	133 ± 25,16

4 weeks	Albumin (g/dl)	Urea (mg/dl)	GPT (U/l)	GOT (U/I)
Saline HT1080	4,2 ± 0,52	41,67 ± 2,52	70 ± 12,17	111,33 ± 6,03
EDS1 HT1080	3,4 ± 0,28	30,5 ± 3,54	29 ± 1,41	109 ± 26,87
Saline Panc-1	3,69 ± 0,23	42,86 ± 7,69	41,57 ± 8,02	114,86 ± 22,03
EDS1 Panc-1	3,53 ± 0,23	39,67 ± 9,07	33,67 ± 7,29	122,33 ± 37,41

Table 24. Blood biochemical analysis of the biodistribution study in HT1080 & Panc-1 xenograft models. Above: analysis after 1 week, below: analysis at the end of the experiment (mean (SD)).

EDS did not show signs of toxicity when administered to tumor bearing mice, despite of its high accumulation in the liver. The animals did not lose weight, show abnormal morphology or damage in the tissues with the highest gold accumulation. Blood biochemical analysis showed no signs of hepatic, renal or pancreatic damage.

3.2 Characterization of EDS-Drug

Double-conjugate characterization was started by studying first different strategies to link the drug to the nanocarrier followed by stability, cell viability and blood circulation time studies. The final candidate was chosen based on these studies and the chemical characterization of this candidate was performed. Internalization studies followed chemical characterization and finally the efficacy and toxicity of the double conjugates *in vitro* and *in vivo* were studied.

Cisplatin was the first drug used as the delivered anti-cancer agent. As the other members of this class – carboplatin and oxaliplatin – it crosslinks to DNA interfering with cell division which ultimately triggers apoptosis of the cancer cells.

3.2.1 Drug conjugation strategies

The three different conjugation strategies for cisplatin produced the three candidates presented in the Materials and Methods-section. To define the best candidate for further studies, candidates A, B and C were compared by determining gold and platinum quantities in solution after synthesis and in blood after intraperitoneal and intravenous injections.

3.2.1.1 ICP-MS

The concentrations of Au and Pt of candidates A, B and C were quantified (Table 25). Different concentrations of Cisplatin in synthesis were included in the study. Based on the outcome of the ICP-MS analysis, the Pt/Au ratio of each candidate was calculated.

	Product & $C_{synthesis\ Cis}$	Au (ppm)	Pt (ppm)	Cis (uM)	Pt /Au
A: Linker 1	EDS-L1-CIS 9,95 uM	171,1	2,02	10,35	0,012
	EDS-L1-CIS 825 uM	187,67	9,69	49,67	0,05
B: Linker 2	EDS-Mua-CIS 9,95 uM	205,32	2,64	13,53	0,013
	EDS-Mua-CIS 825 uM	207,3	55,62	285,11	0,27
C: Encapsulation	EDS-CIS 200 uM	791,17	25,57	131,07	0,32
	EDS-CIS 5000 uM	822,25	545,08	2794,08	0,66
	EDS-CIS 20 000 uM	1000,08	1797,77	9215,36	1,8

Table 25. Three different strategies were tested to load cisplatin on the nanosystem. Gold and platinum amounts were determined by ICP-MS, the ratio Pt/Au was calculated.

As candidate A had the lowest drug load of the three candidates, it was discarded at this point and the candidates produced by using the linker Mua and the encapsulation strategy proceeded to further studies.

3.2.1.2 Biological characterization of double conjugates

In order to compare the two drug conjugation strategies (B and C), *in vitro* cytotoxicity testing was performed. Through *in vivo* studies their kinetics in blood circulation were analyzed.

3.2.1.2.1 *In vitro* characterization

To study *in vitro* effects of the two candidates (B: EDS + Mua + CIS & C: EDS + CIS) destined for further studies, cytotoxicity studies in the lung cancer cell line A549 were performed. Candidate B was found less toxic of the two candidates, and the IC50 between different production batches could vary almost 10-fold (from 7,6 to 52,1 uM Cis). EDS-Drug C on the other hand showed more reproducibility, IC50 between batches were quite similar (Figure 44).

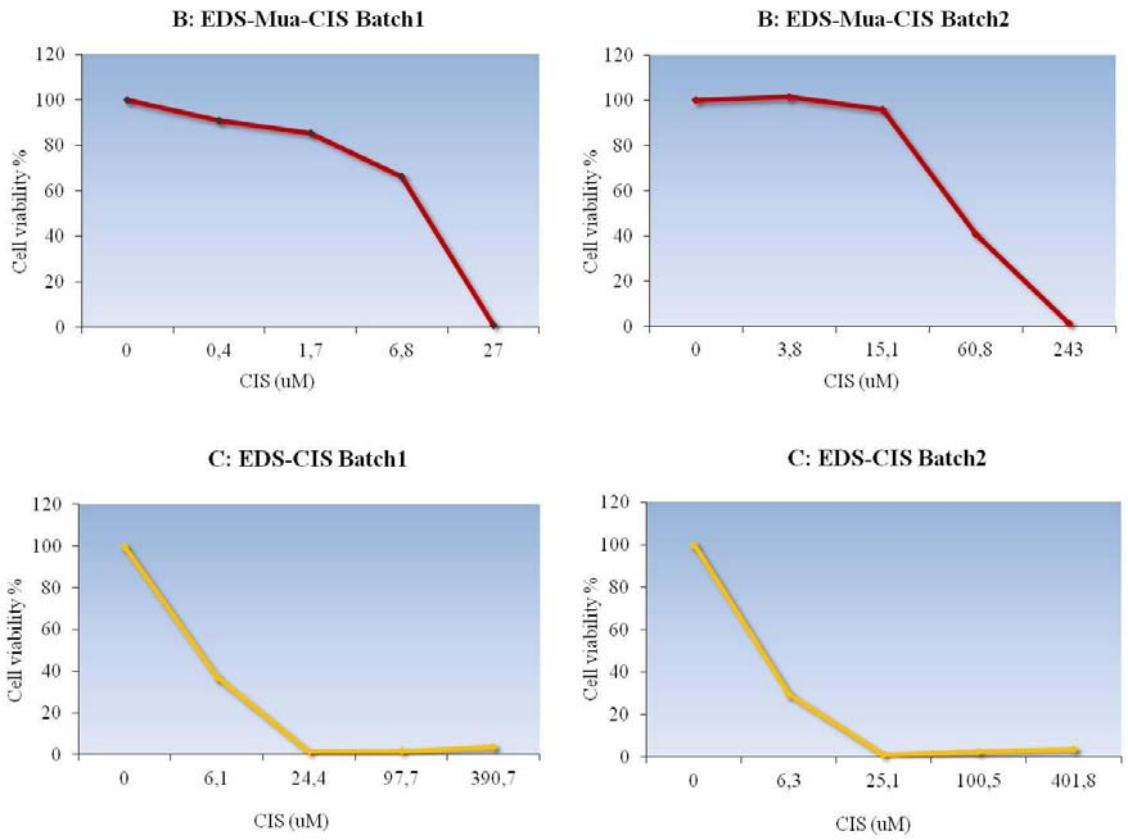

Figure 44. EDS-Mua-Cis and EDS-Cis cytotoxicity in A549.

3.2.1.2.2 *In vivo* characterization

In order to compare the behavior of candidates B (EDS + Mua + CIS) and C (EDS + CIS) *in vivo*, they were injected intravenously and intraperitoneally in athymic nude mice. Candidate B was cleared very fast from circulation after IV injection: 1h after injection we did not detect practically any gold or platinum. Also after IP injection candidate B was almost completely cleared from blood 4h post-injection and the levels at 1h were significantly lower than with candidate C. Candidate C produced higher concentrations of both Au and Pt in blood at all time points and its clearance was greatly slower (Figure 45).

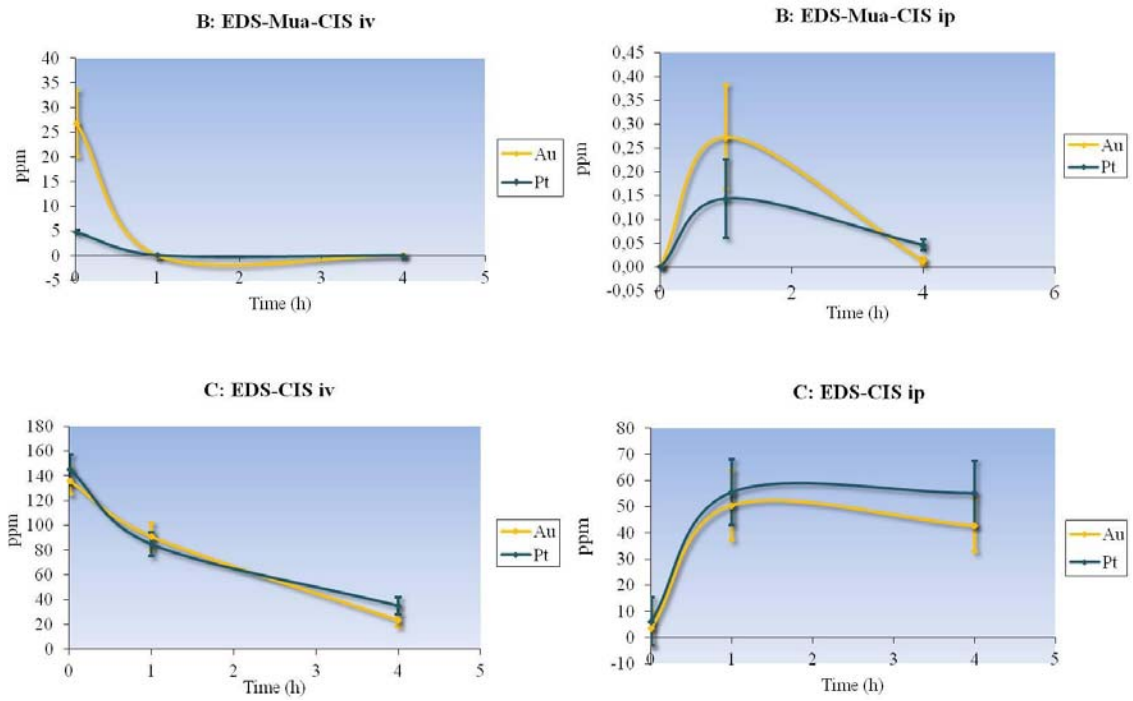

Figure 45. Au and Pt levels in blood after IV and IP injections of drug conjugation candidates B (EDS + Mua + CIS) and C (EDS + CIS) until 4 h post-injection (mean (SD)).

Due to results of Pt/Au ratios and in vitro & in vivo stability studies, candidate C, that was produced by encapsulating the drug in the HA-coating of the NPs, was chosen as the final candidate and proceeded to chemical characterization. With this candidate we were able to reach the highest drug load per nanoparticle and it showed higher stability and a longer blood circulation time than the other candidates.

Further on in this study, candidate C will be referred to as EDS-CIS, meaning the three-part drug delivery system (gold NP – hyaluronic acid – cisplatin) resulting in approximately 9 mM cisplatin in 1000 ppm gold solution.

3.2.2 Chemical characterization of EDS-CIS

3.2.2.1 TEM

EDS-CIS was visualized by TEM after double conjugation in order to study the size and state of dispersion of the nanosystem. Similar to the nanocarrier before addition of the drug, AuNPs showed a size of 11,22 ± 2,50 nm and there was no sign of aggregation due to addition of the drug (Figure 46).

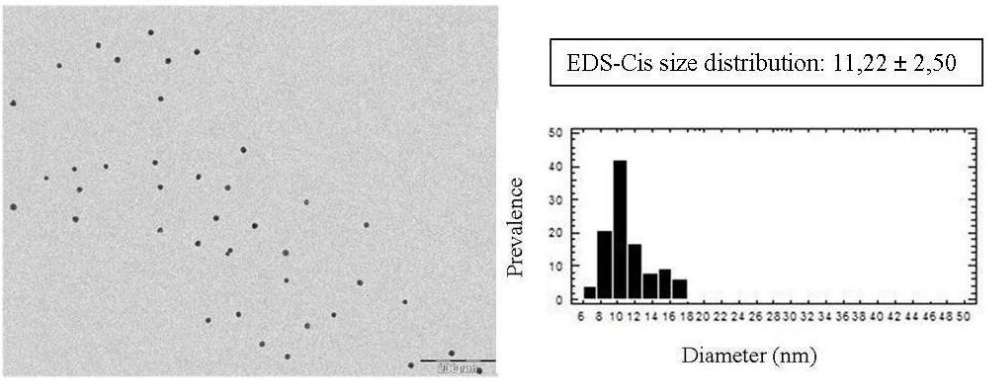

Figure 46. TEM image of EDS-CIS. NPs were found disperse and of low size distribution.

3.2.2.2 UV-VIS

The UV-VIS analysis of EDS and EDS-CIS showed that the absorbance peak of the nanosystem shifted slightly from 524 nm to 532 nm, when the drug was conjugated (Figure 47).

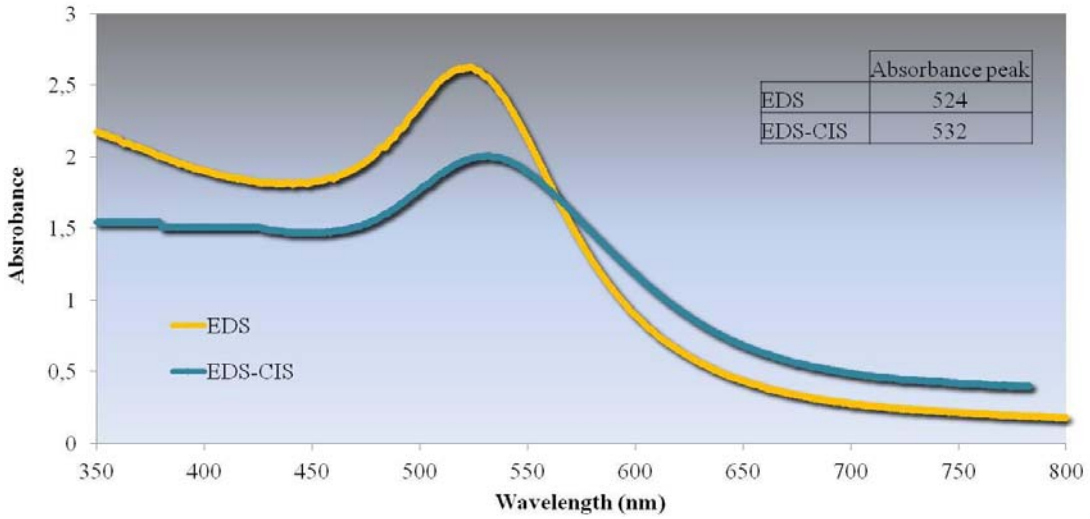

Figure 47. Absorption spectra of EDS and EDS-CIS showing the slight shift to the right of EDS-CIS.

3.2.2.3 DLS

DLS revealed the hydrodynamic diameter of EDS-CIS to be slightly smaller than that of EDS. This could be due to the crosslinking effect of cisplatin; it may link to different HA-chains and pulling the chains closer to each other. The average size of EDS was at 97,7 nm and that of EDS-CIS at 83 nm (Figure 48).

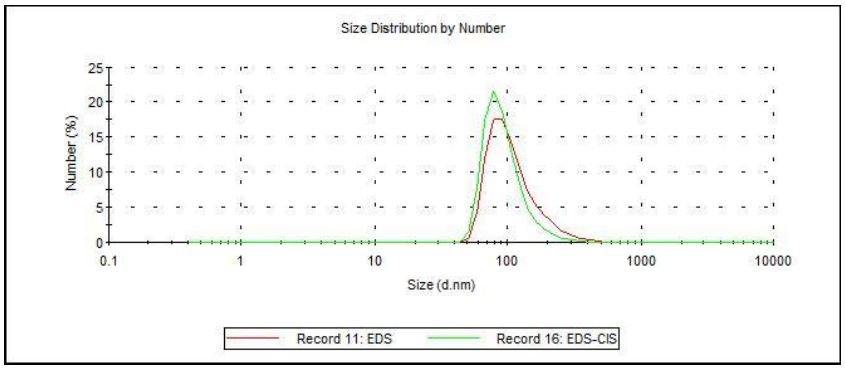

Nanosystem	Size (nm)
AuNPs	11,56 ± 0,2
EDS	97,7 ± 6,9
EDS-CIS	83,0 ± 7,2

Figure 48. Size distribution of EDS-CIS and EDS (mean (SD)).

3.2.2.4 Z-potential

Z potential of bare NPs was -38,5 mV and when coated with the HA, surface charge remained very similar. As cisplatin in the double conjugate is encapsulated in the HA, it had no effect in the surface charge of the conjugate (Table 26).

Nanosystem	Z pot (mV)
AuNPs	-38,5 ± 1,8
EDS	-38,2 ± 1,3
EDS-CIS	-40,7 ± 4,5

Table 26. Z-potential comparing bare gold nanoparticles, EDS and EDS-CIS (below) (mean (SD)).

3.2.2.5 ICP-MS & EA

We determined the concentrations of gold and platinum in the EDS-CIS solution by ICP-MS, then calculated the Au/Pt ratio and the number of gold nanoparticles in the solution. Finally we calculated the number of HA chains around one NP by utilizing the results achieved from EA to quantify HA in the solution (Table 27).

	C_{Au} by ICP (ppm)	C_{Pt} by ICP (ppm)	C_{CIS} (µM)	Pt/Au	HA chains / NP
EDS	948, 96 ± 27,76	-	-	-	2158 ± 127
EDS-CIS	1018,31 ± 31,77	1563,19 ± 331,73	8015,08 ± 1702,21	1,9	2018 ± 349

Table 27. Concentrations of Au, Pt and HA in EDS and EDS-CIS solutions (mean (SD)).

Conjugating cisplatin to EDS does not change significantly its physico-chemical characteristics; TEM shows disperse NPs with an equal size when compared to EDS, absorbance peak only slightly shifts to right and surface charge remains similar. We detected a minor change in the hydrodynamic radius when conjugated to cisplatin.

3.2.3 Stability of EDS-CIS

For the drug to be able to exert its effect in a cancer cell it needs to be freed from the carrier. On the other hand, if drug is released before reaching the tumor, the nanocarrier cannot perform the targeting it is designed to reach. Accordingly, drug release and blood circulation time studies were the next step of this project.

3.2.3.1 *In vitro* drug release

EDS-CIS has been shown to be stable in water, releasing less than 10 % of the conjugated cisplatin (data from the doctoral thesis of Laura Vivero: "Diseño y caracterización de sistemas de liberación de fármacos basados en nanopartículas metálicas y ácido hialurónico", not presented here) during a time period of 3 months. Drug release from EDS-CIS was studied in PBS – representing biological media – at time points from 30 minutes to 72 hours. Close to 80 % of the drug loaded to the nanosystem, was released over time (Figure 49).

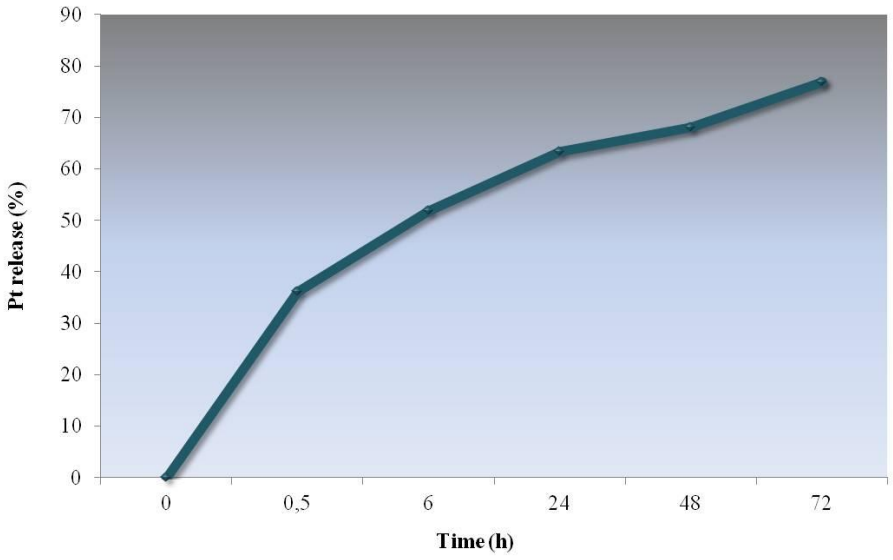

Figure 49. Drug release from the double conjugates in PBS. EDS-CIS showed a gradual release of Pt during the 72 h time course.

3.2.3.2 *In vivo* stability

EDS-CIS was injected into Panc-1 tumor bearing athymic nude mice intraperitoneally and intravenously in order to study the blood circulation time of the nanosystem. Blood was collected and plasma separated from the treated mice at 4 hours, 24 hours and 48 hours post injection and analyzed by ICP-MS. At 4 hours after treatment, the levels of gold were 14 % (ip) and 6 % (iv) of the initial dosis, while platinum levels were slightly lower, 8 % (ip) and 5 % (iv). At 24 hours practically all gold and platinum had been cleared from circulation (Figure 50). The injections and blood collecting of this *in vivo* stability study were performed by CIBBIM Nanomedicine (Vall d'Hebron Institut de Recerca).

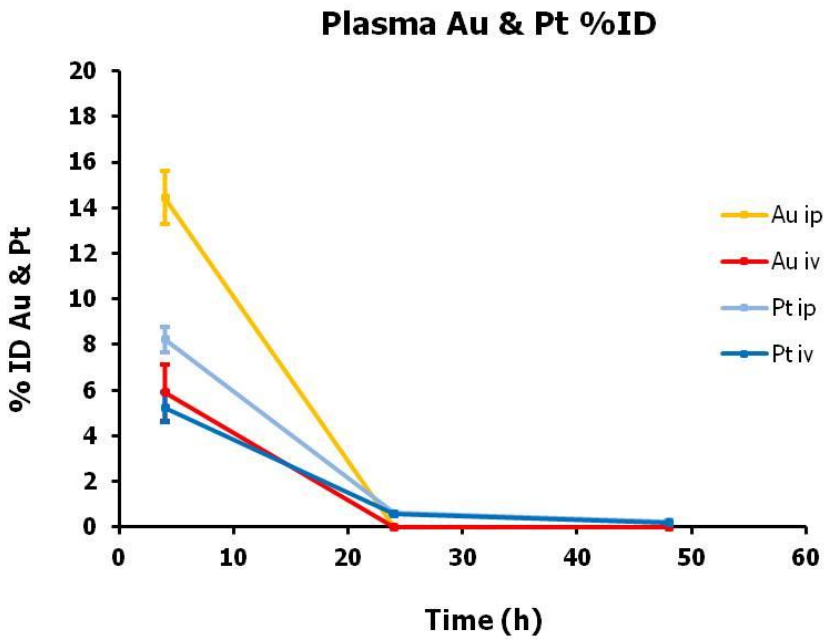

Figure 50. Plasma levels of Au and Pt after IP and IV injections of EDS-CIS during a 48 h time course (mean ± SEM).

Stability studies showed that the drug is gradually released from the nanocarrier in vitro. After in vivo injections, the quantities of Au and Pt in blood differed some especially when administered intraperitoneally (% ID), but the nanosystem shows to be quite stable in vivo.

3.2.4 Internalization of EDS-CIS

EDS-CIS internalization was studied in Panc-1 (high CD44 levels) and HEPG2 (low CD44 levels) to examine the possible differences in uptake when a drug was encapsulated in the carrier. Besides gold quantity, the amount of the Pt-based drug cisplatin internalized by the cells could be also analyzed with ICP-MS. Consistent with the earlier results, we found gold in Panc-1 pellets, but only very low amounts in HEPG2 (Figure 51). On the other hand while there was no internalized Au in HEPG2, we found Pt, which shows that the drug is released from the carrier and enters the cells, most probably due to hyaluronidase activity.

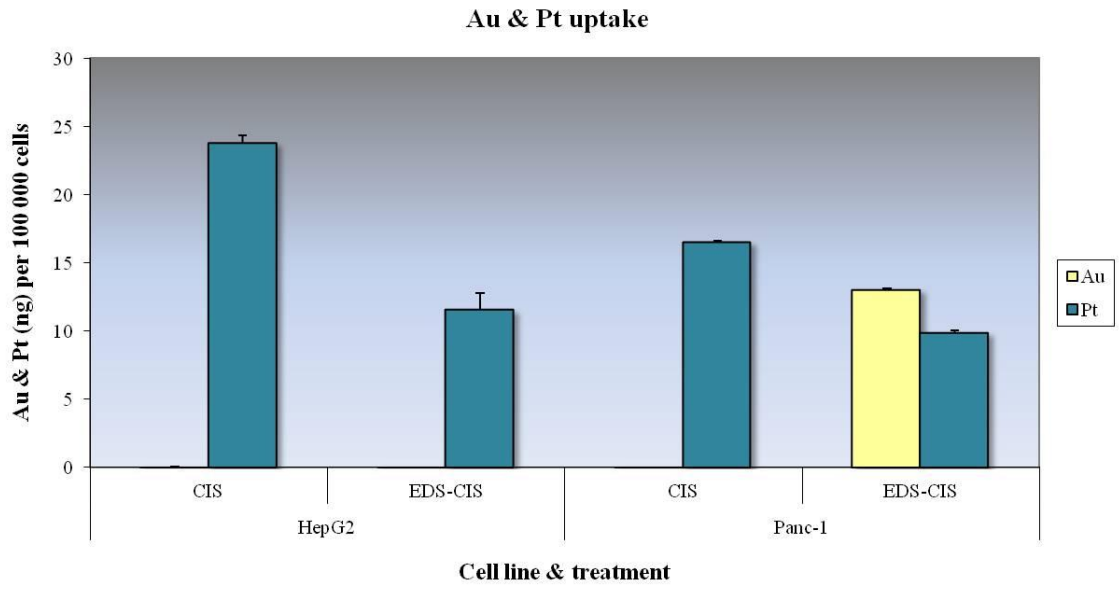

Figure 51. Quantities of Au and Pt in HEPG2 and Panc-1 after treating the cells with EDS-CIS and free drug (mean (SD)). Pt was found in both cell lines, when Au was only internalized by CD44-positive Panc-1 cells.

As with the nanocarrier, we then continued our uptake experiments by silencing the main receptor for HA (CD44) and a secondary receptor that is only known to bind HA (RHAMM) in Panc-1. As seen with the nanocarrier without the drug, knocking down CD44 led to lower levels of internalization of gold, but this reduction in uptake was not again seen when silencing RHAMM. On the other hand, the levels of Pt were very similar in both siRNA-treated cells compared to cells without previous siRNA-treatment (Figure 52).

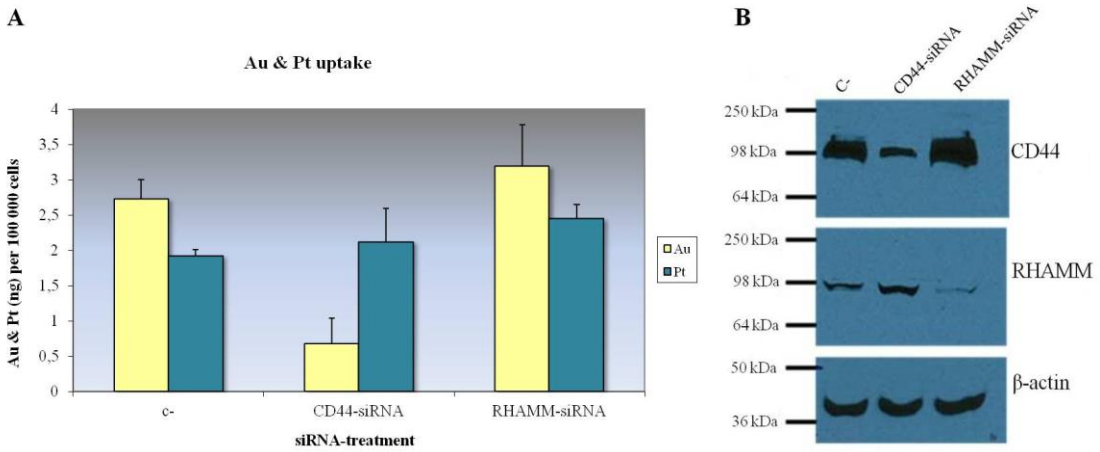

Figure 52. Uptake of Au & Pt in Panc-1 with CD44- and RHAMM-silencing (A). CD44 and RHAMM protein expression in silenced and non-silenced cells (B) (mean (SD)).

The internalization studies showed that the uptake of gold with the double conjugates is CD44-dependent, as it was for the nanocarrier itself. But we also found that the uptake of cisplatin was not. This drug release from the nanosystem can be caused by extracellular hyaluronidase activity besides being in physiological media.

3.2.5 Efficacy & toxicity of EDS-CIS

Efficacy of EDS-CIS was studied *in vitro* by colony forming and cytotoxicity assays, and *in vivo* by measuring the antitumoral activity of EDS-CIS compared to free drug. The tumor accumulation and biodistribution of gold and platinum were quantified by ICP-MS. Toxicity was evaluated by measuring animal weight during the efficacy experiment and by histology.

3.2.5.1 Colony formation assay

In vitro efficacy of the double conjugates was studied by colony forming assay. An optimized number of Panc-1 to achieve countable single colonies was seeded on cell culture plates and treated the following day with different concentrations free drug or corresponding concentrations of drug encapsulated in the nanocarrier. The drug seemed to have a slightly greater effect when encapsulated to the nanosystem, but the differences were not significant (Figure 53).

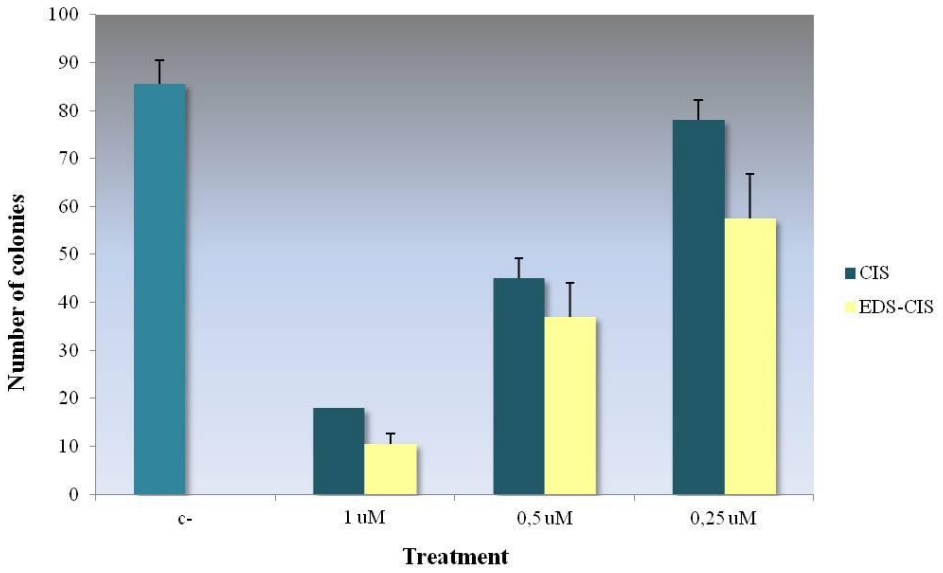

Figure 53. Number of colonies formed after 11 days when single cells of Panc-1 were treated with EDS-CIS and CIS as a free drug (mean (SD)).

3.2.5.2 Cell viability & IC50

The most suitable cell viability assay for gold nanoparticles was validated while characterizing the nanocarrier before double conjugation to the drug. The IC50 of EDS-CIS was studied using the optimized assay in different cell lines expressing varying levels of the receptor for the targeting ligand. The IC50 values showed to be slightly lower with EDS-CIS compared to the free drug in Panc-1 (high CD44 expression) and in A549 (intermediate CD44 expression), but very similar in HEPG (no CD44 expression) (Table 28). The experiments were repeated at least three times and the IC50 were calculated as a mean of the experiments.

Panc-1	uM CIS	ppm Au
CIS	11,5 ± 2,6	-
EDS-CIS	8,3 ± 4	1,9 ± 1

A549	uM CIS	ppm Au
CIS	4,8 ± 1,7	-
EDS-CIS	3,1 ± 3,6	2,2 ± 2,6

HEPG2	uM CIS	ppm Au
CIS	3,6	-
EDS-CIS	3 ± 1,6	1 ± 0,8

Table 28. IC50 of EDS-CIS and free drug in Panc-1, A549 and HEPG2.

3.2.5.3 EDS-CIS biodistribution

EDS-CIS was injected into Panc-1 tumor bearing athymic nude mice intraperitoneally and intravenously and various organs were collected 4 h, 24 h and 48 h post injection for ICP-MS analysis. In Au organ accumulation a difference was seen in pancreas between intraperitoneal and intravenous injections:

- Au ip: liver > spleen > pancreas > kidney > lung > tumor
- Au iv: liver > spleen > kidney > lung > tumor > pancreas

Pt accumulation did not show great differences between interperitoneal and intravenous injections: liver > spleen > kidney > tumor > pancreas > lung. The injections and organ collecting of this biodistribution study were performed by CIBBIM Nanomedicine (Vall d'Hebron Institut de Recerca).

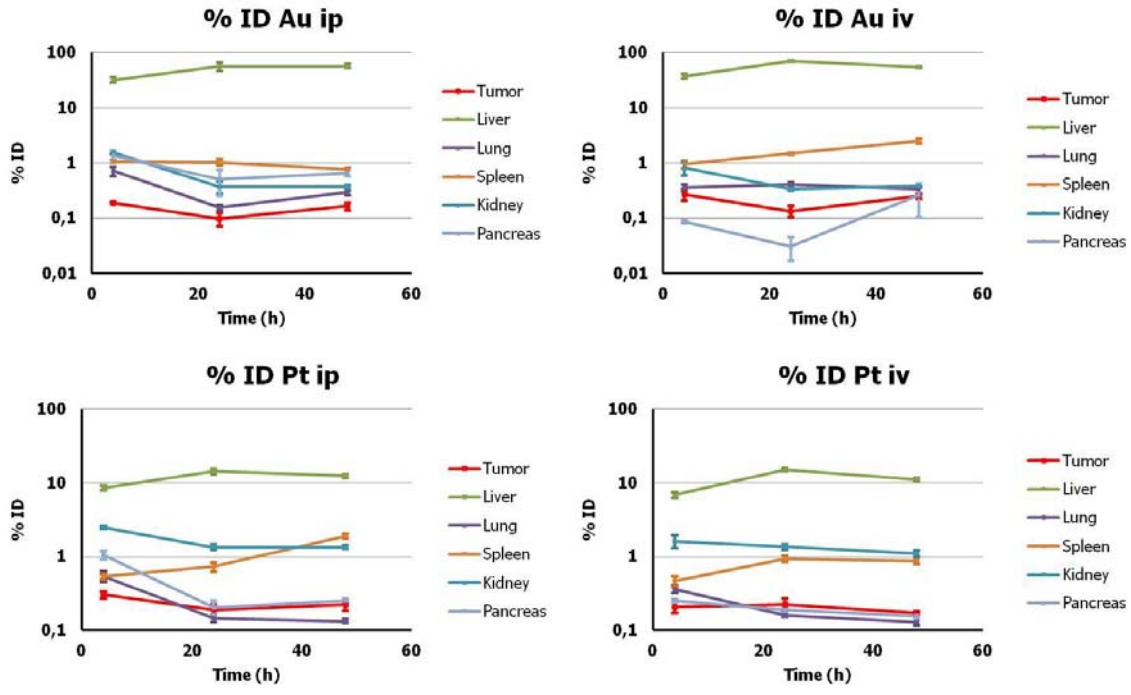

Figure 54. Organ distribution of Au & Pt after single intravenous & intraperitoneal EDS-CIS dose at 4 h, 24 h and 48 h (mean ± SEM).

3.2.5.4 *In vivo* antitumoral efficacy

The next step of this project was to study the effect of our drug delivery system compared to free drug in an *in vivo* xenograft model of OVCAR-3 in collaboration with Leitat Technological Centre.

On day 39 of the experiment, EDS-CIS with both tested concentrations showed a similar antitumoral effect; 56,83 % (2 mg/ml) and 57,25 % (4 mg/ml) growth inhibition compared to saline, while free cisplatin inhibited tumor growth by 13,35 % (2 mg/ml) and 39,90 % (4 mg/ml) (Figure 55 & Table 29).

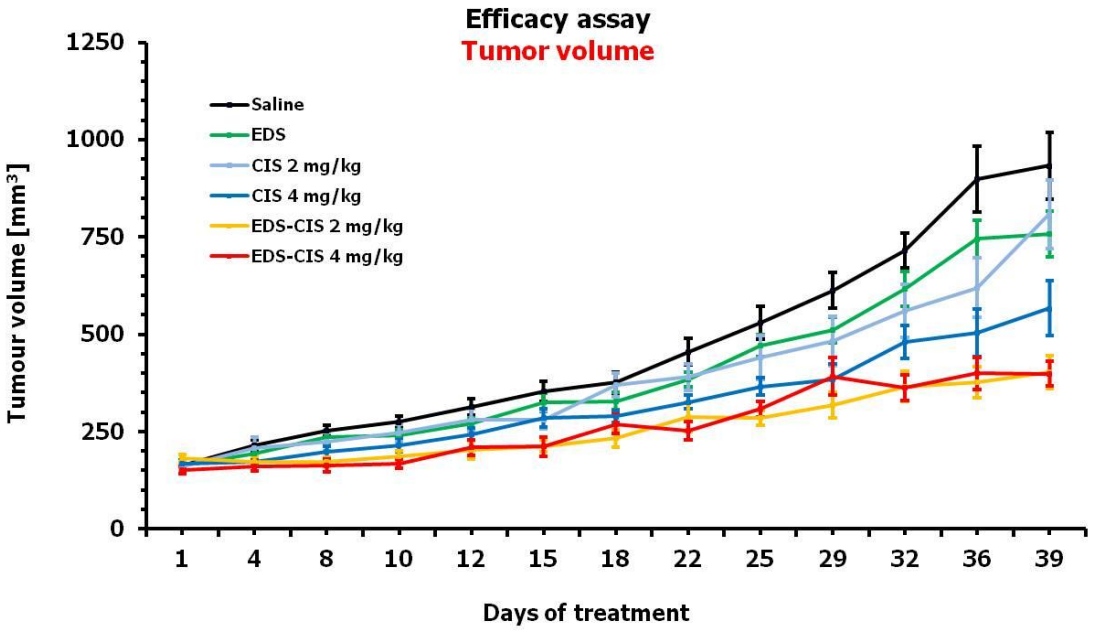

Figure 55. In vivo tumor growth of OVCAR-3 in athymic nude mice receiving different doses of EDS-CIS and CIS (mean ± SEM). EDS-conjugated cisplatin showed higher antitumoral effect than free drug.

Treatment	Difference in tumor growth (%)
Saline vs EDS	-18,75
Saline vs CIS 2 mg/kg	-13,35
Saline vs CIS 4 mg/kg	-39,30 *
Saline vs EDS-CIS 2 mg/kg	-56,83 *
Saline vs EDS-CIS 4 mg/kg	-57,25 *
EDS vs CIS 2 mg/kg	6,65
EDS vs CIS 4 mg/kg	-25,29
EDS vs EDS-CIS 2 mg/kg	-46,86 *
EDS vs EDS-CIS 4 mg/kg	-47,39
CIS 2 mg/kg vs CIS 4 mg/kg	-29,94
CIS 2 mg/kg vs EDS-CIS 2 mg/kg	-50,18 *
CIS 2 mg/kg vs EDS-CIS 4 mg/kg	-50,67 *
CIS 4 mg/kg vs EDS-CIS 2 mg/kg	-28,88
CIS 4 mg/kg vs EDS-CIS 4 mg/kg	-57,25
EDS-CIS 2 mg/kg vs EDS-CIS 4 mg/kg	-1,00

Table 29. Differences in tumor growth between the treatments (the latter compared to the former). The asterisk (*) shows significant differences between treatments ($p < 0,05$).

EDS-CIS with both tested concentrations caused some weight loss after the first administrations as did free cisplatin. Mice that received free cisplatin recovered shortly, while the weight of EDS-CIS receiving mice remained slightly lower almost throughout the experiment (Figure 56).

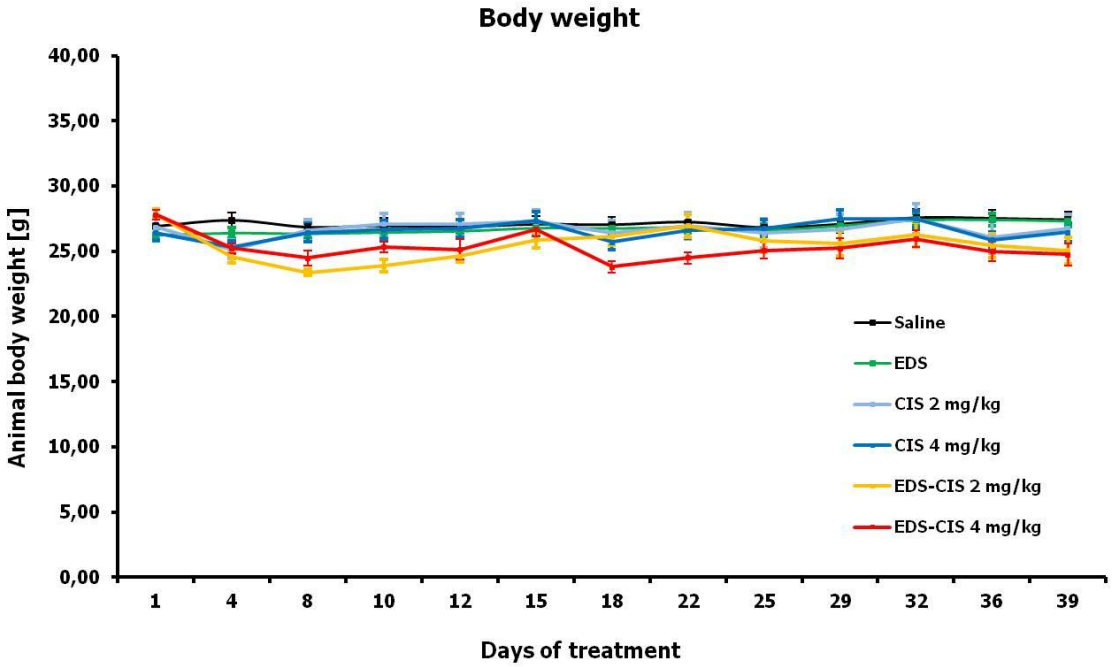

Figure 56. Mouse body weight during the efficacy study (mean ± SEM).

3.2.5.5 Drug accumulation in tumor

ICP-MS analysis of the tumors revealed that when delivered by EDS, there was an increase of 104 % with 2 mg/ml dose and an increase of 408 % with 4 mg/ml dose of platinum in drug accumulation compared to the free drug (Figure 57).

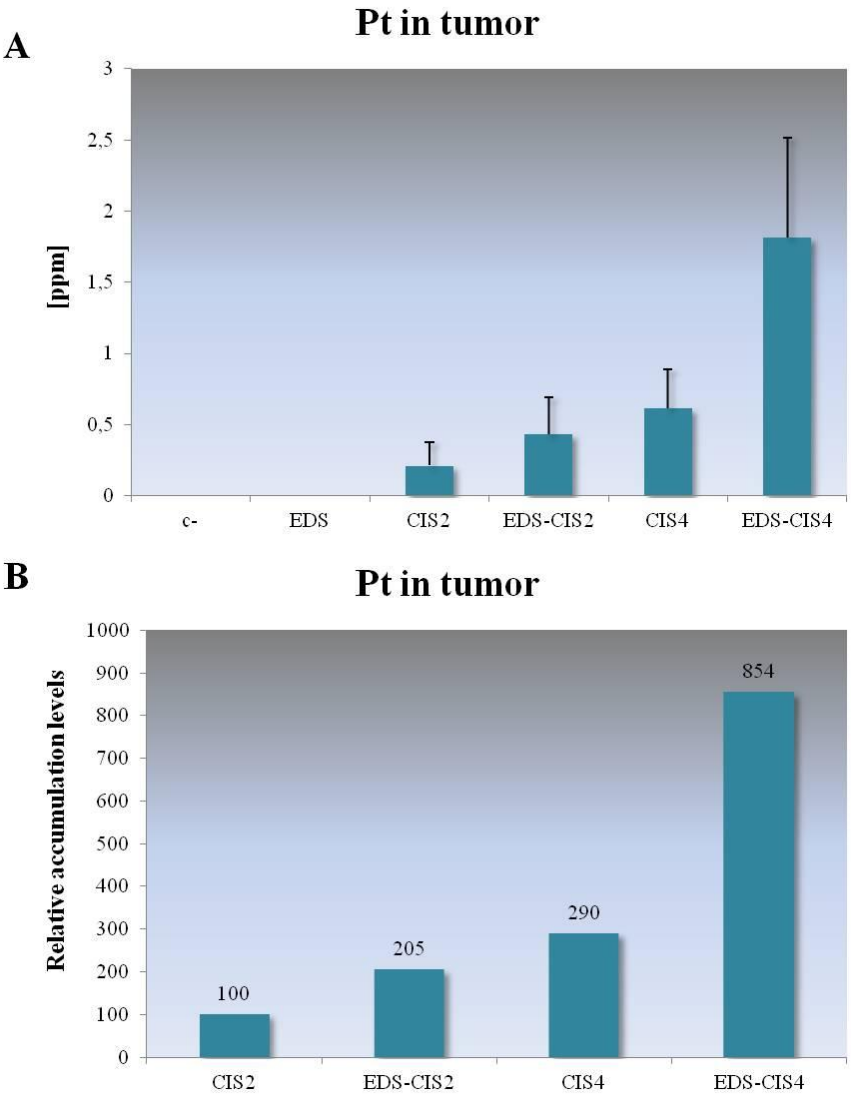

Figure 57. Pt-levels of CIS- and EDS-CIS-treated mice in tumors after sacrifice of the *in vivo* efficacy study. A: accumulation in ppm (mean (SD)), B: relative accumulation levels. Cisplatin conjugated to EDS showed higher accumulation than free drug with both tested concentrations.

3.2.5.6 Au & Pt accumulation in tumor and liver

We found the gold accumulation in liver to be similar between EDS and the two different doses of EDS-CIS administered during the study. Platinum accumulation in liver on the other hand was greater with the two different doses of EDS-CIS than with free drug (Figure 58, above). Gold accumulation in tumor was similar between EDS-CIS 4 mg/ml and the corresponding dose of EDS, and lower with EDS-CIS 2 mg/ml as expected. When comparing platinum accumulation in tumor, we found that when

conjugated to the nanocarrier, more platinum was deposited to the tumor than when mice were administered free drug (Figure 58, below) as already shown before.

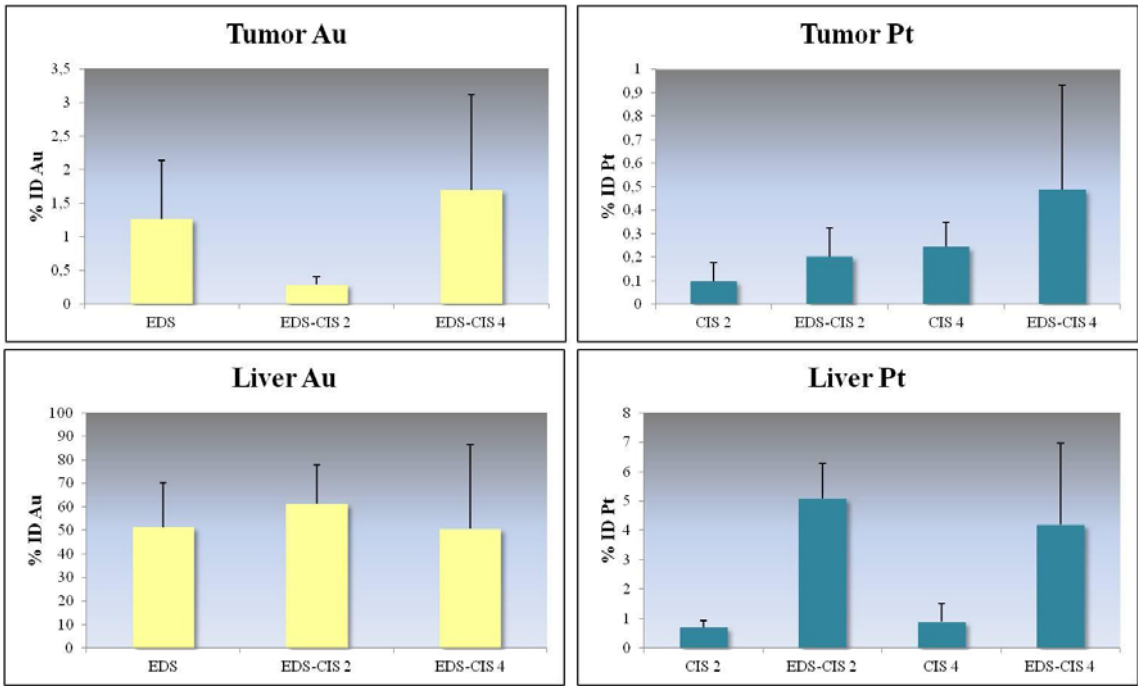

Figure 58. Gold and platinum accumulation (% of initial dose) in liver (above) and tumor (below) in the *in vivo* antitumoral efficacy study of EDS-CIS (mean (SD)). Pt accumulated more in the tumor when conjugated to the nanosystem, but conjugation also led to higher liver accumulation.

3.2.5.7 Liver histology

Despite the increase of Pt accumulation in liver when administered with EDS, histological analysis did not show severe tissue damage in liver (Figure 59).

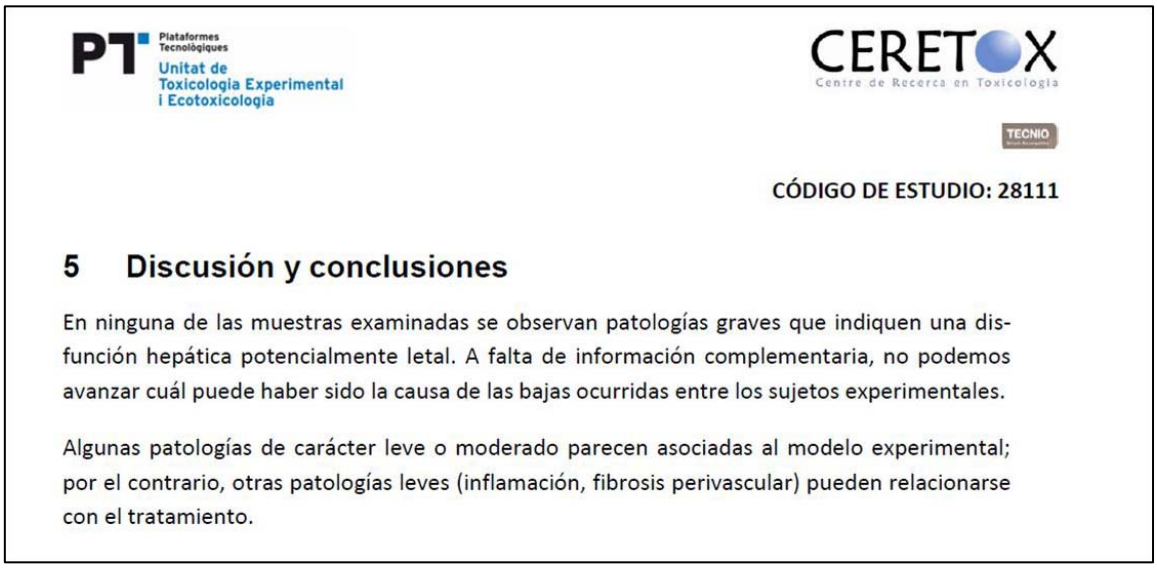

Plataformes Tecnològiques
Unitat de Toxicologia Experimental i Ecotoxicologia

CERETOX
Centre de Recerca en Toxicologia

TECNIO

CÓDIGO DE ESTUDIO: 28111

5 Discusión y conclusiones

En ninguna de las muestras examinadas se observan patologías graves que indiquen una disfunción hepática potencialmente letal. A falta de información complementaria, no podemos avanzar cuál puede haber sido la causa de las bajas ocurridas entre los sujetos experimentales.

Algunas patologías de carácter leve o moderado parecen asociadas al modelo experimental; por el contrario, otras patologías leves (inflamación, fibrosis perivascular) pueden relacionarse con el tratamiento.

Figure 59. Conclusions of the histological analysis of liver damage in the efficacy study stating that no severe liver damage was found with any of the treatments.

The IC50 of EDS-CIS was very slightly lower than that of the free drug in all the tested cell lines in vitro. This, taken together with the results from the colony formation assay further concludes that the drug is delivered in its active form. The in vivo efficacy study suggests that the antitumoral effect of cisplatin is enhanced when it is delivered by the nanocarrier and this could lead to achieving the same therapeutical effect with a lower dose of the drug. EDS-CIS showed an increase in the accumulation of the drug in the liver of the animals compared to free cisplatin. But while Pt accumulated more in the liver when administered encapsulated in the nanocarrier, it also showed an increase in tumor accumulation, and no severe liver damage was detected, even though animals suffered of some weight loss during the experiment.

DISCUSSION

4. DISCUSSION

Gold as the core of nanosized drug delivery vehicles is non-toxic and chemically inert. AuNPs are easy to produce and modify and their large surface area enables efficient conjugation and protection of anticancer therapeutics. For these reasons AuNPs surrounded by an organic monolayer provide an attractive platform for drug delivery systems. Targeted drug delivery can be achieved by functionalizing the AuNPs with ligands that specifically target cell surface receptors which leads to receptor-mediated endocytosis of the NPs (Han et al., 2007).

Different types of AuNPs have been used in the development of diagnostic and therapeutic systems to increase tumor targeting of conventional imaging and anticancer agents. The most popular targeting moieties include antibodies to EGFR and HER2 and folate that targets folate receptors (Ahmad et al., 2013).

Due to its water solubility, viscoelasticity and biocompatibility, HA has been used to enhance drug stability, solubility and bioavailability in formulations for various administration routes (Jin et al., 2010). Drug delivery systems composed of HA, that targets the cell surface receptor CD44, and an anticancer agent have been described and characterized *in vitro* (Jeong et al., 2008; Coradini et al., 1999) and their tissue distribution has been studied (Cai et al., 2008a; Ossipov, 2010). HA-anticancer drug conjugates have also shown increased antitumoral efficacy when adiministered locoregionally in mouse xenograft models (Auzenne et al., 2007) and intratumoral injections of HA-drug conjugates have been well tolerated *in vivo* (Venable et al., 2012).

We chose an approach that employs AuNPs as the core of a CD44-targeting drug carrier system, since AuNPs have been shown to improve the stability and efficacy of chemotherapeutic agents (Craig et al., 2012; Afifi et al., 2014). The addition of AuNPs compared to delivery systems consisting only of HA can result in higher stability (there should be no dissolution of the HA complex before it reaches the tumor environment), higher concentration of HA molecules and targeting capacity (HA molecules are more available for recognition by CD44). 12 nm AuNPs were chosen for this project since

nanoparticles with this size should be big enough to avoid first pass elimination through the kidneys while still being small enough to escape from being sequestered by sinusoids in the spleen and by the liver (Venturoli & Rippe, 2005).

The first drug to be studied with our drug delivery system was cisplatin. Cisplatin is used to treat different types of cancer, including testicular, ovarian, bladder, cervical, head and neck, esophageal and small cell lung cancer. However cisplatin causes toxic effects that limit its dose (Cepeda et al., 2007). Delivery of platinum drugs has already been widely studied with different types of NPs (Butler & Sadler, 2013), and their efficacy could be greatly improved and systemic toxicity reduced by nanocarriers that specifically target tumor tissue.

4.1 Chemical characterization

The past few decades have seen a rapid increase in the development of many different nanomaterials. Among numerous nanomaterials there are great differences in structural, chemical and physical properties and regulation struggles to keep up with the rapid development of NMs, especially regarding health and environmental hazard identification. The biological activity of NMs most probably depends on their physico-chemical features. These features might not be regarded in traditional routine toxicity studies. Therefore it is of high importance to conduct a thorough characterization to understand the effects that NMs can have in biological milieus. The NM properties that should be included in the characterization study include:

- Particle size and size distribution
- Agglomeration state
- Shape
- Crystal structure
- Chemical composition
- Surface area
- Surface chemistry
- Surface charge
- Porosity (Oberdörster et al., 2005)

The physico-chemical properties of NMs dictate their cellular uptake. The mechanism of uptake depends on the size of the NMs, particles with a size above 250 nm are phagocytosed while particles smaller than 200 nm rather use clathrin- or caveolin-mediated endocytosis. The shape of the NMs can affect intracellular trafficking and cytoplasmic or nuclear localization and positive surface charge leads to most efficient uptake due to negatively charged plasma membrane (Panariti et al., 2012).

A detailed characterization cascade can give information about possible toxicity of NMs as well as their state: agglomerated NMs may function in a completely different way compared to disperse NMs and aggregates could even not be considered nanomaterials anymore due to their superior size.

EDS

Our physico-chemical characterization strategy for the NM used in this study included various techniques established in the NCL cascade (http://ncl.cancer.gov/). When bare AuNPs were conjugated to HA, TEM showed no change in the shape or size of the gold core, AuNPs remained spherical with a low size distribution. Also the surface charge remained unchanged at around -38 mV. The hydrodynamic radius of AuNPs turned from 12 nm to 98 nm after HA conjugation. ICP-MS analysis confirmed the theoretical concentration resulting from the AuNP synthesis and showed that EDS could be concentrated up to 100X. Through elemental analysis we could analyze the amount of HA after conjugation and determine the number of HA chains surrounding each AuNP core of the drug delivery system (approximately 2000 HA chains per NP).

We found no need for further uptake-related physico-chemical characterization, since HA acts as a targeting ligand and CD44-targeting was studied later during the project. Due to targeting, the negative surface charge should not hinder internalization.

EDS-CIS

There are various different possibilities for loading the drug in the nanocarrier. Pro-drug delivery and drug release can be executed by cleavable linkages through covalent conjugation, using e.g. photoregulated release or glutathione (GSH) –mediated release to trigger the discharge of the drug. Photoregulated release is achieved by irradiating the light-responsive NPs by a laser, which creates “hot” electrons that trigger the release of the payload. GSH-mediated drug release exploits the high intracellular GSH content and the capability of GSH to displace the drug attached to the surface of the NP by thiols. NPs can also be non-covalently loaded by hydrophobic drugs. Incorporation of the drug is accomplished by encapsulating it in the AuNP-surrounding monolayer, such as PEG (Duncan et al., 2010; Vigderman & Zubarev, 2013).

In this project, three strategies for drug loading and release were tested. Two involved covalent binding through a linker molecule attached on the AuNPs surface through thiol bonding, and to cisplatin through their carboxyl groups. The strategy we finally chose

for drug loading is covalent incorporation of cisplatin in the HA-coating of the AuNPs. This approach resulted in highest drug loading and showed the most reproducibility and stability. Encapsulation of cisplatin in HA has already been described by others (Cafaggi et al., 2011; Jeong et al., 2008) and it has showed no decrease in the activity of the drug *in vitro* or *in vivo*. The drug is released due to acidic pH of the tumor environment and when HA is degraded, starting on the tumor cell surface by HYALs and continued in the lysosomes.

Cisplatin conjugation did not significantly change the characteristics of EDS. The EDS-CIS NPs were disperse and UV-VIS showed only a slight shift of the peak to right, while surface charge remained very similar. DLS analysis displayed a minor decrease in the hydrodynamic radius that we believe to result from a compressing effect of cisplatin to the HA chains.

4.2 Stability

To achieve stability in biological milieu is of high importance when designing and producing NP-based applications for nanomedicine. Physiological media are complex liquids that contain various components – such as salts, proteins and enzymes – that can give rise to aggregation of NPs, which could lead to undesired responses. NPs need to be stabilized through surface functionalization in order to avoid this aggregation (Fratila et al., 2014).

PEG is a polyether polymer that has been widely used to tackle this problem of aggregation since it provides steric stabilization and biocompatibility and enhances blood circulation time of NPs through evading the MPS (Bogliotti et al., 2011; Cho et al., 2010; Lipka et al., 2010). We expected HA to provide AuNPs with all the same advantages as PEG and furthermore active targeting to cancer cells.

EDS

Our data showed that conjugation with HA had a stabilizing effect on the AuNPs. Besides TEM, this was demonstrated by visual analysis and UV-VIS. EDS retained the burgundy color characteristic to 12 nm AuNPs, when diluted on PBS, while bare AuNP solution turned blue in PBS, which implies aggregation. Aggregation was also detected by UV-VIS, which manifested widening and an ample shift to the right in the absorbance peak. Aggregation of bare AuNPs, but not EDS, could be detected in cell culture as well using light microscopy. Cell culture media caused aggregation and the aggregated AuNPs were seen as clusters big enough for visualization surrounding the cells, while EDS remained disperse, and could not be seen.

EDS-CIS

EDS-CIS showed high stability in aqueous solution; during a three-month storage resulted in only a 10 % release of platinum from the complex (data from the doctoral thesis of Laura Vivero, “Diseño y caracterización de sistemas de liberación de fármacos basados en nanopartículas metálicas y ácido hialurónico”, not presented here). In

physiological solution, the drug was released gradually from the nanocarrier; after 30 minutes 36 % of the platinum was released and after 6 h, the release was 56 %. 72 h, the last time point tested, showed a release of 77 % of the drug.

The *in vivo* stability study showed that both platinum and gold were practically cleared from blood at 24 h. There was not much difference between intraperitoneal and intravenous injections at the time points included in this study (4 h, 24 h & 48 h) – IP injections resulted in longer blood circulation time – which justifies the use of ip injections in further studies.

4.3 Internalization

HA has been earlier used to functionalize different types of NPs to achieve tumor targeting. These studies have shown that HA-coated NPs selectively target tumor cells that express CD44 and indicate that NPs with HA-coating have potential as diagnostic and therapeutic applications in cancer (Lim et al., 2011; Mizrahy et al., 2014).

The use of HA to functionalize AuNP-based anticancer drug delivery systems has been reported in a few studies. Li et al. describe the chacterization and *in vitro* uptake of porous NP-conjugates consisting of cyclodextrin-modified HA-coated AuNPs bearing adamantine moieties loaded with different anticancer agents (Li et al., 2014), and Manju & Sreenivasan depict improved targeting and efficacy of curcumin, an extract from the plant turmeric that has shown antitumoral properties, conjugating it first to HA and using it as a stabilizing agent to produce folate-PEG-anchored AuNPs (Manju & Sreenivasan, 2012).

Our approach is simpler and more easily controlled, since it consists only of AuNPs conjugated to HA which encapsulates the drug thorugh covalent linking. When designing new drug delivery systems, and especially when utilizing NPs, all the components of the system need to be characterized and quantified. Using various different components can complicate the synthesis and create greater variability between different batches. Keeping the structure plain may facilitate subsequent formulation and the process of translating a nanosystem form bench to bedside.

In order to demonstrate that our nanocarrier targets CD44, we needed to study the responses of cells with varying expression levels of the receptor. For this we started the *in vitro* studies by examining the expression levels of the receptor in various cancer cell lines established from different cancer tissues. Various cell lines expressing different amounts of CD44 were chosen for further studies.

EDS

Uptake studies of EDS by TEM, IF and ICP-MS showed that the nanocarrier targeted CD44 and was found inside CD44 expressing cells *in vitro*, but not in cells that do not express the receptor. Internalized EDS was both visualized by TEM and IF and quantified by ICP-MS. CD44-targeting was further confirmed by knocking down the expression of CD44 by siRNA in Panc-1, a cell line that expresses high levels of the receptor, and found that EDS uptake was greatly decreased when CD44 expression was reduced.

EDS-CIS

EDS-CIS internalization studies showed that while gold was found only inside cells that express CD44, platinum was also internalized by cells that do not express the receptor, or in which the expression is knocked down. This suggests drug release from the nanocarrier *in vitro*, which is most probably due to two different reasons: physiological media and hyaluronidase activity when EDS-CIS reaches cell surface. Under *in vivo* conditions, the acidic pH of the tumor environment may further induce drug release from the delivery system, and yet enhance accumulation of the drug in the tumor, since HA has already targeted the system to the tumor. On the other hand we can conclude that the compressing effect of conjugating cisplatin in EDS did not affect recognition of the HA-coating by CD44.

4.4 Efficacy

OVCAR-3 cell line was chosen for the *in vivo* efficacy study of EDS-CIS, since cisplatin – the drug chosen for characterization of the drug delivery platform – is one of the effective anticancer agents used to treat ovarian carcinoma. OVCAR-3 expresses intermediate levels of CD44 and CD44 antibodies have been studied for the treatment of ovarian carcinoma (Du et al., 2013). Besides antibodies, NP-based drug delivery systems that exploit CD44 expression have been developed for targeted therapy against ovarian carcinoma. HA was used as a targeting ligand in PEG-based toposiomerase 1 inhibitor-carrying NM, and showed specific uptake by CD44-expressing ovarian carcinoma cell lines (Vangara et al., 2013). Shah et al. have described a dendrimer-based nanocarrier that uses luteinizing hormone-releasing peptide as a tumor-targeting moiety to deliver paclitaxel and CD44-siRNA to ovarian cancer cells. Treatment with this drug delivery system resulted in enhanced antitumoral efficacy *in vivo* and reduced toxicity in healthy organs compared to free paclitaxel (Shah et al., 2013).

In order to be efficient, a drug delivery system needs to deliver a drug to its target tissue in a sufficient concentration and in its active state. Therefore we wanted to study the effects of EDS-CIS on tumor-formation *in vitro* and compare it with free cisplatin. Colony formation assay showed that there was a minor increase in the inhibition of colony formation in favor of EDS-CIS compared to free cisplatin, although insignificant, and this shows that CIS arrives to the cells in its active state.

Since we had seen evidence of drug release in internalization studies of EDS-CIS, we resolved that *in vitro* cell viability assays are not susceptible to detect the efficacy of the nanocarrier in delivering the drug to the target cells, even though they are generally used to evaluate the efficacy of anticancer agents. In the case of EDS-CIS, cells are continuously treated with the nanosystem for 72h and drug is most probably released from the carrier and can enter the cells on its own. By studying targeting and efficacy *in vivo*, the differences between free drug and drug delivered by the carrier can be better appreciated. For the drug delivery system to show its full potential, we conducted an *in vivo* antitumoral efficacy experiment and studied the accumulation of the NP-delivered cisplatin in tumor compared to the free drug.

The *in vivo* antitumoral efficacy study showed that EDS as a delivery system for cisplatin can increase the effect of the drug. On the day of sacrifice (day 39) cisplatin at 2 mg/ml inhibited tumor growth by 13 %, while EDS-CIS at the same concentration caused an antitumoral response of 57 %. With a dose of 4 mg/ml the difference between free drug and EDS-CIS was lesser; on the day of the sacrifice the inhibition percentages were 39 % (free cisplatin) and 57 % (EDS-CIS).

EDS-CIS administration at a dose of 2 mg/kg lead to a two-fold increase in tumor-accumulation of platinum compared to free cisplatin at the end of the *in vivo* efficacy study, even though biodistribution of a single dose of EDS-CIS showed quite low tumor accumulation. The increase in tumor accumulation when conjugated to the nanocarrier with a dose of 4 mg/ml of the drug was approximately three-fold, even though we did not detect such a big difference in antitumoral efficacy between EDS-CIS and free cisplatin at this dose at the end of the study. Nevertheless, tumor inhibition of 2 mg/ml EDS-CIS was greater than that of CIS 4 mg/ml on day 39, which means that the same and even higher efficacy could be achieved with half the drug dose, when it is targeted with the nanocarrier.

4.5 Toxicity

When it comes to nanomaterials a thorough characterization that includes profound safety assessment is fundamental since a lack of information occurs due to the novelty of the field. The same features that give NPs their great potential in biomedicine also might contribute to their possible toxicity. Use of NPs as nanoscale carriers could lead to increases in drug efficacy while reducing side-effects, but their size can also lead to unexpected toxicological effects. It is highly important to study possible toxicological effects of nanomaterials engineered for biomedical applications (Nyström & Fadeel, 2012).

The toxic effects of nanoparticles depend considerably on their surface modifications (Chompoosor et al., 2010; Das et al., 2012; Kim et al., 2013). The toxicity of HA-coated AuNPs has been studied previously. Bare AuNPs induced some DNA damage without causing severe cytotoxicity, but when coated with HA, the cytotoxicity was reduced. However, the toxicity of both bare and HA-coated AuNPs was considered low and they were concluded to be suitable for therapeutic applications (Di Guglielmo et al., 2012). Nevertheless, we considered it consequential to study the possible toxicity of both EDS and EDS-CIS. In some experiments we considered the use of a NP-control essential, but due to the facile aggregation of bare AuNPs and loss of their dispersity in biological media, we chose to use PEG-coated AuNPs instead (see Materials and Methods).

EDS

We discovered the importance of assay validation by starting cytotoxicity evaluation with the most common test available: MTT assay. We soon took note that residual and internalized AuNPs can cause interference due to chemical reactions between the NPs and the assay components and/or to NPs having their absorption peak close to the wavelength the assay uses to quantify absorbance. Limitations of established *in vitro* toxicity assays with NM have been reported previously (Kroll et al., 2009) and NP toxicity studies require a thorough characterization and validation of the employed assays.

Our *in vitro* studies showed that EDS does not cause genotoxicity or oxidative damage, and cytotoxicity testing showed decrease in cell viability with high concentrations. *In vivo* administration of EDS did not show systemic toxicity, the animals did not suffer of any weight loss. Blood biochemical analysis did not suggest any hepatic, renal or pancreatic damage. ICP-MS analysis revealed highest accumulation of gold in liver and skin followed by tumor, but histological analysis of the healthy organs did not show abnormalities in morphology or tissue damage. Since liver, unlike skin in which we found the second highest accumulation, does not express high levels of CD44, we did not expect levels this high. Instead of CD44, liver expresses another HA-receptor, HARE that is involved in the clearance of HA (see Introduction), that could be responsible for the accumulation.

The exhaustive review of Khlebtsov & Dykman summarizes that AuNPs tend to accumulate in the organs of the MPS, including liver and spleen (Khlebtsov & Dykman, 2011). HA-based NPs have also been reported to accumulate in the liver (Choi et al., 2011), but this is believed to be size-dependent. HMW HA is rapidly cleared from the body after injection, but clearance can be reduced by using LMW HA, attaching HA to NPs or crosslinking HA chains and forming nanogels (Ossipov, 2010). However, there is great discrepancy in HA studies using various different sizes and even the concepts of LMW and HMW HA. Nevertheless, EDS showed high liver accumulation that could cause problems in drug delivery to the tumor.

On the other hand, CYT6091, an AuNP-based drug delivery system that is currently in Phase 2 clinical trials, has shown high liver accumulation of gold in pre-clinical studies as well. When 63 to 74 % (depending on the xenograft model) of the injected gold accumulated in liver in case of 4 doses EDS, a single CYT6091 injection lead to liver accumulation 45 % of the gold. The amount of accumulated gold gradually decreased in their studies during a 4-month period, but 27 % of the gold still remained in the liver at the end of the study. Yet CYT6091 still demonstrated enhanced uptake of the delivered drug by tumor tissue and was able to proceed to clinical trials (Goel et al., 2009).

The blood circulation time of EDS after intraperitoneal injection showed a peak at 4 h, approximately half of the EDS was cleared after 12 h and practically all EDS was cleared at 24 h.

EDS-CIS

EDS-CIS cytotoxicity testing demonstrated that there were minor, yet insignificant differences between the IC50 values of the free drug and drug encapsulated in the nanocarrier: EDS-CIS was very slightly more toxic. The differences between cell lines in case of EDS-CIS are not due to differing levels of CD44 expression, but to varying sensibilities of the cells to the drug. Based on the colony formation assay results and the IC50 values obtained from the cell viability assays we can conclude that the nanocarrier does not inhibit the efficacy of the drug itself.

Since liver was the organ that accumulated the most gold after EDS-CIS administration, we chose to study the accumulation in liver besides tumor in the *in vivo* antitumoral efficacy study. The animals that had been administered with the two different doses of EDS-CIS (2 mg/ml and 4 mg/ml cisplatin) had suffered weight loss in the beginning of the experiment. Similar initial decrease in body weight has been reported with HA- and CIS-loaded chitosan NPs, but the mice recovered this weight during the experiment (Cafaggi et al., 2011).

Compared to the free drug, EDS-CIS administration resulted in higher platinum liver accumulation. The increase was from less than 1 % ID to 5 % ID with a dose of 2 mg/ml cisplatin. The increase was similar with a dose of 4 mg/kg. Even though severe liver toxicity was not detected by histological analysis, this increase in the drug liver accumulation is a major drawback, and can lead to redesigning the drug delivery system to avoid such high healthy organ accumulation.

Intravenous injections of EDS-CIS showed that at 4h the amount of Pt had decreased less than 10 % from the initial dose. This blood circulation profile is comparable to that of CYT6091 that has been functionalized with PEG to avoid clearance by the MPS (Paciotti et al., 2004). Therefore it is possible that the delivery system is not recognized by the MPS, but cleared by HARE and for this reason accumulates in the liver.

4.6 Future prospects

Our next studies will be focused on determining the reasons for the weight loss of the animals following EDS-CIS administration and liver accumulation of both Au and Pt. Conjugation strategies may be re-evaluated and approaches to improve tumor targeting and reduce healthy organ accumulation will be studied.

Besides defining the motives for toxicity, the drug delivery platform will be studied for the delivery of other chemotherapeutic agents, such as gemcitabine (GEM). GEM, a deoxycytidine analog, is the first choice treatment for pancreatic cancer. It has been conjugated to various types of NPs to increase its efficacy, stability and specificity, and reduce side-effects (Khaira et al., 2014; Zhang et al., 2012). AuNPs have been loaded with GEM as well using cetuximab as the targeting agent, and with these nanosystems increased antitumoral efficacy has been achieved *in vivo* (Kudgus et al., 2013; Patra et al., 2008).

Conjugation of HA and CIS to AuNPs did not change the unique characteristics of the NPs. Altogether both EDS and EDS-CIS demonstrated high stability and biocompatibility. EDS was shown to target CD44, and while CIS was released from the nanocarrier both in vitro and in vivo, it reaches the tumor environment before the release takes place. Conjugation to EDS does not inhibit the activity of CIS and higher tumor accumulation and tumor growth inhibition is reached than with the free drug. EDS showed no evidence of toxicity, but EDS-CIS still needs further toxicity testing to ensure its safety.

CONCLUSIONS

5. CONCLUSIONS

EDS

Chemical characterization. The chemical characterization of EDS showed evidence of a controlled synthesis. HA converted AuNPs biocompatible in physiological solutions, avoiding aggregation that bare AuNPs are susceptible to due to their surface charge becoming neutral. Quantification showed that there were approximately 2000 HA molecules per NP and the nanocarrier demonstrated high stability.

Biological characterization: internalization and toxicity. EDS uptake was shown to be CD44-dependent, this was proven by studies with cell lines that exhibit differing CD44 expression levels as well as down-regulating the expression of the HA receptor in a cell line that expresses high levels of CD44. Internalized EDS was detected both visually and quantitatively. EDS showed no signs of genotoxicity or oxidative damage even though high concentrations showed a decrease in cell viability. *In vivo* studies showed highest accumulation in liver, followed by skin and tumor in mouse xenografts, but the animals did not suffer weight loss, abnormal histology or tissue damage as a result of this accumulation.

EDS-Drug

Chemical characterization. After studying different conjugation strategies for drug loading and selecting the candidate for further studies, EDS-Drug (EDS-CIS, since the chemotherapeutic cisplatin was used) did not show significant changes in its physico-chemical characteristics compared to EDS. EDS-CIS was stable in solution and indicated a gradual drug release.

Biological characterization: internalization, efficacy & toxicity. Conjugation of cisplatin to EDS did not prevent the drug from performing its action *in vitro*, the drug showed very slightly higher toxicity when encapsulated compared to the free drug. However, even though EDS uptake was proven to be CD44-dependent, platinum was found to be internalized by both CD44-positive and CD44-negative cells, which is most probably

due to pH changes in the tumor environment and HYAL activity on the cell surface. Nevertheless, *in vitro* assays are not the most adequate methods to assess the efficacy of a drug delivery system. The *in vivo* antitumoral effect of EDS-CIS was increased compared to free cisplatin, a higher effect was reached with less drug and tumor accumulation of the drug increased. However more toxicity testing is needed to fully determine the safety of EDS-Drug compounds.

The research conducted for this thesis demonstrates that hyaluronic acid-coated gold nanoparticles can be used as a platform for the synthesis of drug delivery systems for antitumoral agents, significantly increasing the accumulation of the drug in tumor thus achieving the same efficacy with a lower drug dose.

REFERENCES

REFERENCES

Afifi, M. M., Austin, L. A., Mackey, M. A., & El-Sayed, M. A. (2014). XAV939: from a small inhibitor to a potent drug bioconjugate when delivered by gold nanoparticles. *Bioconjugate Chemistry*, *25*(2), 207–15.

Agasti, S., Chompoosor, A., You, C.-C., Ghosh, P., Kim, C. K., & Rotello, V. M. (2009). Photoregulated release of caged anticancer drugs from gold nanoparticles. *Journal of the American Chemical Society*, *131*(16), 5728–5729.

Ahmad, M. Z., Akhter, S., Rahman, Z., Akhter, S., Anwar, M., Mallik, N., & Ahmad, F. J. (2013). Nanometric gold in cancer nanotechnology: current status and future prospect. *The Journal of Pharmacy and Pharmacology*, *65*(5), 634–51.

Ahn, S., Jung, S. Y., & Lee, S. J. (2013). Gold nanoparticle contrast agents in advanced X-ray imaging technologies. *Molecules (Basel, Switzerland)*, *18*(5), 5858–90.

Al-Hajj, M., Wicha, M. S., Benito-Hernandez, A., Morrison, S. J., & Clarke, M. F. (2003). Prospective identification of tumorigenic breast cancer cells. *Proceedings of the National Academy of Sciences of the United States of America*, *100*(7), 3983–8.

American Cancer Society. http://www.cancer.org

Amoozgar, Z., & Yeo, Y. (2012). Recent advances in stealth coating of nanoparticle drug delivery systems. *Wiley Interdisciplinary Reviews: Nanomedicine and Nanobiotechnology*, *4*(2), 219–233.

Are, C., Rajaram, S., Are, M., Raj, H., Anderson, B. O., Chaluvarya Swamy, R., Vijayakumar, M., Song, T., Pandey, M., Edney, J. A., Cazap, E. L. (2013). A review of global cancer burden: trends, challenges, strategies, and a role for surgeons. *Journal of Surgical Oncology*, *107*(2), 221–6.

Arvizo, R., Bhattacharyya, S., Kudgus, R., Giri, K., Bhattacharya, R., & Mukherjee, P. (2012). Intrinsic therapeutic applications of noble metal nanoparticles: past, present and future. *Chemical Society Reviews*, *41*(7), 2943–2970.

Arvizo, R., Saha, S., Wang, E., Robertson, J., Bhattacharya, R., & Mukherjee, P. (2013). Inhibition of tumor growth and metastasis by a self-therapeutic nanoparticle. *Proceedings of the National Academy of Sciences of the United States of America*, *110*(17), 6700–6705.

Auzenne, E., Ghosh, S. C., Khodadadian, M., Rivera, B., Farquhar, D., Price, R. E., Ravoori, M., Kundra, V., Freedman, R. S., Klostergaard, J. (2007). Hyaluronic Acid- Paclitaxel: Antitumor Efficacy against CD44(+) Human Ovarian Carcinoma Xenografts. *Neoplasia*, *9*(6), 479–486.

Baird, R. D., & Caldas, C. (2013). Genetic heterogeneity in breast cancer: the road to personalized medicine? *BMC Medicine*, *11*(151), 151.

Bayr, H. (2005). Reactive oxygen species. *Critical Care Medicine*, *33*(Suppl), S498–S501.

Belizário, J. (2009). Immunodeficient mouse models: an overview. The *Open Immunology Journal*, *2*, 79–85.

Bhattacharya, R., & Mukherjee, P. (2008). Biological properties of "naked" metal nanoparticles. *Advanced Drug Delivery Reviews*, *60*(11), 1289–306.

Black, K. E., Collins, S. L., Hagan, R. S., Hamblin, M. J., Chan-Li, Y., Hallowell, R. W., Powell, J. D., Horton, M. R. (2013). Hyaluronan fragments induce IFNβ via a novel TLR4-TRIF-TBK1-IRF3-dependent pathway. *Journal of Inflammation (London, England)*, *10*(1), 23.

Bogliotti, N., Oberleitner, B., Di-Cicco, A., Schmidt, F., Florent, J.-C., & Semetey, V. (2011). Optimizing the formation of biocompatible gold nanorods for cancer research: functionalization, stabilization and purification. *Journal of Colloid and Interface Science*, *357*(1), 75–81.

Bouga, H., Tsouros, I., & Bounias, D. (2010). Involvement of hyaluronidases in colorectal cancer. *BMC Cancer*, *10*, 499.

Bourguignon, L. (2008). Hyaluronan-mediated CD44 activation of RhoGTPase signaling and cytoskeleton function promotes tumor progression. *Seminars in Cancer Biology*, *18*(4), 251–259.

Butler, J. S., & Sadler, P. J. (2013). Targeted delivery of platinum-based anticancer complexes. *Current Opinion in Chemical Biology*, *17*(2), 175–88.

Cafaggi, S., Russo, E., Stefani, R., Parodi, B., Caviglioli, G., Sillo, G., Bisio, A., Aiello, C., Viale, M. (2011). Preparation, characterisation and preliminary antitumour activity evaluation of a novel nanoparticulate system based on a cisplatin-hyaluronate complex and N-trimethyl chitosan. *Investigational New Drugs*, *29*(3), 443–55.

Cai, S., Xie, Y., Bagby, T., Cohen, M., & Forrest, M. (2008a). Intralymphatic chemotherapy using a hyaluronan–cisplatin conjugate. *Journal of Surgical Research*, *147*(2), 247–252.

Cai, W., Gao, T., Hong, H., & Sun, J. (2008b). Applications of gold nanoparticles in cancer nanotechnology. *Nanotechnology, Science and Applications*, (1), 17–32.

Cao, Y., Jin, R., & Mirkin, C. (2002). Nanoparticles with Raman spectroscopic fingerprints for DNA and RNA detection. *Science*, *297*(5586), 1536–1540.

Cancer Research UK: http://www.cancerresearchuk.org/

Cepeda, V., Fuertes, M. a, Castilla, J., Alonso, C., Quevedo, C., & Pérez, J. M. (2007). Biochemical mechanisms of cisplatin cytotoxicity. *Anti-Cancer Agents in Medicinal Chemistry*, *7*(1), 3–18.

Cho, W.-S., Cho, M., Jeong, J., Choi, M., Han, B. S., Shin, H.-S., Hong, J., Chung, B. H., Jeong, J., Cho, M.-H. (2010). Size-dependent tissue kinetics of PEG-coated gold nanoparticles. *Toxicology and Applied Pharmacology*, *245*(1), 116–23.

Choi, K. Y., Min, K. H., Yoon, H. Y., Kim, K., Park, J. H., Kwon, I. C., Choi, K., Jeong, S. Y. (2011). PEGylation of hyaluronic acid nanoparticles improves tumor targetability in vivo. *Biomaterials*, *32*(7), 1880–9.

Chompoosor, A., Saha, K., Ghosh, P. S., Macarthy, D. J., Miranda, O. R., Zhu, Z.-J., Arcaro, K.F., Rotello, V. M. (2010). The role of surface functionality on acute cytotoxicity, ROS generation and DNA damage by cationic gold nanoparticles. *Small*, *6*(20), 2246–9.

Chu, P., Clanton, D. J., Snipas, T. S., Lee, J., Mitchell, E., Nguyen, M.-L., Hare, E., Peach, R. J. (2009). Characterization of a subpopulation of colon cancer cells with stem cell-like properties. *International Journal of Cancer. Journal International Du Cancer*, *124*(6), 1312–21.

Colnot, D., Ossenkoppele, G., Roos, J., Quak, J., de Bree, R., Börjesson, P., Juijgens, P. C., Snow, G. B., van Dongen, G. (2002). Reinfusion of unprocessed, granulocyte colony-stimulating factor-stimulated whole blood allows dose escalation of 186Relabeled chimeric monoclonal antibody U36 radioimmunotherapy in a phase I dose escalation study. *Clinical Cancer Research*, *8*(11), 3401–3406.

Colnot, D., Roos, J., de Bree, R., Wilhelm, A., Kummer, J., Hanft, G., Heider, K. H., Stehle, G., Snow, G. B., van Dongen, G. (2003). Safety, biodistribution, pharmacokinetics, and immunogenicity of 99mTc-labeled humanized monoclonal antibody BIWA 4 (bivatuzumab) in patients with squamous cell carcinoma of the head and neck. *Cancer Immunology, Immunotherapy*, *52*(9), 576–582.

Coradini, D., Pellizzaro, C., Miglierini, G., Daidone, M., & Perbellini, A. (1999). Hyaluronic acid as drug delivery for sodium butyrate: improvement of the anti-proliferative activity on a breast-cancer cell line. *International Journal of Cancer*, *81*(3), 411–416.

Craig, G. E., Brown, S. D., Lamprou, D. a, Graham, D., & Wheate, N. J. (2012). Cisplatin-tethered gold nanoparticles that exhibit enhanced reproducibility, drug loading, and stability: a step closer to pharmaceutical approval? *Inorganic Chemistry*, *51*(6), 3490–7.

Dang, S., Peng, Y., Ye, L., Wang, Y., Qian, Z., Chen, Y., Wang, X., Lin, Y., Zhang, X., Sun, X., Wu, Q., Cheng, Y., Nie, H., Jin, M., Xu, H. (2013). Stimulation of TLR4 by LMW-HA induces metastasis in human papillary thyroid carcinoma through CXCR7. *Clinical & Developmental Immunology*, *2013*, 712561.

Daniel, M.-C., & Astruc, D. (2004). Gold nanoparticles: assembly, supramolecular chemistry, quantum-size-related properties, and applications toward biology, catalysis, and nanotechnology. *Chemical Reviews*, *104*(1), 293–346.

Das, S., Debnath, N., Mitra, S., Datta, A., & Goswami, A. (2012). Comparative analysis of stability and toxicity profile of three differently capped gold nanoparticles for biomedical usage. *Biometals, 25*(5), 1009–22.

Day, E., Zhang, L., Thompson, P., Zawaski, J. A, Kaffes, C., Gaber, M., Blaney, S. M., West, J. (2012). Vascular-targeted photothermal therapy of an orthotopic murine glioma model. *Nanomedicine*, *7*(8), 1133–1148.

Diamond, M. P., Burns, E. L., Accomando, B., Mian, S., & Holmdahl, L. (2012). Seprafilm(®) adhesion barrier: (2) a review of the clinical literature on intraabdominal use. *Gynecological Surgery*, *9*(3), 247–257.

Di Guglielmo, C., De Lapuente, J., Porredon, C., Ramos-López, D., Sendra, J., & Borràs, M. (2012). In vitro safety toxicology data for evaluation of gold nanoparticles-chronic cytotoxicity, genotoxicity and uptake. *Journal of Nanoscience and Nanotechnology*, *12*(8), 6185–6191.

Doane, T. L., & Burda, C. (2012). The unique role of nanoparticles in nanomedicine: imaging, drug delivery and therapy. *Chemical Society Reviews*, *41*(7), 2885–911.

Dreaden, E. C., Alkilany, A. M., Huang, X., Murphy, C. J., & El-Sayed, M. a. (2012). The golden age: gold nanoparticles for biomedicine. *Chemical Society Reviews*, *41*(7), 2740–79.

Du, Y.-R., Chen, Y., Gao, Y., Niu, X.-L., Li, Y.-J., & Deng, W.-M. (2013). Effects and mechanisms of anti-CD44 monoclonal antibody A3D8 on proliferation and apoptosis of sphere-forming cells with stemness from human ovarian cancer. *International Journal of Gynecological Cancer*, *23*(8), 1367–75.

Duncan, B., Kim, C., & Rotello, V. M. (2010). Gold nanoparticle platforms as drug and biomacromolecule delivery systems. *Journal of Controlled Release*, *148*(1), 122–7.

Duncan, R., & Gaspar, R. (2011). Nanomedicine(s) under the microscope. *Molecular Pharmaceutics*, *8*(6), 2101–41.

ESF Forward Look on *Nanomedicine* 2005:

http://www.nanopharmaceuticals.org/files/nanomedicine.pdf

European Comission Recommendation on the Definition of Nanomaterial (2011): http://ec.europa.eu/environment/chemicals/nanotech/pdf/commission_recommendation.pdf

Espinosa, E., Zamora, P., Feliu, J., & González Barón, M. (2003). Classification of anticancer drugs—a new system based on therapeutic targets. *Cancer Treatment Reviews*, *29*(6), 515–523.

Fadeel, B., & Garcia-Bennett, A. E. (2010). Better safe than sorry: Understanding the toxicological properties of inorganic nanoparticles manufactured for biomedical applications. *Advanced Drug Delivery Reviews*, *62*(3), 362–74.

Fishburn, C. (2008). The pharmacology of PEGylation: balancing PD with PK to generate novel therapeutics. *Journal of Pharmaceutical Sciences*, 1–17.

Flanagan, S. P. (1966). "Nude", a new hairless gene with pleiotropic effects in the mouse. *Genetic Research*, *8*(3), 295–309.

Franzmann, E., Schroeder, G., Goodwin, W., Weed, D., Fisher, P., & Lokeshwar, V. (2003). Expression of tumor markers hyaluronic acid and hyaluronidase (HYAL1) in head and neck tumors. *International Journal of Cancer*, *106*(3), 438–445.

Fratila, R. M., Mitchell, S. G., Del Pino, P., Grazu, V., & De La Fuente, J. M. (2014). Strategies for the biofunctionalization of gold and iron oxide nanoparticles. *Langmuir*, *Jun 9*, *[Epub ahead of print]*.

Gaffney, J., Kumar, S., & Slevin, M. (2009). Oligosaccharides of hyaluronan induce angiogenesis through distinct CD44 and RHAMM-mediated signalling pathways involving Cdc2 and Á -adducin. *International Journal of Oncology*, *35*(4), 761–773.

Gibson, J. D., Khanal, B. P., & Zubarev, E. R. (2007). Paclitaxel-functionalized gold nanoparticles. *Journal of the American Chemical Society*, *129*(37), 11653–61.

Goel, R., Shah, N., Visaria, R., Paciotti, G., & Bischof, J. (2009). Biodistribution of TNF-α-coated gold nanoparticles in an in vivo model system. *Nanomedicine*, *4*(4), 401–410.

Gold, M. (2009). The science and art of hyaluronic acid dermal filler use in esthetic applications. *Journal of Cosmetic Dermatology*, *8*(4), 301–307.

Gonzalez de Castro, D., Clarke, P. a, Al-Lazikani, B., & Workman, P. (2013). Personalized cancer medicine: molecular diagnostics, predictive biomarkers, and drug resistance. *Clinical Pharmacology and Therapeutics*, *93*(3), 252–9.

Goodison, S., Urquidi, V., & Tarin, D. (1999). CD44 cell adhesion molecules. *Molecular pathology*, *52*(4), 189–96.

Han, G., Ghosh, P., & Rotello, V. M. (2007). Multi-functional Gold Nanoparticles for Drug Delivery. *Bio-applications of Nanoparticles* (pp. 48–55).

Hanahan, D., & Weinberg, R. A. (2000). The hallmarks of cancer. *Cell*, *100*, 50–70.

Hanahan, D., & Weinberg, R. A. (2011). Hallmarks of cancer: the next generation. *Cell*, *144*(5), 646–674.

Hall, C. L., Wang, C., Lange, L. a, & Turley, E. a. (1994). Hyaluronan and the hyaluronan receptor RHAMM promote focal adhesion turnover and transient tyrosine kinase activity. *The Journal of cell biology*, *126*(2), 575–88.

Hamilton, S., Fard, S., & Paiwand, F. (2007). The hyaluronan receptors CD44 and Rhamm (CD168) form complexes with ERK1, 2 that sustain high basal motility in breast cancer cells. *Journal of Biological Chemistry*, *282*(22), 16667–16680.

Higby, G. J. (1982). Gold in medicine: a review of its use in the West before 1900. *Gold Bulletin*, *15*(4), 130–40.

International Agency for Research on Cancer and Cancer Research UK. *World Cancer Factsheet*. Cancer Research UK, London, 2014. http://publications.cancerresearchuk.org/downloads/product/CS_REPORT_WORLD.pdf

Isacke, C. M., & Yarwood, H. (2002). The hyaluronan receptor, CD44. *The International Journal of Biochemistry & Cell Biology*, *34*(7), 718–21.

Itano, N. (2008). Simple primary structure, complex turnover regulation and multiple roles of hyaluronan. *Journal of Biochemistry*, *144*(2), 131–7.

Itano, N., & Kimata, K. (2008). Altered hyaluronan biosynthesis in cancer progression. *Seminars in Cancer Biology*, *18*(4), 268–74.

Itano, N., Zhuo, L., & Kimata, K. (2008). Impact of the hyaluronan-rich tumor microenvironment on cancer initiation and progression. *Cancer science*, *99*(9), 1720–5.

Jackson, D. G. (2004). Biology of the lymphatic marker LYVE-1 and applications in research into lymphatic trafficking and lymphangiogenesis. *Acta Pathologica, Microbiologica, et Immunologica Scandinavica*, *112*(7-8), 526–38.

Jackson, D. G. (2009). Immunological functions of hyaluronan and its receptors in the lymphatics. *Immunological Reviews*, *230*(1), 216–31.

Jeong, Y.-I., Kim, S.-T., Jin, S.-G., Ryu, H.-H., Jin, Y.-H., Jung, T.-Y., Kim, I.-Y., Jung, S. (2008). Cisplatin-incorporated hyaluronic acid nanoparticles based on ion-complex formation. *Journal of Pharmaceutical Sciences*, *97*(3), 1268–1276.

Jiang, D., Liang, J., & Noble, P. W. (2011). Hyaluronan as an Immune Regulator in Human Diseases, 221–264.

Jin, R., He, X., Wang, K., Yang, L., Li, H., Jin, Y., & Tan, W. (2007). Characterization of different sequences of DNA on si substrate by atomic force microscopy and gold nanoparticle labeling. *Journal of Nanoscience and Nanotechnology*, *7*(2), 418–423.

Jin, Y., Ubonvan, T., & Kim, D. (2010). Hyaluronic Acid in Drug Delivery Systems HA in Nonparenteral Delivery, *40*, 33–43.

Kah, J. C. Y., Kho, K. W., Lee, C. G. L., James, C., Sheppard, R., Shen, Z. X., Soo, K. C., Olivo, M. C. (2007). Early diagnosis of oral cancer based on the surface plasmon resonance of gold nanoparticles. *International Journal of Nanomedicine*, *2*(4), 785–98.

Karbownik, M. S., & Nowak, J. Z. (2013). Hyaluronan: Towards novel anti-cancer therapeutics. *Pharmacological Reports: PR*, *65*(5), 1056–74.

Kelkar, S. S., & Reineke, T. M. (2011). Theranostics: combining imaging and therapy. *Bioconjugate Chemistry*, *22*(10), 1879–903.

Kelland, L. (2000). Preclinical perspectives on platinum resistance. *Drugs*, (59), 1–8.

Kelland, L. (2007). The resurgence of platinum-based cancer chemotherapy. *Nature Reviews. Cancer*, *7*(8), 573–84.

Khaira, R., Sharma, J., & Saini, V. (2014). Development and characterization of nanoparticles for the delivery of gemcitabine hydrochloride. *The Scientific World Journal*, *2014*, 560962.

Khlebtsov, N., & Dykman, L. (2011). Biodistribution and toxicity of engineered gold nanoparticles: a review of in vitro and in vivo studies. *Chemical Society Reviews*, *40*(3), 1647–71.

Kim, S., Saha, K., Kim, C., & Rotello, V. (2013). The role of surface functionality in determining nanoparticle cytotoxicity. *Accounts of Chemical Research*, *46*(3), 681–691.

Kimling, J., Maier, M., Okenve, B., Kotaidis, V., Ballot, H., & Plech, a. (2006). Turkevich method for gold nanoparticle synthesis revisited. *The Journal of Physical Chemistry. B*, *110*(32), 15700–7.

Knudson, W., & Knudson, C. B. (1999). The hyaluronan receptor, CD44. *Glycoforum, Glycoscience, Science of Hyaluronan*.

Knudson, W., Chow, G., & Knudson, C. B. (2002). CD44-mediated uptake and degradation of hyaluronan. *Matrix Biology*, *21*(1), 15–23.

Knudson, W., & Knudson, C. B. (2004). The hyaluronan receptor CD44, an update. *Glycoforum, Glycoscience, Science of Hyaluronan*.

Kroll, A., Pillukat, M. H., Hahn, D., & Schnekenburger, J. (2009). Current in vitro methods in nanoparticle risk assessment: limitations and challenges. *European Journal of Pharmaceutics and Biopharmaceutics*, *72*(2), 370–7.

Kudgus, R. A, Szabolcs, A., Khan, J. A., Walden, C. a, Reid, J. M., Robertson, J. D., Bhattacharya, R., Mukherjee, P. (2013). Inhibiting the growth of pancreatic adenocarcinoma in vitro and in vivo through targeted treatment with designer gold nanotherapeutics. *PloS One*, *8*(3), e57522.

Kumar, D., Saini, N., Jain, N., Sareen, R., & Pandit, V. (2013). Gold nanoparticles: an era in bionanotechnology. *Expert Opinion on Drug Delivery*, *10*(3), 397–409.

Kurkina, T., & Balasubramanian, K. (2012). Towards in vitro molecular diagnostics using nanostructures. *Cellular and molecular life sciences*, *69*(3), 373–88.

Laurent, T. C., Laurent, U. B., & Fraser, J. R. (1996). The structure and function of hyaluronan: An overview. *Immunology and Cell Biology*, *74*(2), A1–7.

Lee, D.-E., Koo, H., Sun, I.-C., Ryu, J. H., Kim, K., & Kwon, I. C. (2012). Multifunctional nanoparticles for multimodal imaging and theragnosis. *Chemical Society reviews*, *41*(7), 2656–72.

Lewinski, N., Colvin, V., & Drezek, R. (2008). Cytotoxicity of nanoparticles. *Small, 4*(1), 26–49.

Li, Y., Wark, A., Lee, H., & Corn, R. (2006). Single-nucleotide polymorphism genotyping by nanoparticle-enhanced surface plasmon resonance imaging measurements of surface ligation reactions. *Analytical Chemistry*, *78*(9), 3158–3164.

Li, N., Chen, Y., Zhang, Y.-M., Yang, Y., Su, Y., Chen, J.-T., & Liu, Y. (2014). Polysaccharide-gold nanocluster supramolecular conjugates as a versatile platform for the targeted delivery of anticancer drugs. *Scientific Reports*, *4*, 4164.

Liang, X., Chen, C., & Zhao, Y. (2008). Biopharmaceutics and therapeutic potential of engineered nanomaterials. *Current Drug Metabolism*, *9*(8), 697–709.

Liao, W., McNutt, M. a, & Zhu, W.-G. (2009). The comet assay: a sensitive method for detecting DNA damage in individual cells. *Methods, 48*(1), 46–53.

Libutti, S. K., Paciotti, G. F., Byrnes, A. A, Alexander, H. R., Gannon, W. E., Walker, M., Seidel, G. D., Yuldasheva, N., Tamarkin, L. (2010). Phase I and pharmacokinetic studies of CYT-6091, a novel PEGylated colloidal gold-rhTNF nanomedicine. *Clinical Cancer Research*, *16*(24), 6139–49.

Lim, E.-K., Kim, H.-O., Jang, E., Park, J., Lee, K., Suh, J.-S., Huh, Y-M., Haam, S. (2011). Hyaluronan-modified magnetic nanoclusters for detection of CD44-overexpressing breast cancer by MR imaging. *Biomaterials*, *32*(31), 7941–50.

Lipka, J., Semmler-Behnke, M., Sperling, R. A., Wenk, A., Takenaka, S., Schleh, C., Kissel, T., Parak, W. J., Kreyling, W. G. (2010). Biodistribution of PEG-modified gold nanoparticles following intratracheal instillation and intravenous injection. *Biomaterials*, *31*(25), 6574–81.

Liu, X., Dai, Q., Austin, L., Coutts, J., Knowles, G., Zou, J., Chen, H., Huo, Q. (2008). A one-step homogeneous immunoassay for cancer biomarker detection using gold nanoparticle probes coupled with dynamic light scattering. *Journal of the American Chemical Society*, *130*(9), 2780–2782.

Llevot, A., & Astruc, D. (2012). Applications of vectorized gold nanoparticles to the diagnosis and therapy of cancer. *Chemical Society Reviews*, *41*(1), 242–57.

Lövestam, G., Rauscher, H., Roebben, G., Klüttgen, B. S., Gibson, N., Putaud, J., & Stamm, H. (2010). *Considerations on a Definition of Nanomaterial for Regulatory Purposes*.

Manju, S., & Sreenivasan, K. (2012). Gold nanoparticles generated and stabilized by water soluble curcumin-polymer conjugate: blood compatibility evaluation and targeted drug delivery onto cancer cells. *Journal of Colloid and Interface Science*, *15*(368), 144–151.

Maxwell, C. A., McCarthy, J., & Turley, E. (2008). Cell-surface and mitotic-spindle RHAMM: moonlighting or dual oncogenic functions? *Journal of Cell Science*, *121*(Pt 7), 925–32.

Medley, C., Smith, J., Tang, Z., Wu, Y., Bamrungsap, S., & Tan, W. (2008). Gold nanoparticle-based colorimetric assay for the direct detection of cancerous cells. *Analytical Chemistry*, *80*(4), 1067–1072.

Mimeault, M., & Batra, S. K. (2014). Molecular biomarkers of cancer stem/progenitor cells associated with progression, metastases, and treatment resistance of aggressive cancers. *Cancer Epidemiology, Biomarkers & Prevention*, *23*(2), 234–54.

Minelli, C., Lowe, S. B., & Stevens, M. M. (2010). Engineering nanocomposite materials for cancer therapy. *Small (Weinheim an der Bergstrasse, Germany)*, *6*(21), 2336–57.

Mittal, A. K., Chisti, Y., & Banerjee, U. C. (2013). Synthesis of metallic nanoparticles using plant extracts. *Biotechnology Advances*, *31*(2), 346–56.

Mizrahy, S., Goldsmith, M., Leviatan-Ben-Arye, S., Kisin-Finfer, E., Redy, O., Srinivasan, S., Shabat, D., Godin, D., Peer, D. (2014). Tumor targeting profiling of hyaluronan-coated lipid based-nanoparticles. *Nanoscale*, *6*(7), 3742–52.

Mortelmans, K., & Riccio, E. S. (2000). The bacterial tryptophan reverse mutation assay with Escherichia coli WP2. *Mutation Research*, *455*(1-2), 61–9.

Mortelmans, K., & Zeiger, E. (2000). The Ames Salmonella/microsome mutagenicity assay. *Mutation Research*, *455*(1-2), 29–60.

Morton, C. L., & Houghton, P. J. (2007). Establishment of human tumor xenografts in immunodeficient mice. *Nature Protocols*, *2*(2), 247–50.

Morton, J., Day, E., Halas, N., & West, J. (2010). Nanoshells for photothermal cancer therapy. *Methods in Molecular Biology*, (624), 101–117.

Mukherjee, P., Bhattacharya, R., & Wang, P. (2005). Antiangiogenic properties of gold nanoparticles. *Clinical Cancer Research*, *11*(9), 3530–3534.

Munshi, A., Hobbs, M., & Meyn, R. E. (2005). Clonogenic cell survival assay. *Methods in Molecular Medicine*, *110*, 21–8.

Nanotechnology Characterization Laboratory: http://ncl.cancer.gov/

National Cancer Institute: http://www.cancer.gov/cancertopics/treatment/types-of-treatment

Nedvetzki, S., Gonen, E., Assayag, N., Reich, R., Williams, R. O., Thurmond, R. L., Huang, J.-F., Neudecker, B., Wang, F.-S, Wang, F.-S., Turley, E. A., Naor, D. (2004). RHAMM, a receptor for hyaluronan-mediated motility, compensates for CD44 in inflamed CD44-knockout mice: a different interpretation of redundancy. *Proceedings of the National Academy of Sciences of the United States of America*, *101*(52), 18081–6.

Nyström, A. M., & Fadeel, B. (2012). Safety assessment of nanomaterials: implications for nanomedicine. *Journal of controlled release*, *161*(2), 403–8.

Oberdörster, G., Maynard, A., Donaldson, K., Castranova, V., Fitzpatrick, J., Ausman, K., Carter, J., Karn, B., Kreyling, W., Lai, D., Olin, S., Monterio-Riviere, N., Warheit, D., Yang, H. (2005). Principles for characterizing the potential human health effects from exposure to nanomaterials: elements of a screening strategy. *Particle and Fibre Toxicology*, *2*, 8.

Ossipov, D. a. (2010). Nanostructured hyaluronic acid-based materials for active delivery to cancer. *Expert Opinion on Drug Delivery*, *7*(6), 681–703.

Paciotti, G. F., Myer, L., Weinreich, D., Goia, D., Pavel, N., McLaughlin, R. E., & Tamarkin, L. (2004). Colloidal gold: a novel nanoparticle vector for tumor directed drug delivery. *Drug Delivery*, *11*(3), 169–83.

Panariti, A., Miserocchi, G., & Rivolta, I. (2012). The effect of nanoparticle uptake on cellular behavior: disrupting or enabling functions? *Nanotechnology, Science and Applications*, *5*, 87–100.

Patra, C. R., Bhattacharya, R., Wang, E., Katarya, A., Lau, J. S., Dutta, S., Muders, M., Wang, S., Buhrow, S. A., Safgren, S. L., Yaszemski, M. J., Reid, J. M., Ames, M. M., Mukherjee, P., Mukhopadhyay, D. (2008). Targeted delivery of gemcitabine to pancreatic adenocarcinoma using cetuximab as a targeting agent. *Cancer Research*, *68*(6), 1970–8.

Platt, V. M., & Szoka, F. C. (2008). Anticancer Therapeutics: Targeting Macromolecules and Nanocarriers to Hyaluronan or CD44 , a Hyaluronan Receptor. *Molecular Pharmaceutics*, *5*(4), 474–486.

Ponta, H., Sherman, L., & Herrlich, P. a. (2003). CD44: from adhesion molecules to signalling regulators. *Nature reviews. Molecular cell biology*, *4*(1), 33–45.

Prestwich, G. (2011). Hyaluronic acid-based clinical biomaterials derived for cell and molecule delivery in regenerative medicine. *Journal of Controlled Release*, *155*(2), 193–199.

Qin, W. J., & Yung, L. Y. L. (2007). Nanoparticle-based detection and quantification of DNA with single nucleotide polymorphism (SNP) discrimination selectivity. *Nucleic Acids Research*, *35*(17).

Reineck, P., Gómez, D., Ng, S., & Karg, M. (2013). Distance and Wavelength Dependent Quenching of Molecular Fluorescence by Au@ SiO2 Core-Shell Nanoparticles. *ACS Nano*, *7*(8), 6636–6648.

Rupp, U., Schoendorf-Holland, E., Eichbaum, M., Schuetz, F., Lauschner, I., Schmidt, P., Schneeweiss, A. (2007). Safety and pharmacokinetics of bivatuzumab mertansine in patients with CD44v6-positive metastatic breast cancer: final results of a phase I study. *Anticancer Drugs*, *18*(4), 477–485.

Schwartz, J., Price, R., Gill-Sharp, K., Sang, K., Khorchani, J., Goodwin, B., & Payne, J. (2011). Selective nanoparticle-directed ablation of the canine prostate. *Lasers in Surgery and Medicine*, *43*(3), 213–220.

Shah, V., Taratula, O., Garbuzenko, O. B., Taratula, O. R., Rodriguez-Rodriguez, L., & Minko, T. (2013). Targeted nanomedicine for suppression of CD44 and simultaneous cell death induction in ovarian cancer: an optimal delivery of siRNA and anticancer drug. *Clinical Cancer Research*, *19*(22), 6193–204.

Shin, S. J., Beech, J. R., & Kelly, K. a. (2013). Targeted nanoparticles in imaging: paving the way for personalized medicine in the battle against cancer. *Integrative Biology*, *5*(1), 29–42.

Shinde, S. B., Fernandes, C. B., & Patravale, V. B. (2012). Recent trends in in-vitro nanodiagnostics for detection of pathogens. *Journal of controlled release*, *159*(2), 164–80.

Shuster, S., Frost, G., Csoka, A., Formby, B., & Stern, R. (2002). Hyaluronidase reduces human breast cancer xenografts in SCID mice. *International Journal of Cancer*, *102*(2), 192–197.

Siddik, Z. H. (2003). Cisplatin: mode of cytotoxic action and molecular basis of resistance. *Oncogene*, *22*(47), 7265–79.

Sironen, R. K., Tammi, M., Tammi, R., Auvinen, P. K., Anttila, M., & Kosma, V.-M. (2011). Hyaluronan in human malignancies. *Experimental Cell Research*, *317*(4), 383–91.

Slevin, M., Kumar, S., & Gaffney, J. (2002). Angiogenic oligosaccharides of hyaluronan induce multiple signaling pathways affecting vascular endothelial cell mitogenic and wound healing responses. *The Journal of Biological Chemistry*, *277*(43), 41046–59.

Slomiany, M. G., Dai, L., Bomar, P. A., Knackstedt, T. J., Kranc, D. A., Tolliver, L., Maria, B. L., Toole, B. P. (2009a). Abrogating drug resistance in malignant peripheral nerve sheath tumors by disrupting hyaluronan-CD44 interactions with small hyaluronan oligosaccharides. *Cancer Research*, *69*(12), 4992–8.

Slomiany, M. G., Dai, L., Tolliver, L. B., Grass, G. D., Zeng, Y., & Toole, B. P. (2009b). Inhibition of Functional Hyaluronan-CD44 Interactions in CD133-positive Primary Human Ovarian Carcinoma Cells by Small Hyaluronan Oligosaccharides. *Clinical Cancer Research*, *15*(24), 7593–7601.

Sneath, R. J., & Mangham, D. C. (1998). The normal structure and function of CD44 and its role in neoplasia. *Molecular pathology*, *51*(4), 191–200.

Son, S., & Lee, S. (2007). A platform for ultrasensitive and selective multiplexed marker protein assay toward early-stage cancer diagnosis. *Nanomedicine*, *2*(1), 79–82.

Sperling, R., Gil, P., Zhang, F., Zanella, M., & Parak, W. J. (2008). Biological applications of gold nanoparticles. *Chemical Society Reviews*, *37*(9), 1896–1908.

Sperling, R., & Parak, W. J. (2010). Surface modification, functionalization and bioconjugation of colloidal inorganic nanoparticles. *Philosophical Transactions of the Royal Society A Mathematical Physical and Engineering Sciences*, *368*(1915), 1333–1383.

Stern, R., & Jedrzejas, M. J. (2008). The Hyaluronidases: Their Genomics, Structures, and Mechanisms of Action. *Chemical Society Reviews*, *106*(3), 818–839.

Sugahara, K. N., Hirata, T., Hayasaka, H., Stern, R., Murai, T., & Miyasaka, M. (2006). Tumor cells enhance their own CD44 cleavage and motility by generating hyaluronan fragments. *The Journal of Biological Chemistry*, *281*(9), 5861–8.

Sultana, S., Khan, M. R., Kumar, M., Kumar, S., & Ali, M. (2013). Nanoparticles-mediated drug delivery approaches for cancer targeting: a review. *Journal of Drug Targeting*, *21*(2), 107–25.

Tan, J.-X., Wang, X.-Y., Su, X.-L., Li, H.-Y., Shi, Y., Wang, L., & Ren, G.-S. (2011). Upregulation of HYAL1 expression in breast cancer promoted tumor cell proliferation, migration, invasion and angiogenesis. *PloS One*, *6*(7), e22836.

Tang, D., Yuan, R., & Chai, Y. (2007). Biochemical and immunochemical characterization of the antigen-antibody reaction on a non-toxic biomimetic interface immobilized red blood cells of crucian carp and gold nanoparticles. *Biosensors and Bioelectronics*, *22*(6), 1116–1120.

Teng, B. P., Heffler, M. D., Lai, E. C., Zhao, Y., Levea, C. M., Vita, M., & Dunn, K. M. B. (2011). Inhibition of Hyaluronan Synthase-3 Decreases Subcutaneous Colon Cancer Growth by Increasing Apoptosis. *Anti-Cancer Agents in Medicinal Chemistry*, *11*(7), 620–628.

Toole, B. P., Ghatak, S., & Misra, S. (2008). Hyaluronan oligosaccharides as a potential anticancer therapeutic. *Current pharmaceutical biotechnology*, *9*(4), 249–52.

Toole, B. P. (2004). Hyaluronan: from extracellular glue to pericellular cue. *Nature reviews. Cancer*, *4*(7), 528–39.

Underhill, C. (1992). CD44: the hyaluronan receptor. *Journal of Cell Science*, *103*, 293–8.

Vangara, K. K., Liu, J. L., & Palakurthi, S. (2013). Hyaluronic acid-decorated PLGA-PEG nanoparticles for targeted delivery of SN-38 to ovarian cancer. *Anticancer Research*, *33*(6), 2425–34.

Veiseh, M., Breadner, D., Ma, J., Akentieva, N., Savani, R. C., Harrison, R., Mikilus, D., Collis, L., Gustafson, S., Lee, T.-Y., Koropatnick, J., Luyt, L. G., Bissel, M. J., Turley, E. A. (2012). Imaging of homeostatic, neoplastic, and injured tissues by HA-based probes. *Biomacromolecules*, *9*(13), 12–22.

Venable, R. O., Worley, D. R., Gustafson, D. L., Ryan, J., Iii, E. J. E., Cai, S., Cohen, M. S., Forrest, L. (2012). Effects of intratumoral administration of a hyaluronan-cisplatin nanoconjugate to five dogs with soft tissue sarcomas. *American Journal of Veterinary Research*, *73*(12), 1969–1976.

Venturoli, D., & Rippe, B. (2005). Ficoll and dextran vs. globular proteins as probes for testing glomerular permselectivity: effects of molecular size, shape, charge, and deformability. *American Journal of Physiology-Renal Physiology*, *288*(4), F605–613.

Vigderman, L., & Zubarev, E. R. (2013). Therapeutic platforms based on gold nanoparticles and their covalent conjugates with drug molecules. *Advanced Drug Delivery Reviews*, *65*(5), 663–76.

Wagner, V., Dullaart, A., Bock, A.-K., & Zweck, A. (2006). The emerging nanomedicine landscape. *Nature biotechnology*, *24*(10), 1211–7.

Wang, L.-S., Chuang, M.-C., & Ho, J.-A. A. (2012). Nanotheranostics--a review of recent publications. *International journal of nanomedicine*, *7*, 4679–95.

Wang, S., Earle, C., Wong, G., & Bourguignon, L. (2013). Role of hyaluronan synthase 2 to promote CD44-dependent oral cavity squamous cell carcinoma progression. *Head Neck*, *35*(4), 511–520.

Wheate, N. J., Walker, S., Craig, G. E., & Oun, R. (2010). The status of platinum anticancer drugs in the clinic and in clinical trials. *Dalton Transactions*, *39*(35), 8113–27.

Williams, K., Motiani, K., Giridhar, P. V., & Kasper, S. (2013). CD44 integrates signaling in normal stem cell, cancer stem cell and (pre)metastatic niches. *Experimental biology and medicine (Maywood, N.J.)*, *238*(3), 324–38.

Yu, Z., Pestell, T. G., Lisanti, M. P., & Pestell, R. G. (2012). Cancer stem cells. *The international journal of biochemistry & cell biology*, *44*(12), 2144–51.

Zhang, Y., Satoh, K., & Li, M. (2012). Novel therapeutic modalities and drug delivery in pancreatic cancer - an ongoing search for improved efficacy. *Drugs in Context*, *2012*, 212244.

Zhou, J., Ralston, J., Sedev, R., & Beattie, D. A. (2009). Functionalized gold nanoparticles: synthesis, structure and colloid stability. *Journal of Colloid and Interface Science*, *331*(2), 251–62.